

博士学位论文

Structural Health Monitoring through
Dynamic and Geometric Characteristics of
Bridges Extracted from GPS Measurements

Mosbeh Rashed Mosbeh Kaloop

哈尔滨工业大学

2010年6月

国内图书分类号: U445.7:U447

国际图书分类号: 624.2

工学博士学位论文

STRUCTURAL HEALTH MONITORING THROUGH DYNAMIC AND GEOMETRIC CHARACTERISTICS OF BRIDGES EXTRACTED FROM GPS MEASUREMENTS

博士研究生: Mosbeh Rashed Mosbeh Kaloop
导 师: 李 惠 教授
申请学位级别: 工学博士
学 科、专 业: 土木工程、防灾减灾工程及防护工程
所 在 单 位: 土木工程学院
答 辩 日 期: 2010 年 6 月
授予学位单位: 哈尔滨工业大学

Classified Index: U445.7:U447

U.D.C.: 624.2

Dissertation for the Doctoral Degree in Engineering

**STRUCTURAL HEALTH MONITORING
THROUGH DYNAMIC AND GEOMETRIC
CHARACTERISTICS OF BRIDGES EXTRACTED
FROM GPS MEASUREMENTS**

Candidate:	Mosbeh Rashed Mosbeh Kaloop
Supervisor:	Prof. Hui Li
Academic Degree Applied for:	Doctor of Engineering
Specialty:	Disaster Prevention and Reduction Engineering and Protective Engineering
Affiliation:	School of Civil Engineering
Date of Oral Examination:	June, 2010
University:	Harbin Institute of Technology

*To my Parents, my Wife, my Daughter (Razan)
and my Son (Khaled)*

摘要

结构健康监测(SHM)是土木工程界的一个新兴研究领域, 该项技术的应用使得连续、实时地评估土木工程结构的安全性能成为可能。通过结构健康监测技术, 根据已有的结构状态信息, 可有效地采取一定的预防措施来延长结构寿命, 并且防止灾难事故的发生。

全球卫星定位系统(GPS)是一种应用于结构健康监测的主要方法。虽然GPS已被证明可有效记录结构的相对位移, 但是, 如何利用GPS采集得到的结构相对位移仍是GPS在健康监测应用中所面临的主要挑战。

针对上述问题, 本文提出一个基于RTK-GPS监测数据的数学框架, 从而实现GPS在结构健康监测中的应用。本文采用某大桥的GPS监测数据进行研究, 该桥梁结构的健康监测系统由哈尔滨工业大学结构健康监测与控制研究中心建立。

由于在该桥重建一年之后, 在距离一号桥墩48.2m处产生了一个明显的裂缝, 因此, 本文对该桥梁结构的移动及损伤进行了研究。此外, 对各种因素所产生的裂缝(如风速, 环境温度、车辆荷载等)以及桥塔的横向及纵向位移进行了分析。

本文分别采用信号处理方法(Kalman滤波器, 自适应滤波器, 参数化最小二乘法对GPS数据进行光滑和去噪处理, 小波分析(短时傅立叶变换, 连续小波变换, 离散小波变换)对GPS数据进行时域和频域分析并识别不同的桥梁运动和可能的损伤)和几何分析方法(平面模型, 跨度模型和极坐标模型)应用于桥梁运动和损伤分析。

为了分析GPS信号的周期性成分, 本文采用高通滤波方法确定桥梁移动信号的高频成分。利用功率谱分析及短时傅里叶变换完成时域信号到频域的转换, 在此基础上, 对转换后的频域信号进行了谱分析。

本文得到如下结论: (1) 车辆荷载是造成桥梁损伤的主要因素; (2) 永和桥使用后六个月, 该桥梁结构的最大变形产生于离第距离一号桥墩48.2m处; (3) 相比传统傅里叶变换而言, 短时傅里叶变换在结构响应分析方面具有明显的优势; (4) GPS信号的灵敏度并不依赖于GPS传感器的位置; (5) 几何分析方法便于计算桥塔的运动, 而物理分析方法更有利于识别桥梁结构损伤; (6) GPS信号20 HZ的采样频率并不适合于采集结构固有频率; (7) Kalman滤波方法适合于结构动力分析; (8) 自功率谱及短时傅里叶变换方法能够有效反映桥梁预期移动和损伤; (9) 南塔运动引起的剪力以及车辆荷载引起的桥梁

非线性运动是造成永和桥损伤的主要原因。

此外，通过分析 GPS 和加速度技术采集的永和桥桥塔的横向位移、加速度和扭转位移数据，得到如下结论：（1）GPS 信号是含有噪声的；（2）Wden 函数的采用能够提高 20%的准确性；（3）能量谱密度是识别桥塔位移的有效参数；（4）GPS 可作为一种可靠的方法研究低频桥梁结构的动力特性。

除了上述提及的分析方法，本文采用多入单出（MISO）的鲁棒拟合回归模型、神经网络 ARMAX（NNARMAX）模型用于识别桥梁的运动。分析结果表明：（1）考虑了鲁棒回归分析的 NNARMAX [4411]和[5415] 模型比 NNARMAX[0100] 模型能够更准确的估计桥梁结构的移动状态；（2）鲁棒拟合回归模型能够较好地映射荷载效应与桥塔位移之间的关系，此外，环境温度和湿度对整个桥梁的阵型影响不大。

关键词：全球卫星定位系统；结构健康监测；桥梁工程；Kalman 滤波；参数最小二乘法；小波变换；神经网络 ARMAX 模型；监测

Abstract

Structural Health Monitoring (SHM) is an emerging field in civil engineering that offers the potential for continuous and periodic assessment of the safety and integrity of civil infrastructures. Based on previous structure condition knowledge, certain preventive measures can be adopted to prolong the service life of the structure and prevent catastrophic failure.

Global Positioning System (GPS) is one of the major methods utilized in SHM. However, as the technical feasibility of using GPS for recording relative displacements has been proven, the challenge issue for users is to determine how to make use of the relative displacements being recorded.

This thesis proposes a mathematical framework that supports the use of Real Time Kinematics (RTK)-GPS data for structural monitoring. The used GPS data is acquired by the Research Center of Structural Health Monitoring and Control of Harbin Institute of Technology (HIT), to monitor the loads and responses of one cable-stayed bridge.

After one year of reconstruction of this bridge, cracks were observed at 48.2 m from the first abutment again. The analysis will include the movements and damages of the bridge, the current applied operational safety methods, and the bridge cracks cause under different stress factors such as wind speed, temperature change and traffic loads. In addition, the bridge towers lateral, longitudinal movements are to be analyzed

Signal processing methods (Kalman and Adaptive filtering, parametric least square methods were utilized to smooth and denoise the recorded GPS signals) and (Wavelet analysis algorithm (STFT,CWT,DWT) are to be used to transform the GPS signals into the frequency time domain and detect different bridge movements and possible damage). The geometrical analysis methods (plane model, span length model and polar coordinates model) are to be used for the bridge movements and damages analysis.

For the analysis of the periodic components of the GPS signals, a high-pass filtering process is applied to the signal to determine the high frequencies components of the bridge movements. The transformation of the recorded signals from the time domain to the frequency domain are formed by power spectrum

density (PSD) and short time Fast Fourier Transformation (STFT), then the power spectrums of the transformed signals are analyzed.

The following are some of the analysis the results: (1) The traffic loads are the main factor that affects the bridge damage, (2) The maximum deformation was pronounced at 48.2 m from the first abutment six months after the bridge use, (3) The STFT is a significant step forward from the traditional FFT in terms of structural response analysis, (4) The sensitivity of the recorded GPS signals does not depend on the position of the GPS sensors, (5) The geometric analysis method provides an easy way to calculate the bridge tower movement, whereas, the physical analysis method is better for detecting the bridge damage, (6) The observed frequency using a 20 HZ GPS is not suitable for monitoring the observed structure natural frequency, (7) The Kalman Filtering is suitable for the dynamic study, (8) It was found that the PSD and STFT analysis results reflect the bridge expected movements and cracks, and (9) It was found that the bridge cracks are mainly caused by the shear force due to movement of the south tower and the bridge non-linear movements due to traffic loads.

GPS and accelerometer techniques are used to collect the lateral displacements, acceleration and torsion displacements data of the bridge tower. Analysis the collected data provide the following results: (1) The recorded GPS signals are noisy, (2) The Wden function provides a 20% increase of accuracy, (3) Power spectral density is a good parameter to detect the tower movements, and (4) GPS can be used as a trustworthy tool for characterizing the dynamic behavior of the low frequency bridges.

In addition to previous analysis methods, two identification models namely; Multi Input-Single Output (MISO) robust fit regression and Neural Network Auto-Regression Moving Average with eXogenous input (NNARMAX) models are used for the identification of the bridge movements. The analysis of test results indicate that: (1) The NNARMAX [4411] and [5415] models defined by taking into account the results of robust regression analysis estimate structural movements are more accurate than the NNARMAX[0100] model, and (2) The robust fit regression models have good capacities for mapping the relationship between the applied loads effects factors and the tower displacements. Temperature and humidity effects on the entire modals shapes are insignificant.

Keywords: Global Position System; Structural Health Monitoring; Bridge; Kalman Filter; Parametric Least Square method; Wavelet Transformation; Neural Network Auto-Regression Moving Average with eXogenous; Monitoring.

Contents

摘要	I
Abstract	III
List of Abbreviations and Acronyms.....	IX
Chapter 1 Introduction	1
1.1 General.....	1
1.2 Scope of the thesis	2
1.3 Global Positioning System (GPS) Background.....	2
1.3.1 Real Time Kinematics GPS positioning.....	4
1.3.2 Error sources in GPS observations.....	7
1.3.3 GPS Accuracy Enhancement.....	8
1.4 Structural Health Monitoring (SHM) Background.....	8
1.4.1 Methods of Determining Deformation.....	10
1.4.2 Structural Health Monitoring Using GPS	13
1.5 GPS signal processing.....	16
1.5.1 Kalman Filter (KF)	17
1.5.2 Adaptive Filter (AF)	18
1.5.3 Parametric least square method.....	21
1.5.4 Wavelet transform processing.....	22
1.6 Geometrical monitoring models.....	24
1.6.1 Plane Monitoring Model.....	25
1.6.2 Polar Coordinates Monitoring Model	26
1.6.3 Span Length Monitoring Model.....	27
Chapter 2 Bridge Movement Analysis Based on GPS Technique	29
2.1 Introduction.....	29
2.2 Bridge Descriptions.....	29
2.3 GPS and Data Collection Information.....	31
2.3.1 Data Processing Strategy	35
2.4 Analysis the Tower Bridge Movement	36
2.4.1 Prediction and analysis of movements.....	36
2.4.1.1 KF Method.....	38
2.4.1.2 PLS Method	39

2.4.1.3 Statistical deformation analysis	41
2.4.2 Filtering and deformation analysis.....	43
2.4.2.1 Investigation of the loading effects on the tower movements	43
2.4.2.2 Analysis of the observed displacement	46
2.4.2.3 2D- Frequency time series analysis.....	48
2.4.2.4 Tower Statistical Deformation analysis.....	55
2.4.3 Adaptive filter and analysis of tower movement.....	57
2.4.4 Sensitivity and statistics of GPS signals based on damage observations and WT analysis	60
2.4.4.1 Analysis movement of the Tower Bridge	61
2.4.4.2 Wavelet Analysis.....	66
2.4.5 Geometrical Models Analysis	72
2.4.5.1 Plane analysis	75
2.4.5.2 PC analysis	77
2.4.5.3 Span Length analysis	79
2.5 Summary	80
Chapter 3 Multi input / Single Output Model Identification of Bridge Tower Movements Using GPS Monitoring System	81
3.1 Introduction.....	81
3.2 Robust fitted regression	81
3.3 The NNARMAX model	83
3.4 Criterion of parameters and prediction.....	86
3.5 Identification of Tower bridge movements.....	87
3.5.1 Tower displacements.....	87
3.5.2 Identified Models.....	91
3.6 Summary	97
Chapter 4 Bridge Deformation Monitoring Based on GPS/ Accelerometer Integration Technique.....	98
4.1 Introduction.....	98
4.2 Bridge Deformation Monitoring Based on GPS and Accelerometer background.....	98
4.3 GPS/Acceleration integration analysis Tower bridge movement	103
4.3.1 Wden Matlab Function (WMF).....	104
4.3.2 GPS Displacement	104

4.3.3 Acceleration measurements.....	109
4.3.4 Torsional displacement	110
4.3.5 Deformation analysis	111
4.4 Summary	113
Conclusions and Recommendations.....	114
References	118
Appendix (A): Some used MATLAB programs	130
Appendix (B): Some Observations Movements Results	135
List of Figure Captions	139
List of Table Captions	144
Published Papers in the Ph.D.Period.....	145
Statement of Copyright.....	Error! Bookmark not defined.
Letter of Authorization	Error! Bookmark not defined.
Acknowledgements.....	148
Resume	149

List of Abbreviations and Acronyms

GPS- Global Positioning System
RTK - Real Time Kinematics
MCS - Master Control Station
C/A – Course-Acquisition
SPS - Standard Positioning Service
SPP - Single Point Positioning
DGPS - Differential Global Positioning System
DOP - Dilution of precision
RKP - Relative Kinematic Positioning
UTC - Coordinated Universal Time
FFT - Fast Fourier Transformation
WT - Wavelet Transformation
STFT - Short Time Fourier Transformation
T - Temperature
FE - Finite Element
KF - Kalman Filter
AF - Adaptive Filter
PLS - Parametric Least Square
MISO - Multi Input Single Output
ARMAX - Auto-Regressive Moving Average with eXternal input
NN - Neural Network
 λ_0 - Value of the loss function
FPE - Akaike's Final Prediction Error
ACF - Auto-Correlation Function
AC - Auto-Correlation
R - R-square
MLP - Multilayer Perceptron
LS - Least Square
PC - Polar Coordinate
WMF - Wden Matlab Function
DWT - Discrete Wavelet Transform

CWT - Continuous Wavelet Transform

MSE - minimize the mean square estimation error

FIIR - Finite-duration Impulse Response

PSD - Power Spectrum Density

SD - Standard Deviation

IIR - Tenth-order Butterworth Infinite impulse response

α - Coefficient of thermal expansion

BCS - Bridge Coordinate System

WGS-84 - World Geodetic System 1984

CCD - Charge Couple Device

AASHTO - American Association of State Highway and Transportation Officials

GIS - Geographical Information System

MA - Moving average

SD - Standard Deviation

SHM - Structural Health Monitoring

BMS - Bridge Management System

PRN - Pseudorandom Noise

OTF - Kinematic On the Fly

MDL - Minimum Description Length

Chapter 1 Introduction

1.1 General

The security of civil engineering works demands a periodical monitoring of the structures. In many civil structures like bridges, tunnels and dams; the deformations are the most relevant parameters to be monitored, so monitoring the structural deformation and dynamic response to the large variety of external loadings has a great importance for maintaining structures safety and economical design of man-made structures ^[43-44].

Nowadays a few structures have been instrumented to provide continuous data in real time to monitor large and small movements. The main objective in continuous monitoring, commonly known as Structural Health Monitoring (SHM), is to track any changes in the characteristics of the structure, and to detect and locate damage. SHM of complex structures poses new challenges as regards increased safety and operational reliability, while recent sensor technology opens up many possibilities undreamt of methods of analysis. On other hand, another important SHM objective is to track dynamic characteristics of the structure and possible changes that may occurred after a natural or man made extreme events.

The three-dimensional co-ordinates of a moving object are required to a high-level of accuracy and at a high data rate in many situations. Typical applications include studies of bridges and buildings under load, monitoring cranes in operation for deflections and aligning large machinery during construction. In such applications, simultaneous positioning of several points at the sub-centimeter level may be required at data rates of 1 Hz or more. Over the last decade, the Global Positioning System (GPS) has emerged as the technology of choice in such monitoring applications. In particular, GPS has the advantages of high data acquisition rate (typically up to 10 Hz) and autonomous operation. Also, using differential techniques and the appropriate equipment, it can furnish position estimates in real-time with sub centimeter-level accuracy.

1.2 Scope of the thesis

The main objectives of this research are: (1) to examine the real time kinematic (RTK)-GPS technique for structures movement monitoring, (2) to implement the parametric least square with a Kalman Filter in GPS data processing, (3) to use the Adaptive filter (AF) technique in GPS data processing for movement analysis, (4) to find out the reasons that may affect bridge damage, (5) To determine the tower bridge deformation and frequency domain analysis using the plane geometric method and STFT technique, (6) to use the Wden function available within Matlab library to de-noise the GPS signals, (7) to evaluate the effects of the applied loads on the bridge tower movements, (8) To determine the bridge deformation using the geometrical analysis, (9) To set a relation between the movement of towers and bridges damage, (10) To estimate the probable bridge time time, (11) to develop parametric models to asses the dynamic behavior of the Yonghe tower bridge utilizing RTK-GPS measurements, (12) to develop transfer functions that express the relationship between the displacements of the southern tower in two directions (X and Y) and the variations of temperature, humidity, wind speed and number of vehicles on the bridge have been defined with the use of parametric MISO NNARMAX and robust fit regression models.

1.3 Global Positioning System (GPS) Background

GPS is a positioning system that has been developed and operated by the U.S. Department of Defense ^[12, 112]. A GPS system is formed from a network of satellites that transmit Continuous coded information, which makes it possible to identify locations on Earth by measuring distances from the satellites; moreover, the receiver also has the ability to obtain information about its velocity and direction.

A GPS network consists of 24 satellites arranged in six orbital planes of about 20200 Km altitude above earth's surface, with an orbital inclination of 55 degree, as depicted in Figure 1.1, so that at any given time a minimum of five satellites can be observed by GPS receivers at any location in the world ^[51; 121].

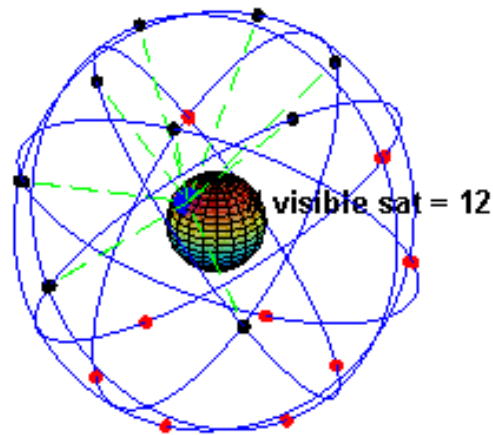


Figure 1.1 GPS satellites arranged in six orbital planes

The GPS system consists of three segments (Space segment, Control segment and user segment) refer to ^[12, 51, 73] (Figure 1.2).

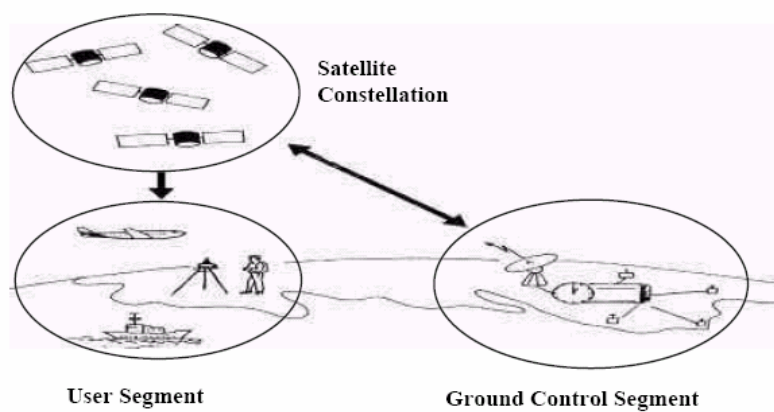


Figure 1.2 GPS elements

Each GPS satellite transmits data on three frequencies: L1 (1575.42 MHz), L2 (1227.60 MHz) and L5 (1176.45 MHz). The L1, L2 and L5 carrier frequencies are generated by multiplying the fundamental frequency by 154, 120 and 115, respectively ^[12; 51].

Pseudorandom noise (PRN) codes, along with satellite ephemerides, ionospheric model, and satellite clock corrections are superimposed onto the carrier frequencies L1, L2 and L5. The measured transmitting times of the signals that travel from the satellites to the receivers are used to compute the

pseudoranges. The Course-Acquisition (C/A) code, sometimes called the Standard Positioning Service (SPS), is a pseudorandom noise code that is modulated onto the L1 carrier. The precision (P) code, sometimes called the Precise Positioning Service (PPS), is modulated onto the L1, L2 and L5 carriers allowing for the removal of the effects of the ionosphere ^[63]. In addition, more detail on GPS system can be found in any of a number of GPS textbooks and thesis, see ^[12; 39; 49; 51-52].

In fact, basic GPS receivers often have four radio channels so that the receiver can observe four GPS satellites at once and obtain a pseudo-range measurement from each satellite signal.

Leva in ^[13] show two different techniques by which a GPS receiver can compute its location from four pseudo-range measurements, minimum required for localization in three dimensions. However, if one of the GPS satellites' signals does not appear, it is hard to identify the location of the GPS receiver from only three measurements. Therefore, the more advanced receivers have been developed to have six or more radio channels. The extra channels keep observing other GPS satellites and put their information in reserve, to use in case one or more of the four signals that is missing.

1.3.1 Real Time Kinematics GPS positioning

The Real Time Kinematics (RTK)-GPS positioning concept is represented in Figure 1.3. In practice, RTK-GPS system uses a single base station receiver and a number of rover stations. The hardware requirements are identical at each station. The reference station is placed at a location with good sky visibility in order to minimize GPS errors that may be introduced due to signal obstructions or reflections. The reference station are collected the data, e.g. raw pseudorange and carrier phase or the GPS satellite ranges, and transmitted to the rover station (s) via a communication link using either proprietary message formats or an industry standard format ^[82]. In the standard RTK configuration, the rover receiver combines this transmitted data with its own measurements in order to calculate its position in real time ^[83-84]. When measurements from two receivers were combined, correlated errors (such as satellite orbital errors, satellite clock errors, ionospheric and tropospheric errors) are significantly reduced. So, the spatial

correlation of the errors is largely dependent on the inter-receiver distance. Beyond 10 or more kilometers, the degree of de-correlation may be higher as to significantly impact on the baseline solution.

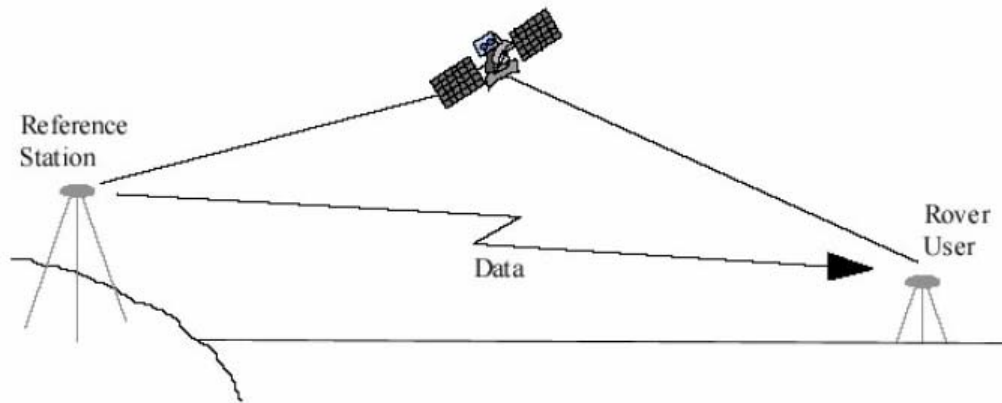


Figure 1.3 the RTK-GPS schem

In order to achieve high positioning accuracies in real-time, the processing of double-differenced carrier phase measurements were carried out. In this case, the integer ambiguities must be determined ^[79-80]. This problem was essentially one of determining the initial ambiguities at signal lock on, which is when the receiver measured the changing number of cycles. The basic approach to determining the integer ambiguities was to use the relatively noisy pseudorange measurements to define a volume, which is assumed to contain the correct set of integer ambiguities. All possible integer ambiguity combinations were then tested to determine the best case, the test criterion often being the set that minimizes the sum squared carrier phase residuals. A ratio test is performed between the sum of squared carrier phase residuals of the best and second best sets, and if the ratio exceeds a certain threshold, then the best set is accepted for fixing the carrier phase ambiguities ^[12; 51].

Figure 1.4 was illustrated the double-differencing data processing strategy for a single epoch. At each of the stations, reference and rover, the observations from the base satellite were subtracted from the observations to all other satellites at that epoch. The differences for the reference station were then subtracted from the differences at the rover station to create a double-difference observable. The satellite-receiver double-difference was generally given as ^[12]:

$$\Delta\nabla = \{(data)^S\} - \{(data)^b\}_{rem} - \{(data)^S\} - \{(data)^b\}_{ref} \quad (1.1)$$

Where:

- $\Delta\nabla$ is the satellite-receiver double difference, the operator Δ implies a between receiver difference and ∇ implies a between satellite difference
- $(data)^S$ is the data from the satellite (other than the base satellite)
- $(data)^b$ is the data from the base satellite
- $\}_{rem}$ and $\}_{ref}$ are respectively the differenced data calculated by the rover station and the reference station

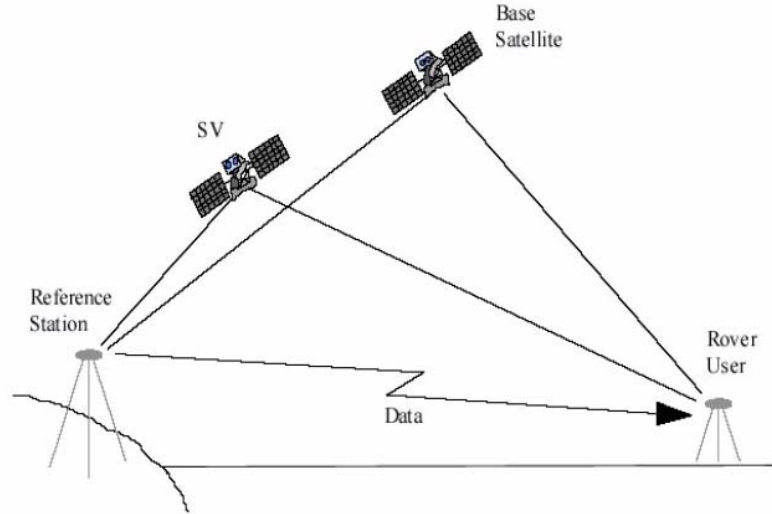


Figure 1.4 satellite-receiver double difference cases

The resulting satellite-receiver double-differenced phase observable was:

$$\Delta\nabla\Phi = \Delta\nabla\rho + \Delta\nabla d\rho + \lambda\Delta\nabla N - \Delta\nabla d_{ion} + \Delta\nabla d_{trop} + \varepsilon\Delta\nabla(\Phi_{rx}) + \varepsilon\Delta\nabla(\Phi_{mult}) \quad (1.2)$$

Where the satellite and receiver clock error terms were eliminated, and the orbital and atmospheric effects were greatly reduced, while the receiver noise and multipath were slightly increased. In single epoch solution, using carrier phase data, accuracies in the range sub-centimeters to sub-decameters can be obtained, depending on the baseline length and other factors ^[53; 79]. Typical single epoch

accuracy is + 1-2 cm for the horizontal components and about + 2 cm for the vertical component, for short baseline (< 10 Km). However, higher accuracies have been claimed with recent receiver technology and refined Kalman filter data processing ^[54-55].

1.3.2 Error sources in GPS observations

The accuracy of GPS in case of relative positioning depends on the distribution (positional geometry) of the observed satellites and on the quality of the observations. The GPS observables are affected by systematic errors and random noise. The errors sources can be classified according to ^[75] into three groups as show Figure 1.5.

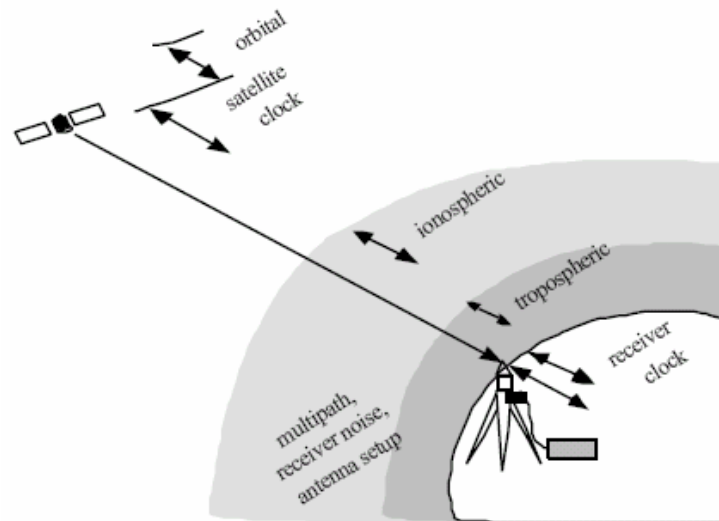


Figure 1.5 Common errors in GPS measurements

(1) Satellite related errors like: orbit errors, satellite clock biased, satellite antenna offsets and satellite antenna phase center variations.

(2) Propagation medium related errors like: tropospheric; ionospheric refraction and multipath.

(3) Receiver environment related errors like: receiver clock offsets, interchannel biases and antenna phase center variations.

The errors in GPS observation depend mainly on two factors:

- (1) The user equivalent range error (noise and systematic)
- (2) Geometry of the satellite used.

The most of errors are due to the effect of hardware, environmental and atmospheric error sources. The summary of errors are concluded as refers [12,52,73]

1.3.3 GPS Accuracy Enhancement

Augmentation methods of improving accuracy rely on external information being integrated into the calculation process. There are many such systems in place and they are generally named or described based on how the GPS sensor receives the information [121]. Some systems transmit additional information about sources of error (such as clock drift, ephemeris, or ionospheric delay), others provide direct measurements of how much the signal was off in the past, while a third group provide additional navigational or vehicle information to be integrated in the calculation process. In addition, more detail on GPS accuracy enhancement can be found in any of a number of GPS textbooks and thesis, see [12; 39; 49; 51-52; 73]

1.4 Structural Health Monitoring (SHM) Background

The process of implementing a damage detection strategy for aerospace, civil and mechanical engineering infrastructure is referred to as Structural Health Monitoring (SHM) or Structronic System [94-96]. Here damage is defined as changes to the material and/or geometric properties of these systems, including changes to the boundary conditions and system connectivity, which adversely affect the system's performance. The damage identification process is generally structured into the following levels [129; 132]:

- Damage detection, where the presence of damage is identified.
- Damage location, where the location of the damage is determined.
- Damage typification, where the type of damage is determined.
- Damage extent, where the severity of damage is assessed.

The SHM process involves the observation of a system over time using periodically sampled dynamic response measurements from an array of sensors, the extraction of damage-sensitive features from these measurements, and the statistical analysis of these features to determine the current state of system health. For long term SHM, the output of this process is periodically

updated information regarding the ability of the structure to perform its intended function in light of the inevitable aging and degradation resulting from operational environments. After extreme events, such as earthquakes or blast loading, SHM is used for rapid condition screening and aims to provide, in near real time, reliable information regarding the integrity of the structure [1].

The SHM problem can be addressed in the context of a statistical pattern recognition paradigm [3]. In this paradigm, the process can be broken down into four parts: (1) Operational Evaluation, (2) Data Acquisition and Cleansing, (3) Feature Extraction and Data Compression, and (4) Statistical Model Development for Feature Discrimination.

When one attempts to apply this paradigm to data from real world structures, it quickly becomes apparent that the ability to cleanse, compress, normalize and fuse data to account for operational and environmental variability is a key implementation issue when addressing Parts 2-4 of this paradigm. These processes can be implemented through hardware or software and, in general, some combination of these two approaches will be used [125-128].

One of the most common feature extraction methods is based on correlating measured system response quantities, such a vibration amplitude or frequency, with the first-hand observations of the degrading system [130]. Another method of developing features for damage identification is to apply engineered flaws, similar to ones expected in actual operating conditions, to systems and develop an initial understanding of the parameters that are sensitive to the expected damage [139-143]. The flawed system can also be used to validate that the diagnostic measurements are sensitive enough to distinguish between features identified from the undamaged and damaged system.

The operational implementation and diagnostic measurement technologies needed to perform SHM produce more data than traditional uses of structural dynamics information [4; 15]. A condensation of the data is advantageous and necessary when comparisons of many feature sets obtained over the lifetime of the structure are envisioned. Also, because data will be

acquired from a structure over an extended period of time and in an operational environment, robust data reduction techniques must be developed to retain feature sensitivity to the structural changes of interest in the presence of environmental and operational variability ^[124]. To further aid in the extraction and recording of quality data needed to perform SHM, the statistical significance of the features should be characterized and used in the condensation process. The SHM System's elements include:

Structure, Sensors, Data acquisition systems, Data transfer and storage mechanism, Data management , and Data interpretation and diagnosis: 1) System Identification, 2) Structural model update, 3) Structural condition assessment, 4) Prediction of remaining service life.

1.4.1 Methods of Determining Deformation

The determination of deformations has traditionally been categorized into two methods; analytic or theoretical methods and experimental methods. For analytic methods, there are several geometric and energy models for computing deflection of structures, some of these models are only suitable to calculate one particular deflection component at an individual point, while others may be used to calculate deflections at several points simultaneously. Each model has its limitation, advantages and disadvantages ^[45].

For experimental methods, the measuring techniques and instrumentation for geometrical monitoring of deformations have traditionally been categorized into two groups according to the two main groups of professionals who use the techniques:

(a) Geodetic surveying, which includes Global Position System (GPS), close range Photogrammetry, terrestrial surveying (leveling, theodolite, total station, laserscanner and very long base line interferometer) and satellite laser ranging. These were always contaminated by atmospheric refraction, which limits their positioning accuracy about + 1 ppm to + 2 ppm of the distance. For instance, with the average distance between the object and reference points of 500m, the absolute displacements of the object points can not be determined with an accuracy better than about + 2 mm at the 95% probability ^[57]. So that, the high precision electro-optical geodetic instruments for

Electronic Distance Measurements (EDM), with accuracies of about ± 0.3 mm over short distances, may be more suitable for relative deformation surveys. As the same, geodetic leveling with achievable accuracies of better than ± 0.1 mm over 20 m distances will provide better accuracy for tilt determination (± 1 second of arc). New developments in three-dimensional coordinate systems with electronic theodolites can provide relative positioning to an accuracy of ± 0.05 mm over distances of several meters [46; 65]. The same applies to photogrammetric techniques with Charge Couple Device (CCD) sensors.

The advent of the GPS technology has facilitated automated structural monitoring with real-time direct precise position information (three dimension coordinates or baseline components). With the advantages of the GPS technology and other new sensor technologies, in addition to the current advances in desktop computational flexibility, the possibilities of automated intelligent signal processing and health monitoring systems were today within reach. Numerous feasibility studies have confirmed that GPS-based hardware and software monitoring systems can be playing a role in monitoring manmade structures. Therefore, for such purposes, the GPS technology also has some limitations if used in isolation from other sensors. Consequently, some studies have recently identified the complementary benefits of integrating GPS positioning with additional sensors. For example, Meng et al. (2007) have carried out a series of tests of an integrated GPS/accelerometer system. Their work showed that the integration of the two sensor sub-systems was possible, and that it results in a system that addresses the shortcomings of each sub-system, in addition to providing higher levels of quality control.

In general, the instruments for measuring deformation can be grouped in the categories listed in Table 1.1 [72].

(b) Geotechnical structural measurements of local deformations using tilt meters, strain meters, extensometers, and joint meters, etc [47].

In addition, other displacement measurement sensors and techniques that can be applied to structural monitoring. A complete list cannot provide in this thesis. Some of the more common include:

- Accelerometer: These are devices for measuring the rate of change of acceleration of point. Hence, measurements require double

integration to arrive at displacement values. Several reports of studies on structural monitoring with such devices can be found in the references [68- 69].

- Laser interferometers: These can determine precise interferometer distances by using monochromatic radiation and optical fiber sensors where changes in length of the optical fiber are sensed electro-optically.

- Dynamic pressure transducers: They compare the measured pressure with atmospheric pressure. Dynamic pressure transducer falls in the class of displacement transducers.

Each type of the measurements has its own advantages and drawbacks. Geodetic surveys, through a network of points interconnected by angle and distance measurements, usually supply a sufficient redundancy of observations, for the statistical evaluation of their quality and for a detection of errors. They give global information on the behavior of the deformable object while the Geotechnical measurements give very localized and, very frequently, locally disturbed information without any check [47].

Table 1.1 Non-GPS instruments for measuring deformation [72].

Instrument category	Type of measured deformation					
	↔	↑↓	A	R	• —	B
Surveying instruments						
Optical and electronic theodolites	√	√	√		√	
EDM	√	√	√		√	
Total stations and survey robots	√	√	√		√	
Optical, digital and laser beam levels		√			√	
Photogrammetric and CCD camera	√	√	√		√	
Geotechnical instruments						
Extensometers	√	√	√			√
Tiltmeters				√	√	√
Inclinometers	√	√	√	√		√
Transverse deformation gauges	√	√	√			√
Liquid level gauges		√				√
Miscellaneous deformation gauges	√	√	√		√	√
Other non-GPS instruments						
Laser interferometer, optical fiber sensors, etc.	√	√	√			

Key: ↔ horizontal deformation ↑ vertical deformation A axial deformation
R Rotation deformation • surface deformation B subsurface deformation

1.4.2 Structural Health Monitoring Using GPS

The GPS is frequently demonstrated as being a valuable surveying-monitoring tool. The use of RTK-GPS has many applications, including its using to monitor the deflection of large structures. This information can be of vital importance to structural engineers in the evaluation of structural integrity ^[49; 59].

GPS is widely used to monitor volcano eruptions ^[18], crustal movements ^[19], vertical land movements ^[20; 30], landslides ^[21], earth structures ^[22], dams ^[23], buildings ^[24-25, 50], and bridges ^[2; 9-10; 16-17; 26-28; 32-38; 60].

The GPS offers several advantages over conventional terrestrial methods ^[62-64]. Intervisibility between stations is unnecessary, thus allowing greater flexibility in the selection of station locations than in the terrestrial geodetic surveys. Measurements can be taken during night or day, under varying weather conditions, which makes GPS measurements economical. With the recently developed rapid static positioning techniques, the time for the measurements at each station is reduced to a few minutes ^[47, 58].

The primary task of GPS surveying is to measure distances between 24 Department of Defense satellites in known orbits about 20,000 km above the earth and locations on the earth. Once distances have been measured, the coordinates of positions on the earth are calculated by triangulation ^[12]. Distances are measured based on the amount of time required for an electromagnetic GPS signal to travel from the satellites to ground-based antennas and receivers. Antennas collect the satellite signal and convert the electromagnetic waves into electric currents that can be recorded by the receiver ^[61, 68]. There are two main GPS surveying methods, kinematics and static surveying. In kinematics applications, receivers are in motion during the measurement period and real-time positioning solutions are available based on the pseudorange observable. In static applications, receivers are stationary for long-measurement periods (generally > 30 minutes) and both pseudorange and carrier-phase data are post-processed for precise positioning solutions ^[78]. Rapid-static applications are the same as static techniques except that occupation times are short, generally ranging from 5 to 20

minutes, and post-processing relies on code and carrier phase observations [78].

The type and accuracy of positioning in kinematics and static surveying is dependent on the number of receivers available [12, 78]. There are two types of positioning, single point and relative. Single-point positioning is the determination of a ground position using one receiver and observable from one or more satellites [73]. Single-point positioning relies on the pseudorange observable. The accuracy of the single-point positioning increases with the number of satellites available. Relative positioning is the determination of a ground position using two or more receivers and two or more satellites. Relative positioning determines the precise vector (baseline) between receiver positions. When the coordinates of one of the receiver positions is known, that receiver is referred to as a base station, and the known coordinates and baseline can be used to determine the precise coordinates of the unknown points [73].

The GPS receiver records raw data on a 24-hour basis. The measurements are stored in the computer of the system and these are available to surveyors or other users, working with GPS in the area of observations. Then, they can use these GPS measurements for post-processing positioning computations.

The accuracy of GPS relative positioning depends on the distribution (positional geometry) of the observed satellites and on the quality of the observations. There are several sources of errors contaminating the GPS measurements.

Different types of errors affect GPS relative positioning in different ways. Some of the errors may have a systematic effect on the measured baselines producing significant scale errors and rotations. Due to the changeable geometrical distribution of the satellites and the resulting changeable systematic effects of the observation errors, repeated GPS surveys for the purpose of monitoring deformations can also be significantly influenced (up to a few ppm) by scale and rotation errors which, if undetected, may contaminate the derived deformation parameters leading to a misinterpretation of the behavior of the deformable body [59].

With GPS, an array of antennae is positioned at selected points on the structure and on remote stable monuments as opposed to using reflectors and EDM. The baselines between the antennae are formulated to monitor differential movement. The relative precision of the measurements is on the order of +5 mm over distances averaging between 5 and 10 km. Formulations can be determined continuously 24 hours a day, depending on GPS constellation availability. Once a deformation monitoring system has been set up using GPS, it can be operated unattended and is relatively easy to maintain [47].

However, as in any deformation monitoring application, the design of the optimal GPS monitoring system requires an understanding of the expected deformation signal. Depending on the application and accuracy requirements, monitoring strategies can be varied from continuous collection of data recorded by permanently installed GPS receivers to sporadic occupation of monitoring points. Permanent GPS networks offer the highest accuracies and temporal resolution [5-8]. In addition, setup errors are minimized, as the requirement for the GPS antenna to be manually centered over the point of interest at the beginning of each occupation is eliminated. The disadvantage of continuous monitoring is the limited spatial resolution of the network of deforming point primarily due to the high cost of establishing such networks (a geodetic quality GPS receiver, antenna and communication link is required in perpetuity at each point) [58].

The results of the refer [56] shows that they arrived demonstrate the following points:

1- Concrete dams are not well suited for GPS-based monitoring operations. For these types of dams, conventional surveying techniques, and other surveying techniques, will continue to be used for the collection of information on surface movements.

2- GPS has the potential to provide accurate, economically viable dam surface monitoring systems. However, for this type of application, the technology is still in its infancy and 'off the shelf' systems cannot achieve the accuracies for most dam monitoring requirements.

3- It must be stressed, however, the success of any GPS monitoring

regime depends strongly on the observing environment and this varies greatly from site to site.

4- GPS offers the Geotechnical engineer another useful option for dam monitoring and GPS should be seen as a potentially useful tool for many dam environments.

Although GPS is a good monitoring technique, but it has some limitations, which ^[78]:

1- GPS observations require clear visibility to the sky, power and data links for GPS receivers

2- GPS signals can be affected by existing structures that reflect incoming GPS signals resulting in a condition known as multi-path.

Over the past 15 years, there has been a significant progress in the development of new methods for the geometrical and physical analyses of deformation surveys ^[46]. Associations and organizations have been leading in the developments, particularly in the areas of integrated geometrical analysis of structural deformations and combined integrated analysis. Therefore, the general worldwide use of the geometrical analysis methods is still poor, including even the basic analysis of geodetic monitoring networks. So a flexible surveying technique is needed to monitor the structural deformation of the ordinary and smart structures and make the process of measurements easier and accurate.

1.5 GPS signal processing

Signal processing refers to techniques for manipulating a signal to minimize the effects of noise, to correct all kinds of unwanted distortions or to separate various components of interest. Most signal processing algorithms include the design and realization of filters. A filter can be described as a system that transforms signals. System theory provides the mathematical background for filter design and realization. A filter as a system has an input and an output, where the output signal $y(t)$ is modified with respect to the input signal $x(t)$ (Figure 1.6). The signal transformation is often called convolution or, if filters are applied, filtering. However, many applied processes resemble analog filters that act over a range of spatial dimensions,

which presented as follow.

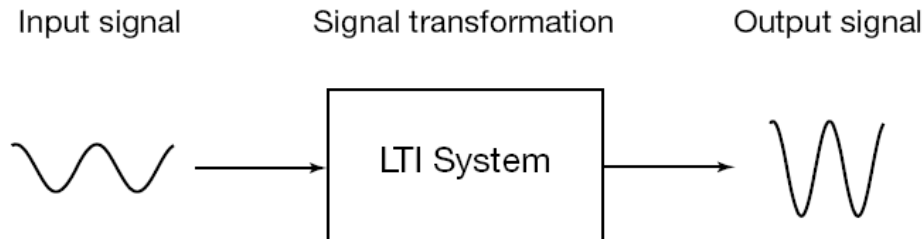


Figure 1.6 Schematic of a linear time-invariant (LTI) system. The input signal is transformed into an output signal.

1.5.1 Kalman Filter (KF)

The celebrated Kalman filter (KF) rooted in the state-space formulation of linear dynamical systems, and provides a recursive solution to the linear optimal filtering problem. It applies to stationary as well as non-stationary environments. The solution is recursive in that each updated estimate of the state is computed from the previous estimate and the new input data, so only the previous estimate requires storage. In addition to eliminating the need for storing the entire past observed data, the Kalman filter is computationally more efficient than computing the estimate directly from the entire past observed data at each step of the filtering process. In this chapter, we present an introductory treatment of Kalman filters to pave the way for their application in subsequent chapters of the thesis. We have chosen to follow the original paper by Kalman^[91, 123, 131] for the derivation; see also the books by Grewal and Andrews^[92]. The Kalman filtering problem, namely, the problem of jointly solving the process and measurement equations for the unknown state in an optimum manner may now be formally stated as follows:

* Use the entire observed data, consisting of the vectors $[y_1 \ y_2 \ \dots \ y_k]$, to find for each $k \geq 1$ the minimum mean-square error estimate of the state x_i . The problem is called filtering if $i = k$, prediction if $i > k$, and smoothing if $1 \leq i < k$.

Table 1.2 Summary of the Kalman filter

State-space model

$$X_{k+1} = F_{k+1,k} X_k + W_k$$

$$y_k = H_k X_k + V_k$$

Where W_k and V_k are independent, zero-mean, Gaussian noise processes of covariance matrices Q_k and R_k , respectively, y_k is the observable at time k and H_k is the measurement matrix, $F_{k+1,k}$ is the transition matrix taking the state X_k from time k to time $k+1$.

Initialization: For $k = 0$, set

$$X^{\wedge}_0 = E[X_0]$$

$$P_0 = E[(X_0 - E[X_0])(X_0 - E[X_0])^T]$$

Computation: For $k = 1; 2; \dots$, compute:

State estimate propagation

$$X_0^- = F_{k,k-1} X_0^-$$

Error covariance propagation

$$P_k^- = F_{k,k-1} P_{k-1} F_{k,k-1}^T + Q_{k-1}$$

Kalman gain matrix

$$G_k = P_k^- H_k^T [H_k P_k^- H_k^T + R_k]^{-1}$$

State estimate update

$$X_k^{\wedge} = X_k^- + G_k (y_k - H_k X_k^-)$$

Error covariance update

$$P_k = (I - G_k H_k) P_k^-$$

1.5.2 Adaptive Filter (AF)

An adaptive filter used for noise suppression is a dual input, closed-loop, adaptive feedback system. The operation of such an adaptive filter involves two basic processes:

1) A filtering process to produce an output in response to an input sequence.

2) An adaptive process for the control of adjustable parameters used in the filtering process. In the present application the dual-inputs to the adaptive filter are the primary input $d(n)$ and the reference input $x(n)$, which have sample size (vector length) N .

The primary input $d(n)$ consists of the desired signal of interest $s(n)$ (for example, bridge deformation) buried in (or contaminated by) multipath noise $x'(n)$, i.e.

$$d(n) = s(n) + x'(n) \quad (1.3)$$

The reference input $x(n)$ supplies multipath noise alone. In order to obtain a relatively noise-free signal using the adaptive filter output, $s(n)$, $x'(n)$, and $x(n)$ have to satisfy the following conditions:

1) The signal and noise in the primary input are uncorrelated with each other, i.e.,

$$E[s(n)x'(n-k)] = 0 \quad n, k = 0, \dots, N-1 \quad (1.4)$$

2) The noise in the reference input is uncorrelated with the signal $s(n)$, but is correlated with the noise component of the primary input $x'(n)$, i.e.,

$$E[s(n)x(n-k)] = 0 \quad n, k = 0, \dots, N-1 \quad (1.5)$$

$$\text{And,} \quad E[x(n)x'(n-k)] = p(k) \quad n, k = 0, \dots, N-1 \quad (1.6)$$

where $p(k)$ is an unknown cross-correlation for lag k .

The Finite-duration Impulse Response (FIR) filter is employed in this application due to its versatility and ease of implementation.

To minimize the mean square estimation error (MSE), the tap-weights of the FIR filter are determined from the relation ^[93, 123]:

$$\sum_{l=0}^{M-1} \hat{w}_l(n) r_{XX}(i-l) = 2r_{dX}(i) \quad i = 0, \dots, M-1 \quad (1.7)$$

This yields the set of linear equations that generate the optimum filter coefficients at time n . To solve the equations, both the auto-correlation sequence $\{r_{XX}(i)\}$ of the reference sequence $\{x(n)\}$ and the cross-correlation sequence $\{r_{dX}(i)\}$ between the primary sequence $\{d(n)\}$ and the reference sequence $\{x(n)\}$ are required.

The structural deformation $s(n)$ is indeed part of the error signal $e(n)$, and the noise component in the adaptive filter output is $x'(n) - y(n)$, as indicated in Equation 1.3.

While $s(n)$ is essentially unaffected by the filter, minimizing E is equivalent to minimizing the output noise $x'(n) - y(n)$. Therefore, the signal-to-noise ratio of the output signal is maximized. There are two special cases to be considered when applying the adaptive filter:

* The adaptive filtering is perfect when $y(n) = x'(n)$ and in this case the system output is noise-free.

* The adaptive filtering will be switched off automatically, as can be seen from Equation 1.7, when the reference signal $x(n)$ is completely uncorrelated with both the signal $s(n)$ and noise component $x'(n)$ of the primary signal $d(n)$, i.e., $E[d(n)x(n-k)] = 0$ for $n, k = 0, \dots, N-1$. In this case, the primary signal is left intact and the output signal-to-noise ratio remains unchanged.

As indicated in Equation 1.7, in order to solve the equations, both the auto-correlation sequence $\{r_{xx}(i)\}$ of the reference sequence $\{x(n)\}$ and the cross-correlation sequence $\{r_{dx}(i)\}$ between the primary sequence $\{d(n)\}$ and the reference sequence $\{x(n)\}$ have to be calculated. This is almost impossible for real-time applications. Therefore the least-mean-square (LMS) algorithm has been introduced as an alternative computational method to adaptively adjust the coefficients (weights) of an FIR filter, $\hat{w}_i(n)$, as in the following equation (tap-weight adaptation):

$$\hat{w}_i(n) = \hat{w}_{i-1}(n) + \mu e(n)x(n-i) \quad (1.8)$$

where μ is the step-size parameter, $i = 0, \dots, M-1$ and $n = 0, \dots, N-1$.

It has been shown that the LMS algorithm expressed in Equation 1.8 can minimize the sum of squared errors, as in the case of Equation 1.7. Evidence has also been presented on the model-independence, and hence robust performance of the LMS algorithm ^[84, 92], making the LMS algorithm the most widely known and implemented of adaptive algorithms. However, special attention has to be paid to two closely related issues: the choice of suitable value for the step-size parameter μ , and the filter length M .

1) It is important to select an appropriate μ which controls the rate of convergence of the LMS algorithm to the optimum solution. The larger the μ selected, the faster the convergence. However, too large a value of μ may

result in the LMS algorithm becoming unstable. To ensure stability, μ should be in the range ^[93]:

$$0 < \mu < \frac{1}{20M p_x} \quad (1.9)$$

where M is the length of the adaptive FIR filter and p_x is the power of the reference signal, which can be approximated by:

$$p_x \approx \frac{1}{M+1} \sum_{n=0}^{N-1} x^2(n) = \frac{r_{xx}(0)}{M+1} \quad (1.10)$$

where $r_{xx}(0)$ is the auto-correlation function of the reference sequence for zero lag.

2) The filter length (i.e., the number of independently adjusted parameters in the filter) should be selected so that the filter best models the regular features of a set of input data.

When the FIR filter and the adaptive algorithm are integrated, an adaptive filter, as shown in Figure 1.7, is obtained. In the next chapter, applying the AF to multipath mitigation and deformation determined.

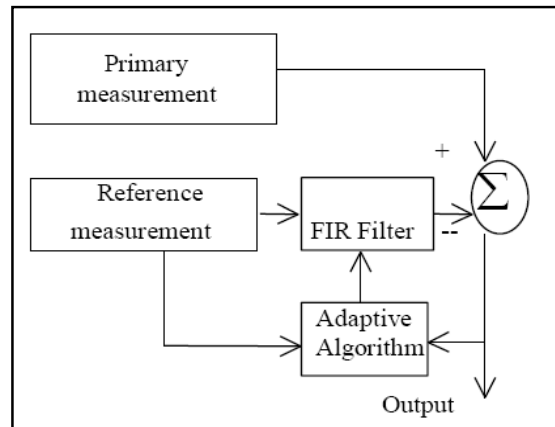


Figure 1.7 Adaptive filter configurations.

1.5.3 Parametric least square method

This method of adjustment makes used observation equations, where observables are expressed as a function of some or all of the parameters, in

the general form $l=f(X)$. To satisfy this relation, actual observations need to be adjusted ^[70]. The linearization of the relation is performed about an approximate set of parameters X_0 .

$$\begin{aligned}
 l-V &= f(X_0) \\
 l-V &= f(X_0 + \delta X) \\
 l-V &= f(X_0) + H\delta X \\
 (l-f(X_0)) - V &= H\delta X
 \end{aligned} \tag{1.11}$$

Where: δX are the corrections to the approximate parameters and H is the design matrix containing the partial derivatives of the observations with respect to the parameters. The expression in brackets is the approximate residual, and is denoted by V_0 . The variance-covariance matrix Q_{ll} of the observations is assumed known. As V_0 differs from l only by a constant, it has the same stochastic behavior. The computational procedure therefore is:

$$V_0 - V = H\delta X \quad \text{with weight matrix } P = Q_{ll}^{-1} \tag{1.12}$$

Solution for the parameters:

$$\delta X^{\wedge} = (H^T P H)^{-1} H^T P V_0 \tag{1.13}$$

With variance covariance matrix of parameters:

$$Q_{x^{\wedge}x^{\wedge}} = (H^T P H)^{-1} \tag{1.14}$$

In all applications on this thesis, the obtained results from KF method were used in the PLS analysis method.

1.5.4 Wavelet transform processing

Consequently, wavelet analysis has recently been considered for damage detection and structural health monitoring (SHM). It provides a powerful tool to characterize local features of a signal. Unlike the Fourier transform, where the function used as the basis of decomposition is always a sinusoidal wave, other basis functions can be selected for wavelet shape according to the features of the signal. The basis function in wavelet analysis is defined by two parameters: scale and translation. This property leads to a multi-resolution representation for non-stationary signals. As mentioned before, a basis function (or mother wavelet) is used in wavelet analysis. For a wavelet of order N , the basis function can be represented as ^[123]:

$$\psi(n) = \sum_{j=0}^{N-1} (-1)^j c_j (2n + j - N + 1) \quad (1.15)$$

where c_j is coefficient. The basis function should satisfy the following two conditions ^[11-12; 77]: The basis function integrates to zero, i.e.

$$\int_{-\infty}^{\infty} \psi(t) dt = 0 \quad (1.16)$$

It is square integral or, equivalently, has finite energy, i.e.

$$\int_{-\infty}^{\infty} |\psi(t)|^2 dt < \infty \quad (1.17)$$

Equation 1.16 suggests that the basis function be oscillatory or have a wavy shape. Equation 1.17 implies that most of the energy in the basis function is confined to a finite duration.

The important properties of basis functions are ‘orthogonality’ and ‘biorthogonality’. These properties make it possible to calculate the coefficient very efficiently. There is no redundancy in the sense that there is only one possible wavelet decomposition for the signal being analyzed. However, not all basis functions have these properties. A frequently mentioned term in the definition of a basis function is ‘compact support’, which means that the values of the basis function are non-zero for finite intervals. This property enables one to efficiently represent signals that have localized features.

The fast Fourier transform (FFT) is a perfect tool for finding the frequency components in a signal. A disadvantage of the FFT is that frequency components can only be extracted from the complete duration of a signal ^[77;85;131]. The frequency components are obtained from an average over the whole length of the signal. Therefore it is not a suitable tool for a non-stationary signal such as the impulse response of cracked beams, vibration generated by faults in a gearbox, and structural response to wind storms, just to name a few. These types of problems associated with FFT can be resolved by using wavelet analysis.

The most standard approach to analyze a signal with time-varying frequency content is to split the time-domain signal into many segments, and then take the Fourier transform of each segment. The Fourier Transform (Equation 1.18) was first adapted and define $S(t, f)$ as follow. Consider a signal $x(t)$, and assume it is stationary when seen through a window $g(t)$ of limited extent, centered at time location τ . The FT (Equation 1.18) of the windowed signals $x(t)g^*(t-\tau)$ yields the Short-Time Fourier Transformation (STFT).

$$X(f) = \int_{-\infty}^{+\infty} x(t)e^{-2j\pi ft} dt \quad (1.18)$$

$$\text{STFT}(\tau, f) = \int x(t)g^*(t-\tau)e^{-2j\pi ft} dt \quad (1.19)$$

Which maps the signal into two-dimensional function in a time-frequency plane (τ, f). Gabor originally only defined a synthesis formula, but the analysis given (Equation 1.19) follows easy^[77].

The main idea of Discrete Wavelet Transformation (DWT) is the same as that of Continues Wavelet Transformation (CWT)^[77; 91-93]. While the CWT requires much calculation effort to find the coefficients at every single value of the scale parameter, DWT adopts dyadic scales and translations (i.e. scales and translations based on powers of two) in order to reduce the amount of computation, which results in better efficiency of calculation. Filters of different cutoff frequencies are used for the analysis of the signal at different scales. The signal is passed through a series of high-pass filters to analyze the high frequencies, and through a series of low-pass filters to analyze the low frequencies.

As opposed to the CWT where only a wavelet function is used, in DWT a scaling function is used, in addition to the wavelet function. These are related to low-pass and high-pass filters, respectively^[77].

1.6 Geometrical monitoring models

In the monitoring process, Armenakis^[98] summarized the methods in two types; which are physical and geometrical. The categories of these methods are illustrated in^[98]. Physical methods are used to measure – usually

unidimensional-relative displacements using various linear mechanical instruments in contact with the object. Geometric methods are capable of monitoring both relative and absolute movements with respect to a given reference datum. These methods range from photogrammetric approaches to conventional- and satellite geodesy techniques.

1.6.1 Plane Monitoring Model

The following derived equation of plane will be accurate position of the surface. The equation of plane in three dimensions can be written in the form:

$$aX + bY + cZ + d = 0 \quad (1.20)$$

Where:

a, b and c are unknown parameters of accurate position of the surface.

The unknown parameters can be calculated by following equation ^[107]:

$$\begin{aligned} a &= Y_1 (Z_2 - Z_3) + Y_2 (Z_3 - Z_1) + Y_3 (Z_1 - Z_2) \\ b &= Z_1 (X_2 - X_3) + Z_2 (X_3 - X_1) + Z_3 (X_1 - X_2) \\ c &= X_1 (Y_2 - Y_3) + X_2 (Y_3 - Y_1) + X_3 (Y_1 - Y_2) \\ d &= -X_1 (Y_2 Z_3 - Y_3 Z_2) - X_2 (Y_3 Z_1 - Y_1 Z_3) - X_3 (Y_1 Z_2 - Y_2 Z_1) \end{aligned} \quad (1.21)$$

Where:

(X_1, Y_1, Z_1) , (X_2, Y_2, Z_2) , (X_3, Y_3, Z_3) are the coordinates of un-deformation plane of points 1, 2 and 3 as shown in Figure 1.8.

The monitoring for the plane was calculated by the parameters of unloaded case and then calculation of the deformation loaded plane as the following equation:

$$\Delta_i = \frac{|aX_i + bY_i + cZ_i + d|}{\sqrt{a^2 + b^2 + c^2}} \quad (1.22)$$

Where:

Δ_i is the deformation value of plane i relative to the un-deformed plane area. This value is perpendicular on the un-deformed plane as shown in Figure 1.8. (a, b, c, d) is the parameters for the un-deformed plane, and (X_i, Y_i, Z_i) is the monitoring coordinate of the movement point i.

The SD of the deformation plane was calculated by the error propagation as the following equation:

$$\sigma_{\Delta}^2 = \left(\frac{\partial \Delta}{\partial a}\right)^2 \sigma_a^2 + \left(\frac{\partial \Delta}{\partial b}\right)^2 \sigma_b^2 + \left(\frac{\partial \Delta}{\partial c}\right)^2 \sigma_c^2 + \left(\frac{\partial \Delta}{\partial d}\right)^2 \sigma_d^2 + \left(\frac{\partial \Delta}{\partial X}\right)^2 \sigma_X^2 + \left(\frac{\partial \Delta}{\partial Y}\right)^2 \sigma_Y^2 + \left(\frac{\partial \Delta}{\partial Z}\right)^2 \sigma_Z^2 \quad (1.23)$$

To determine the deformation values of monitoring points in X-direction and Y-direction were used the plane 2 and plane 1 respectively as shown Figure 1.8.a.

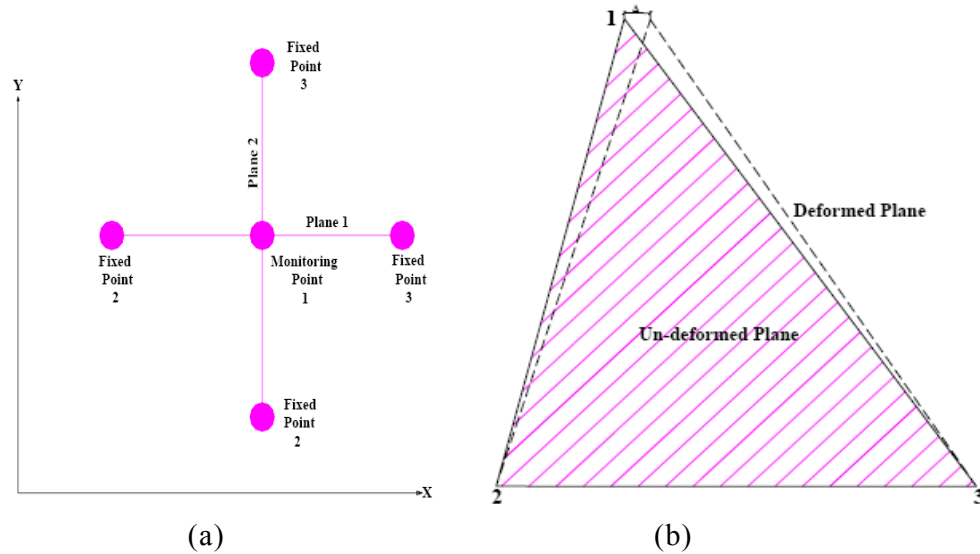


Figure 1.8 The geometry plane deformation monitoring (a) plan, (b) elevation

1.6.2 Polar Coordinates Monitoring Model

The polar coordinates (PC) is a two-dimensional coordinate system in which each point on a plane is determined by an angle and a distance. This monitoring method is depended on the assumed that the origin of the earth is a fixed point to monitoring the rover station point. Figure 1.9 shows the PC system for the study bridge and the local axis of it. The following formula has been used to calculation the PC from the Cartesian coordinates system:

$$r_i = \sqrt{X_i^2 + Y_i^2} \quad i = 1, 2, \dots, n \quad (1.24)$$

$$S_i = \text{Tan}^{-1}\left(\frac{Y_i}{X_i}\right) \quad i = 1, 2, \dots, n \quad (1.25)$$

Where: (r_i, S_i) is the PC of point i and (X_i, Y_i) is the Cartesian coordinates of point i .

From this Figure can be calculated the movement and direction of the movement for the monitoring point as following:

$$\vec{d} = \vec{r}_2 - \vec{r}_1 \quad (1.26)$$

$$\angle dS = \angle S_1 - \angle S_2 \quad (1.27)$$

Where: r_1 and r_2 are the distance of PC, S_1 and S_2 are the angles of PC at time 1 and 2, d is the deformation of member and dS is the direction of deformation.

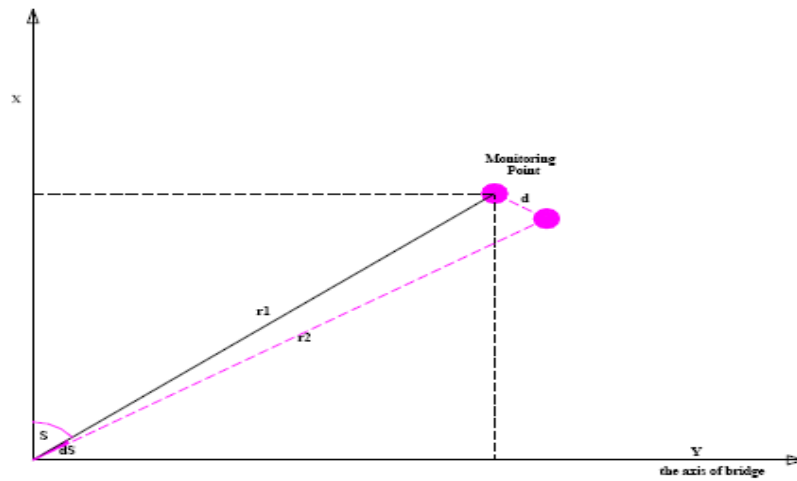


Figure 1.9 The geometry polar coordinates system

1.6.3 Span Length Monitoring Model

The load effects on the bridge affect the span length of bridge. The distance between the two towers of bridge can be calculated from the GPS positioning on the studied bridge. Figure 1.10 shows the effectiveness of traffic loads on top tower movement, as the same for other loads, which affected the tower but may by take another shape.

The distance between two observed points is calculated by the following equation:

$$d(i) = \sqrt{(X_i - X_j)^2 + (Y_i - Y_j)^2} \quad i = 1, 2, \dots, n, \text{ and } j = 1, 2, \dots, n \quad (1.28)$$

Where:

$d(i)$ is the span length between points i and j , and (X_i, Y_i) , (X_j, Y_j) are the coordinates of tower points i and j respectively.

So if the safe span of bridge is observed can be monitoring the span length from the different between the span length at any time observed and the main safe span.

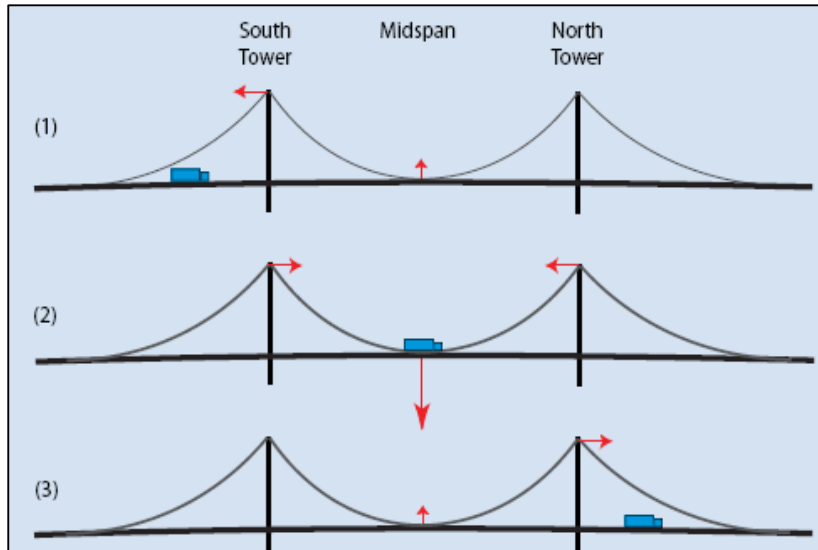


Figure 1.10 The geometry traffic loads affects on the deck and towers movement

Chapter 2 Bridge Movement Analysis Based on GPS Technique

2.1 Introduction

This chapter uses RTK-GPS monitoring system on the Yonghe Bridge, which was completed in 1987, closed in 2006 because cracks over mid span and re opened in 2007 after rehabilitation. After a year from reconstruction of it, cracks were pronounced 48.2 m far from the beginning abutment, southern tower and near mid span bridge. However, this chapter discusses and analyzes in detail the GPS observations of structural health monitoring system, which designed and implemented by the Research Center of Structural Health Monitoring and Control of Harbin Institute of Technology (HIT) to monitor loads and response of the bridge.

To determine the current operational safety and the cause of bridge cracks, its movements were observed under different stress factors such as wind speed, temperature change and traffic load. The observed X and Y-directions of bridge's towers were studied and described using processing and identification methodology.

2.2 Bridge Descriptions

One cable-stayed bridge is employed in this thesis. This bridge was constructed by pre-stressed concrete in December 1987 (Figure 2.1), closed in October 2006 because cracks over mid span and opened in August 2007 after rehabilitation. The whole bridge has four lanes with the total length of 510.00 meters, and main span of the bridge is 260.00 meters.

For safety assurance, a sophisticated long-term structural health monitoring system has been designed and implemented by the Research Center of Structural Health Monitoring and Control of Harbin Institute of Technology to monitor loads and response of the bridge (Figure 2.2).

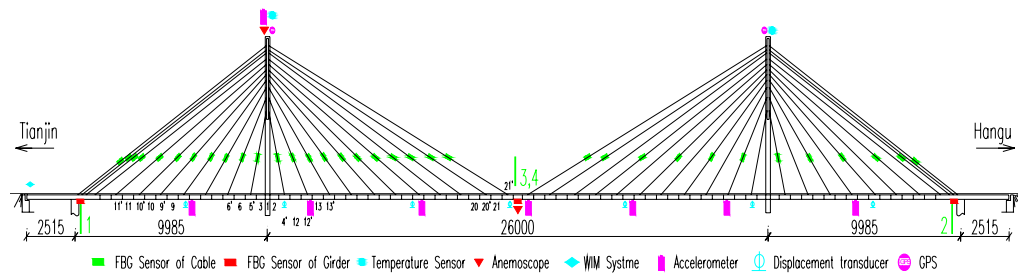


Figure 2.1 Elevation and system of health monitoring of the Bridge

The structural health monitoring system for the bridge comprises a data acquisition and processing system with a total of approximate 179 sensors, including accelerometers, strain gauges, displacement transducers, anemometers, temperature sensors, weight-in-motion sensors and three GPS's. The GPS was permanently installed on the two tower tops of the bridge and bank near the bridge, as shown in Figures 2.1 and 2.4.

Generally, for the cable-stayed bridges and other large-scale buildings, their inherent structure vibration has a lower frequency of 0.1–10 Hz due to their huge mass [74, 99].

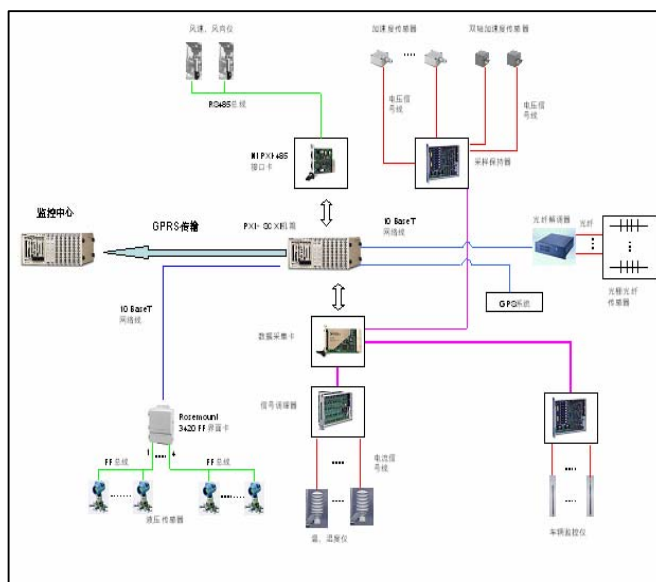


Figure 2.2 The structural health monitoring system of the bridge

2.3 GPS and Data Collection Information

To provide a continuous mapping of the bridge motion under loads, a kinematic GPS survey with data sampling rate of 20 Hz, receivers elevation angle are 13° , and at least 9 satellites were adopted as shown in Figure 2.3.

For these reasons, a setup of three GPS receivers are used: two on the top of the towers (Figure 2.1) and a third one is used as a reference station on stable ground near the bridge as shown in Figure 2.4, 2002 and 2001 denote northern tower (N.Tower) and southern tower (S.Tower), respectively. The positioning of the receivers is related to WGS84 as shown Figure 2.4.

The GPS observations are real time kinematic (RTK) with differential GPS (DGPS) system. The receivers are LEICA GMX902 antenna (24 channel L1/L2 code and phase, 20 HZ data rate, SmartTrack technology for high precision, solid and small, water resistance (IP67) anti vibration, accuracy of $1\text{mm} + 0.5\text{ppm}$ (horz.); $2\text{mm} + 1\text{ppm}$ (ver.)) and Spider 1.2 is used to pre-process the receivers data. The coordinate components for each observation epoch are derived (http://www.gnss.si/images_1/GMX902%20Flyer_en.pdf), as shown in Figure 2.5.

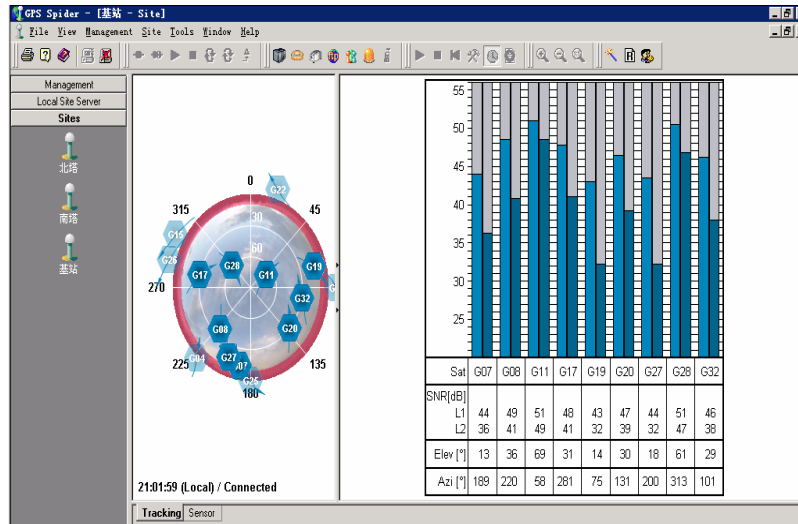


Figure 2.3 The number of satellite and elevation angle of receivers

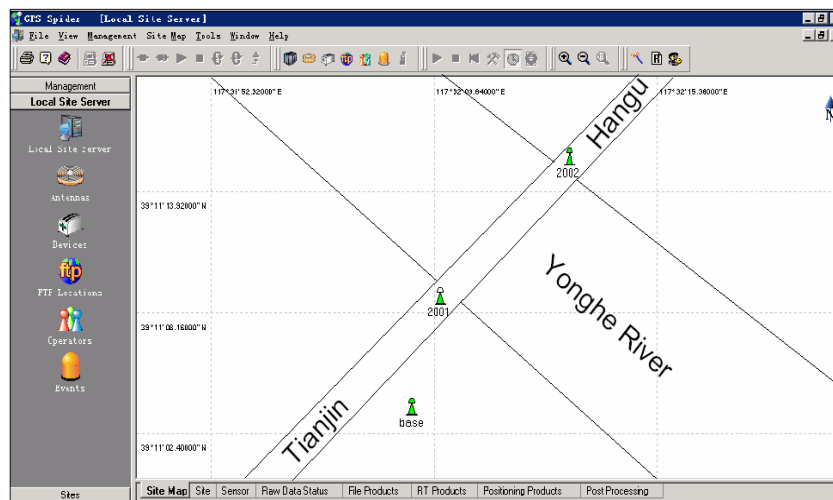


Figure 2.4 GPS Dynamic Monitoring Scheme

Hence, time sequences of positions for each station located on the bridge were generated. More over, hourly-based corresponding atmospheric data as well as traffic volume statistics were collected.

Transformation of the GPS observations from global coordinates to local coordinates of bridges is shown Figure 2.6.a . To transform the coordinates to

local axis the Bursa-Wolf transformation method was used. This transformation is given various names throughout the geodetic literature, such as three-dimensional similarity, three-dimensional conformal, seven-parameter transformation Helmert. This involves an origin shift in three dimensions, a rotation about each axis, and a change in scale, which is usually expressed in parts per million (ppm). The process can be simplified when using small axial rotations by producing a combined rotation matrix ^[29].

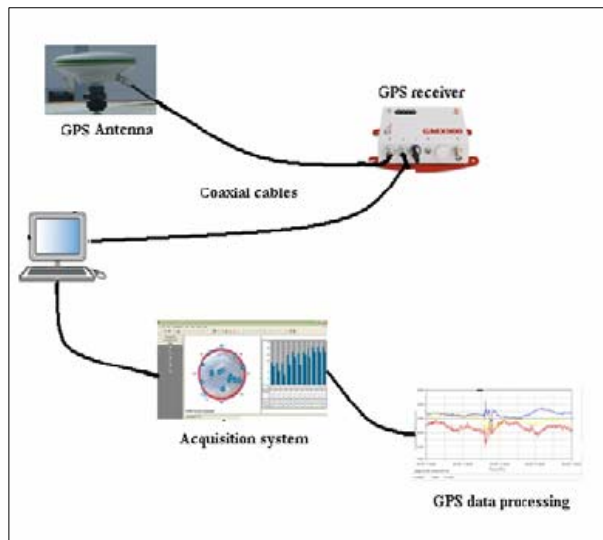


Figure 2.5 GPS network architecture

A local Bridge Coordinate System (BCS) was chosen for the analysis and evaluation procedures of the observations performed. In this coordinate system, the Y-axis shows the traffic direction (span direction), the X-axis shows the lateral direction and the Z-axis gives the vertical direction of the bridge (Figure 2.6). It was assumed that this coordinate system would be beneficial for the evaluation of performed observations, description of the movement of the structure and to allow a better interpretation of the analysis results as it is related to the movement directions of the structure.

Two-rover observation stations were considered along the bridge on the two bridge tower, every rover station is 24 hr observed, the number of data collection are 72000/hr, and each epoch is corrected with the base station. The GPS device must be set up carefully in order to give the appropriate data. Antenna settings must be checked and log on static mode must be turned on in tracking settings of

the GPS device. So, the base station is corrected then each epoch of observation is corrected relative to its related base station. The observation time of base station should be corrected when it is more than that of rover. When all the rover observations are corrected, the data would be compared depending on each epoch of observations ^[109]. GPS coordinates are formed in WGS84 format, which is considered as global degree format. The ellipsoidal coordinates (WGS84- Datum) of two towers are shown in Figure 2.6. Using Equation 2.1 ^[29], the local coordinates of bridge for the two stations were converted to Cartesian coordinates and the results are summarized in Table 2.1.

$$\begin{bmatrix} X \\ Y \\ Z \end{bmatrix}_T = M * \begin{bmatrix} 1 & +R_Z & -R_Y \\ -R_Z & 1 & +R_X \\ +R_Y & -R_X & 1 \end{bmatrix} * \begin{bmatrix} X \\ Y \\ Z \end{bmatrix}_S + \begin{bmatrix} dX \\ dY \\ dZ \end{bmatrix} \quad (2.1)$$

The parameters are commonly referred to define the transformation "from source coordinate system to local coordinate system", where by (X_S, Y_S, Z_S) are the coordinates of the point in the WGS84 and (X_T, Y_T, Z_T) are the coordinates of the point in the local coordinate system of the bridge. (dX, dY, dZ) : a Translation vector, to be added to the point's position vector in the source coordinate system in order to transform from source system to target system; also: the coordinates of the origin of world coordinate system in the target coordinate system. (R_X, R_Y, R_Z) : Rotations are also to applied to the point's vector. M: The scale correction to be made to the position vector in the source coordinate system in order to obtain the correct scale in the target coordinate system. $M = (1 + dS * 10^{-6})$, whereby dS is the scale correction expressed in parts per million (http://posc.org/Epicentre.2_2/Data Model/ Examples of Usage/eu_cs.html).

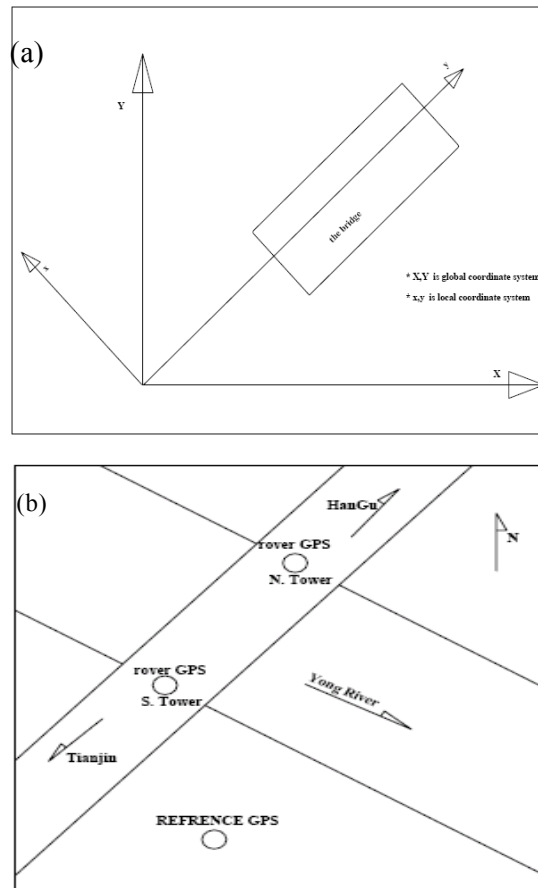


Fig. 2.6. The (a) global and local coordinate system and (b) layout of GPS positions of the bridge

Table 2.1 The local Cartesian coordinates of bridge towers:

Tower	X- coordinate	Y- coordinate
Southern	4337438.924	500401.024
Northern	4337438.925	500662.027

All values in (m)

2.3.1 Data Processing Strategy

Janssen, V ^[112] summarized the data processing as follows, depending on the type of movement expected in a deformation monitoring application, different data processing strategies can be used. If slow deformation at a constant rate is

expected, the data is usually processed in static sessions of a few hours to a few days in length, assuming no movement during the session. This is generally done in post-processing mode, as the deformation does not pose an imminent threat to surrounding structures or the population inhabiting the area. In this case parameters describing precise satellite orbits and polar motion, which are generally not available in real-time, can be used to improve the quality of the solution. This procedure is typically used for processing large scale, global networks in order to detect plate motions where a comparison of several campaigns is usually sufficient to derive the average rate of tectonic motion. However, if the deformational signal is expected to take place over a short period of time ' sudden deformation' and/or varies with time ' continues deformation', the sampling interval must be increased accordingly. This suggests the use of continuous GPS networks, using short static sessions, or epoch-by-epoch solutions. If the deformation can cause failure of the deforming body a real-time, epoch-by-epoch solution is desired in order to detect the deformation as soon as it occurs, to initiate warning and evacuation procedures.

In the case study of this research, bridge deformation monitoring is expected to be of a mixed nature. During periods of quiescence, the deformation will be slow, while increased applied loads will cause bridge movements of increasing magnitude. However, a real-time kinematic solution is preferred in order to detect movements on the deck and tower of bridge over a relatively short period.

2.4 Analysis the Tower Bridge Movement

This section discusses the analysis process of the GPS signals and the bridge tower movement. In addition the statistical analysis will discuss the reasons behind the bridge deck cracks.

2.4.1 Prediction and analysis of movements

In this section, GPS data collection time series were carried out from 11.00 AM to 2.00 PM local time on June 2007 to June 2008, where the traffic loads, temperature, and wind have more effects on the bridge. In this study, we select the south tower as a candidate for before. Study, and a comparison between the monthly data collection is performed to discuss the reasons behind the bridge

movements.

Figure 2.7 shows a sample of the observed environmental effects on the bridge tower and deck. These effects wind speed and wind direction.

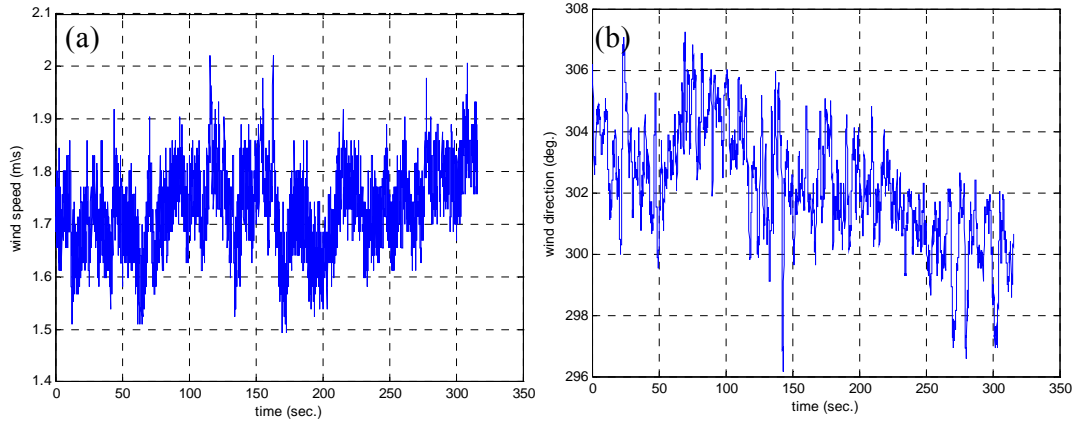


Figure 2.7 The sample of environment data observed (a) wind speed, (b) wind direction

The average minimum temperature in the bridge location is $-3\text{ }^{\circ}\text{C}$ in December and January whereas the average maximum temperature is $25\text{ }^{\circ}\text{C}$ in August. The minimum record temperature is $-13\text{ }^{\circ}\text{C}$ in January and maximum record temperature is $30\text{ }^{\circ}\text{C}$ in August.

$$\delta = \alpha \cdot \Delta T \cdot H \quad (2.2)$$

Table 2.2 Temperature-induced deflection of tower and deck

Property	Value
Coefficient of thermal expansion, α	$12 \times 10^{-6} / ^{\circ}\text{C}$
Maximum temperature	$30\text{ }^{\circ}\text{C}$
Minimum temperature	$-13\text{ }^{\circ}\text{C}$
Change in temperature, ΔT	$43\text{ }^{\circ}\text{C}$
Length of the tower, H	62.50 m
Length of the deck, L	260.00 m
Deflection in tower, δ	0.0323 m
Deflection in deck, δ	0.1342 m

As indicated in Table 2.2, the deflections in the deck and the two bridge towers due to temperature effects are not very large.

2.4.1.1 KF Method

Figures 2.8 and 2.9 show the deformation signals obtained for the south tower before and after KF processing in directions X & Y respectively.

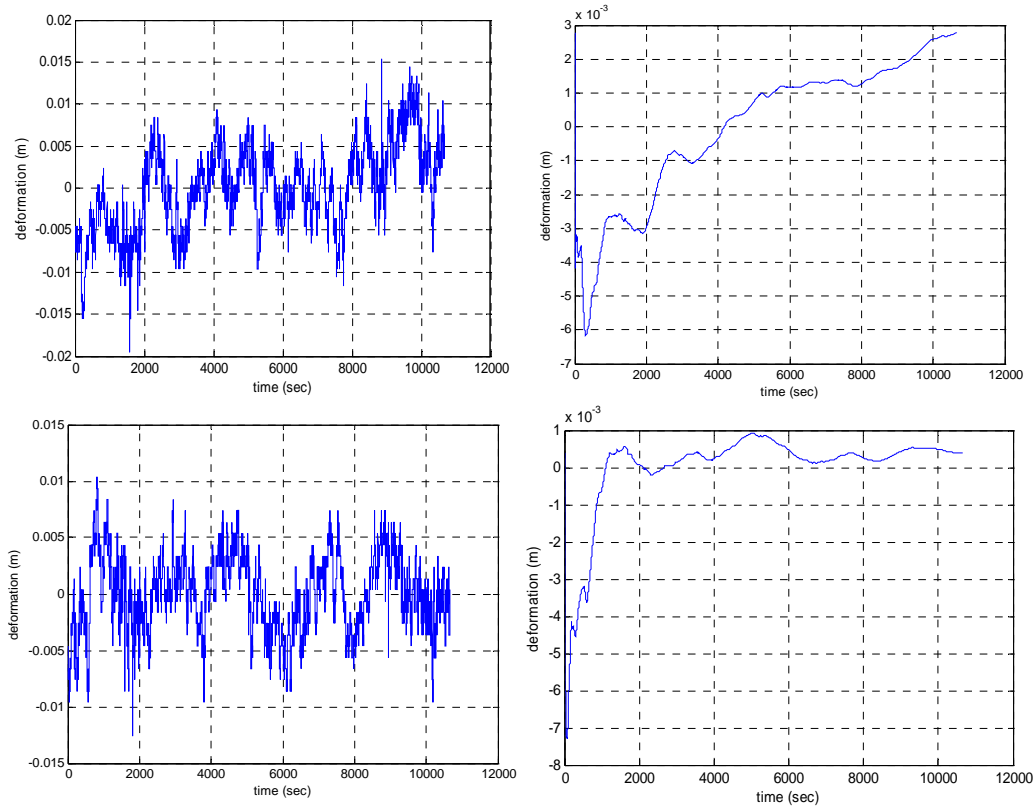


Figure 2.8 The time series of X (up) and Y (down)-direction for S. Tower (before and after KF) (1-8-2007)

From Figures (2.8 and 2.9), it was found that the amplitude of the GPS signals is abnormal. This indicates that the tower is unstable under the applied loads. Also the Figures indicate that the minimum and maximum ranges in the deformation X & Y-directions are 3.11 cm, 2.34 cm and 0.32 cm, 0.42 cm respectively. For these deformations, it was found that the standard deviations (SD) were 8.25 mm and 6.74 mm respectively.

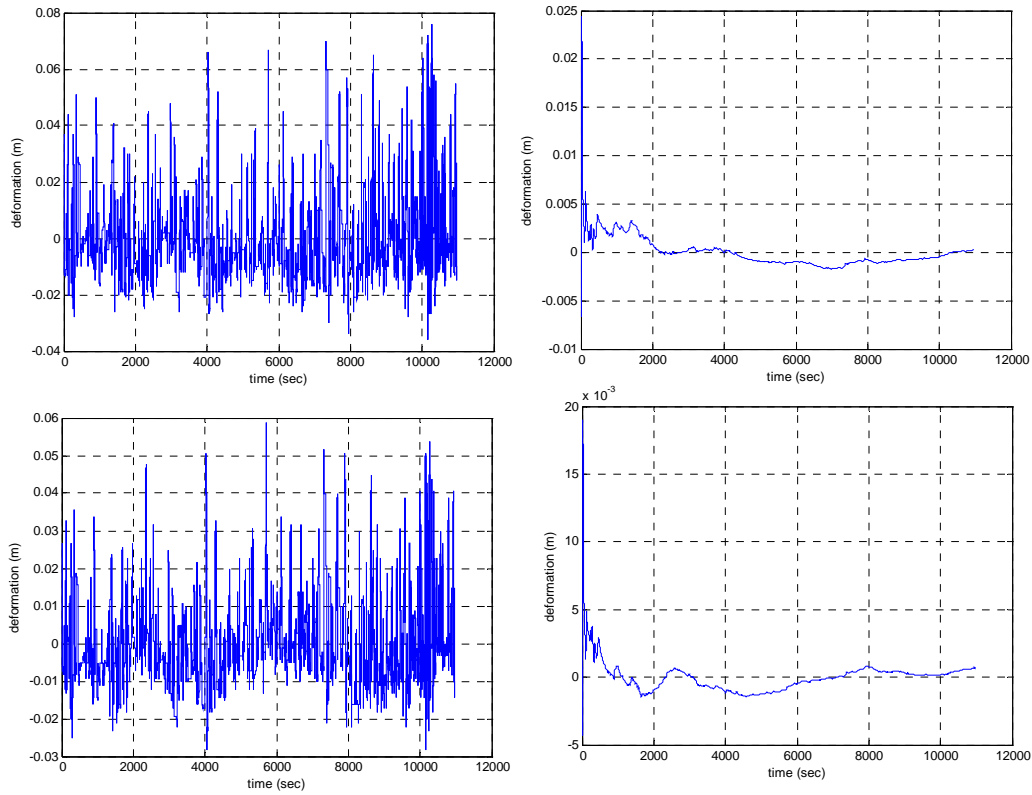


Figure 2.9 The time series of X (up) and Y (down)-direction for S. Tower (before and after KF) (1-6-2008)

2.4.1.2 PLS Method

The relationships between X & Y-coordinates deformations with respect to time are shown in Figures 2.10 and 2.11.

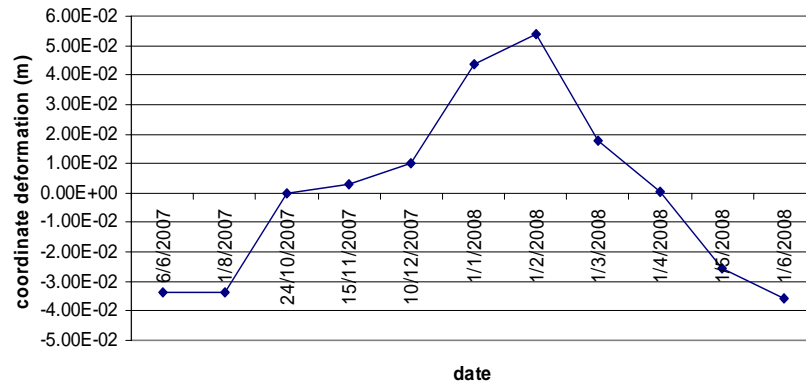


Figure 2.10 Corrected X coordinates deformation of S. Tower from PLS.

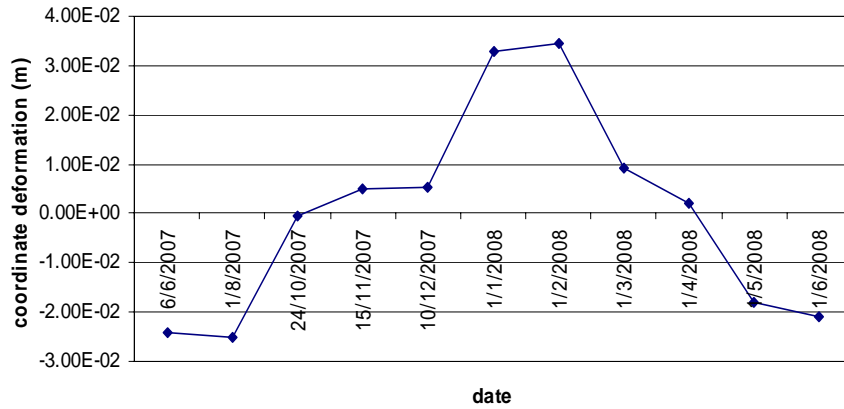


Figure 2.11 Corrected Y coordinate deformation of S. Tower from PLS.

From those Figures, it can be seen that after six months of bridge opening the X&Y directions deformations are 0.087 m and 0.058 m respectively. This can be attributed to the increase in applied traffic loads at mid span.

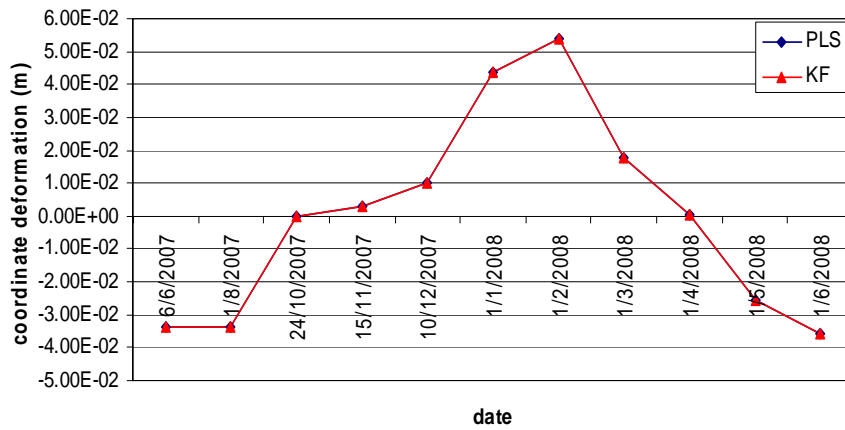


Figure 2.12 Corrected X coordinate deformation of S. Tower from KF and PLS.

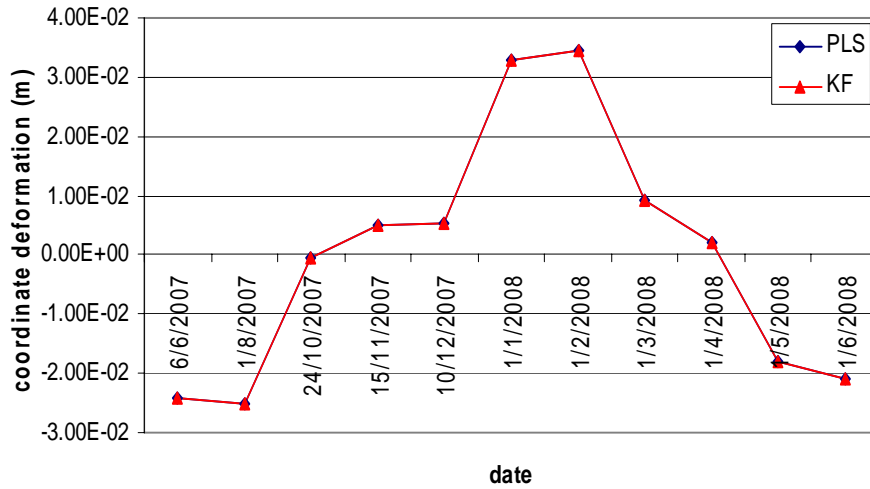


Figure 2.13 Corrected Y coordinate deformation of S. Tower from KF and PLS.

The results also reveals that the accurate coordinates deformation values using KF and PLS are much close (see Figures 2.12 and 2.13). For KF and PLS methods, it was found that the maximum SD in X-direction is 0.003230184 m and $6.95E^{-06}$ m, respectively, whereas the maximum SD in Y-direction is 0.000789298 m and $1.70E^{-06}$ m, respectively.

2.4.1.3 Statistical deformation analysis

SPSS statistical software (SPSS, 1999) ^[132] was used to determine the deformation. Deformation results were statistically analyzed with a 5% level of significance. Damage in the bridge tower has been determined using the similarity transformation approach cited in ^[100-101].

F-test statistical analysis has been adopted to find out the deformation in the tower. In this analysis, the deformation (d) for point i in Equation 2.3 was determined with respect to the p , which was assumed as reference point before bridge loading. Herein, it should be mentioned that all of these points were located on the same datum (c).

$$d = \begin{bmatrix} d_x \\ d_y \end{bmatrix} = \begin{bmatrix} x_c^i - x_c^p \\ y_c^i - y_c^p \end{bmatrix} \quad (2.3)$$

$$|D| = \sqrt{d^T d} \quad (2.4)$$

Whereas: T_J value for the selected point in two directions is computed as follows [90].

$$T_J = \frac{D_{1J}^T Q_{D1J}^{-1} D_{1J}}{2\sigma^2} \approx F(\alpha, 2, df) \quad (2.5)$$

$$\sigma^2 = \frac{(\sigma_1^2)(df_1) + (\sigma_2^2)(df_2)}{df} \quad (2.6)$$

Where:

D_{1J} , and Q_{D1J} are the displacement vector and cofactor matrix of each datum point J.

σ_1, df_1 are a posteriori variance factor and a degree of freedom in epoch 1.

σ_2, df_2 are a posteriori variance factor and a degree of freedom in epoch 2.

$df = df_1 + df_2$, sum of degrees of freedom of epochs 1 and 2.

Then, if $T < F$ the point isn't moved, and if $T > F$ the point is moved [46].
the results are shown in Table 2.3.

Table 2.3. The results of statistical test:

Monitoring Date	$dX=(X_i-X_1)$	F.Test	$dy=(Y_i-Y_1)$	F.Test	Note
1/8/2007	0.000245	N	0.001077	N	No. deformation
24/10/2007	0.033353	Y	0.023527	Y	deformation
15/11/2007	0.036710	Y	0.029160	Y	deformation
10/12/2007	0.043847	Y	0.029606	Y	deformation
1/1/2008	0.077324	Y	0.056974	Y	deformation
1/2/2008	0.087361	Y	0.058642	Y	deformation
1/3/2008	0.051392	Y	0.033368	Y	deformation
1/4/2008	0.034120	Y	0.026366	Y	deformation
1/5/2008	0.007859	N	0.006182	N	No. deformation
1/6/2008	0.002324	N	0.003199	N	No. deformation

Where

(X_1, Y_1) coordinates on 6 July 2007 (Datum).

(X_i, Y_i) coordinates on date i.

All values in (m)

From Table 2.3, it was found that the deformation values in the X-direction occurred on October 2007 to April 2008 varied between 0.033353 m and

0.034120 m, whereas, these values were found to be between 0.023527 m and 0.026366 m in the Y-direction. This is related to the bridge loading that opened on August 2007. It should be mentioned herein, that due to the traffic loads the S-tower has moved towards the bridge inside. Accordingly, the crack width happened on the Abutment is larger than that located on the mid span as shown in Figure 2.14. This is attributed to the weakened bond between the concrete and the steel bars.

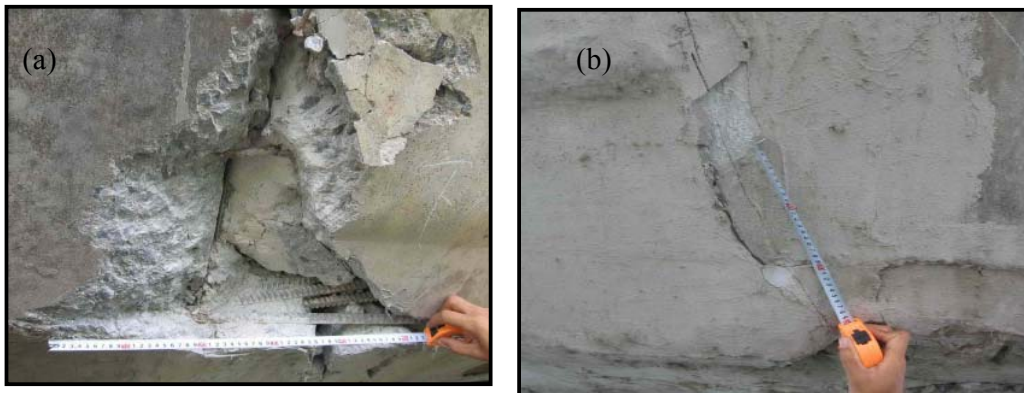


Figure 2.14 Cracks shape at (a) abutment and (b) mid span, respectively.

2.4.2 Filtering and deformation analysis

In this section the tower in one side of the Bridge (southern tower) and the tower on the another side (northern tower) were observed at the same time intervals, to make comparison between both bridge towers movements possible. The evaluation of the observations was performed using BCS and the movements observations with the time will be shown in subsequent figures.

2.4.2.1 Investigation of the loading effects on the tower movements

The Bridge was monitored in January 09 2008 from 12.00 PM to 1.00 PM. At this time, data collection is composed of wind, GPS, temperature and traffic, to study the environmental effects and traffic loads on the bridge tower movements. Figure 2.15 shows the original GPS signals with the linear fitting of it for two towers in two X and Y directions, respectively. In this Figure, it can be

seen that the linear normal residuals for the southern and northern towers in X and Y-directions are 1.3348, 1.0474, 1.4799 and 1.1284, respectively. As shown in the Figures and from the linear equation, it can be seen that the Y-direction slope parameters is greater than that in X-direction. This indicates that the Y-direction deformation increased with time monitoring, whereas from the Finite Element (FE) analysis, it is noted that the movement is in the opposite direction. Also, it can be seen that the peak signals are up and down at the southern and northern towers, respectively. This indicates that the movement of the south and the north towers is non-linear with the applied loads in during the monitoring time. Figure 2.16 shows the load and velocity traffic effects on the study of bridge at the same times as GPS signals are observed in Figure 2.15.

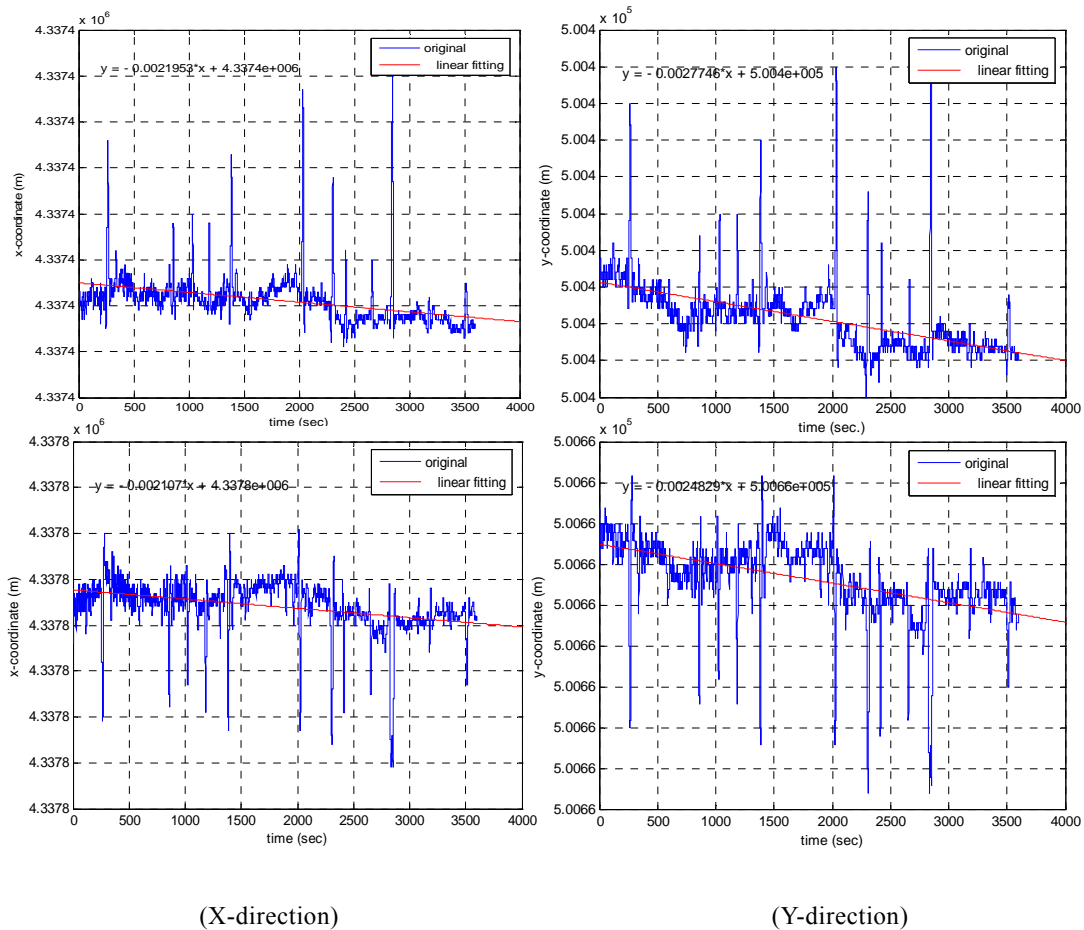


Figure 2.15 The GPS original signals and linear fitting for south (up) and north tower

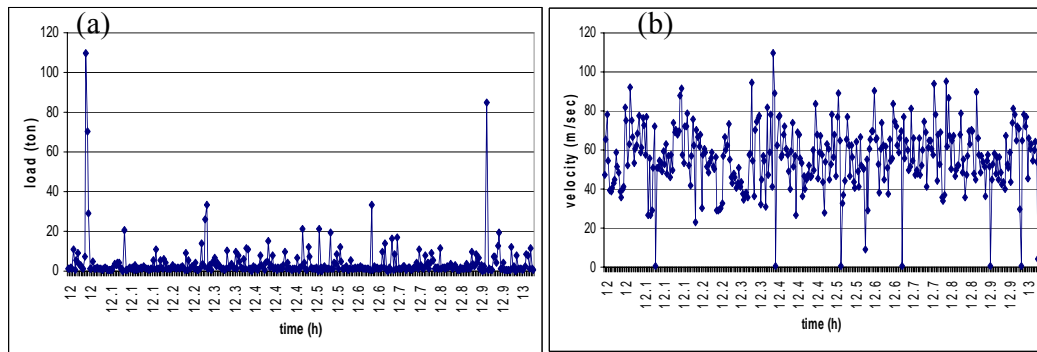


Figure 2.16 The (a) load and (b) velocity traffic effects

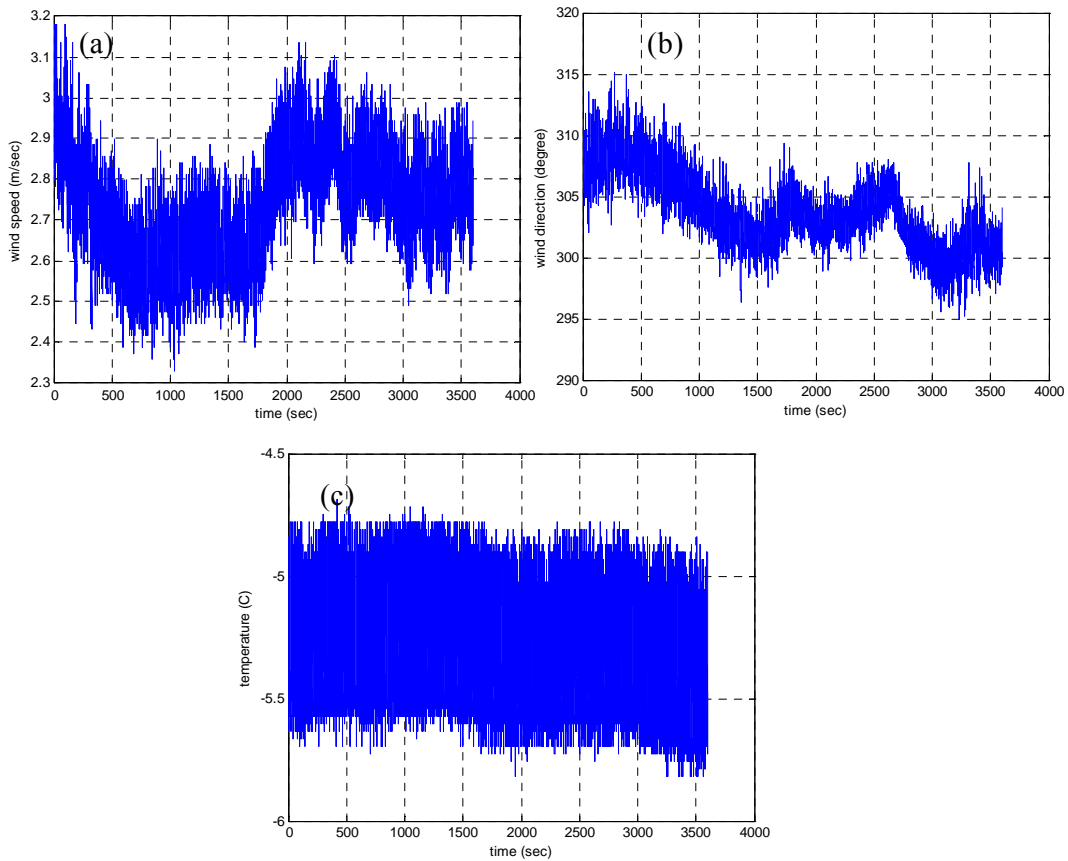


Figure 2.17 The environmental observation data (a) speed, (b) direction of wind and (c) temperature

From these Figures, it can be seen that the traffic loads and there velocities have effect on the towers movements. In addition, it can be found that the

maximum signal deformations in the two directions at the two towers are noticeable with loads and velocity increase, at 12.2 PM to 12.6 PM (750 to 2000 sec.). Figures 2.17.a and 2.17.b show the wind speed and direction, respectively. From these Figures and Figure 2.14, it can be seen that the mean wind speed and direction is 3.3 m/sec and 305° , respectively, approximately perpendicular on the Y-direction. Wind effects may be the reason behind for the X-direction deformation signals decrease at two towers, but actually, it was not the reason for Y-direction deformation signals increased. Figure 2.17.c shows the temperature effects on the towers bridge. From this Figure, it can be seen that the deformation due to the temperature is very small. The change in temperature is also very small (1°C). From these analyses, it can be concluded that traffic loads are the main reason behind bridge damage and the towers movements.

2.4.2.2 Analysis of the observed displacement

Figures 2.18 and 2.19 are shown time series residuals and the scatter residuals of each coordinates pair (X vs Y) at the northern and southern original GPS signals deformations, respectively. These signals were collected from June 2007 to June 2008. All observation data were collected from 11.00 AM to 12.00 PM local China time. Table 2.4 shows the correlation coefficient between the signals at two towers. The residuals are obtained through the Detrend code from Matlab of the positioning signals at each monitoring time.

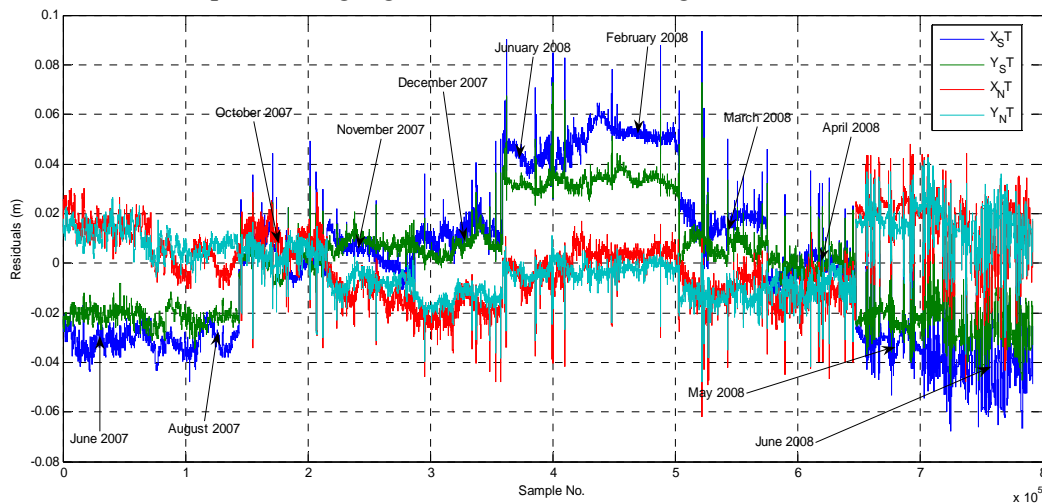


Figure 2.18 The time series original GPS data at north and south tower bridge

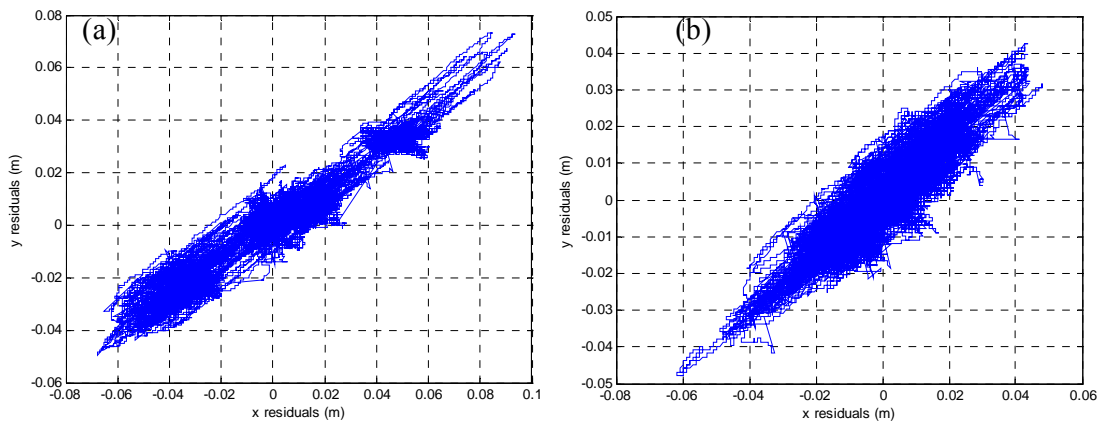


Figure 2.19 The residual of original GPS data at (a) south and (b) north tower bridge

Table 2.4 The correlation coefficient between the GPS signals:

	X_{ST}	Y_{ST}	X_{NT}	Y_{NT}
X_{ST}	1.00	0.9689	-0.3678	-0.5856
Y_{ST}		1.00	-0.3973	-0.3973
X_{NT}			1.00	0.8845
Y_{NT}				1.00

Where, the coordinates of the south and north towers are (X_{ST}, Y_{ST}) and (X_{NT}, Y_{NT}) , respectively.

From these Figures and Table 2.4, it can be seen that the residuals of the southern and northern towers in X and Y directions have similar approximately behavior, and the X and Y-directions correlation coefficient at the southern tower is 0.97, whereas at the northern tower it is 0.88. This indicates that the correlation between movements in two directions for the southern tower is stronger than the northern tower. On the other hand, it can be found that the correlations between the two movements of the towers are 0.39, 0.36, and 0.58 (Table 2.4); this reveals that the movements of the towers in the two directions are not dependent on each other, whereas the bridge was symmetrical (Figure 2.1). Also it can be seen that the drop between signals at the southern tower is very clear compared to the northern tower signals, and the deformation of the northern tower was clear from the start of the observations. That means that the northern tower movements occurred before load effects, this indicates that the

movements of northern tower is abnormal. Also, it can be found that the residuals for the southern tower (-0.60~ 0.80 and -0.40~0.60) are greater than those for the northern tower (-0.60~0.40 and -0.40~0.40) respectively in the two directions (Figure 2.19). And the three peaks residuals are shown in Figure 2.19.a. these indicate that the movements of southern tower is abnormal from October 2007 to the monitoring time end, and may be these movements had some effects on the bridge deck.

2.4.2.3 2D- Frequency time series analysis

To analyze the frequency signals, preprocessing should be first done. That is to minimize the noises and extract the useful signals. Kalman Filter is a strong tool to eliminate noise signals according to the noise characteristics in the kinematics models. The mathematical form of the KF consists of two independent models, the dynamic and measurement models. According to formulas of KF in chapter 1, assuming that the design matrices and the transition matrix are identity matrix and the covariance of observations are assumed equal weight whereas the standard deviations (SD) of the signals are not available. Moreover, the covariance matrix of the dynamic noise model was estimated from accelerometer data. The sample results show that noises can be effectively be removed and the useful signals can be extracted from original signals using KF as shown in Figure 2.20 for the two towers bridge. For the PLS method, it was assumed that the approximated value is the first observation for the KF time series signals and the observed model is ($y^*=Y^* +V$). The residuals and SD of the best positioning of tower were estimated by least square method (LSM) in Equations (1.12-1.14). The deformation calculated from the difference between the mean values of the original and KF signals, while for the PLS, it was calculated from difference between the best-estimated values. The unload case (June 2007, see Figure 2.20) was used as a datum for data monitoring. The movements and SD of those were calculated as shown in Figures 2.20, 2.21 and 2.22 for the southern and northern towers, respectively. From these Figures, it can be seen that the residuals between the original and KF signals are very clear.

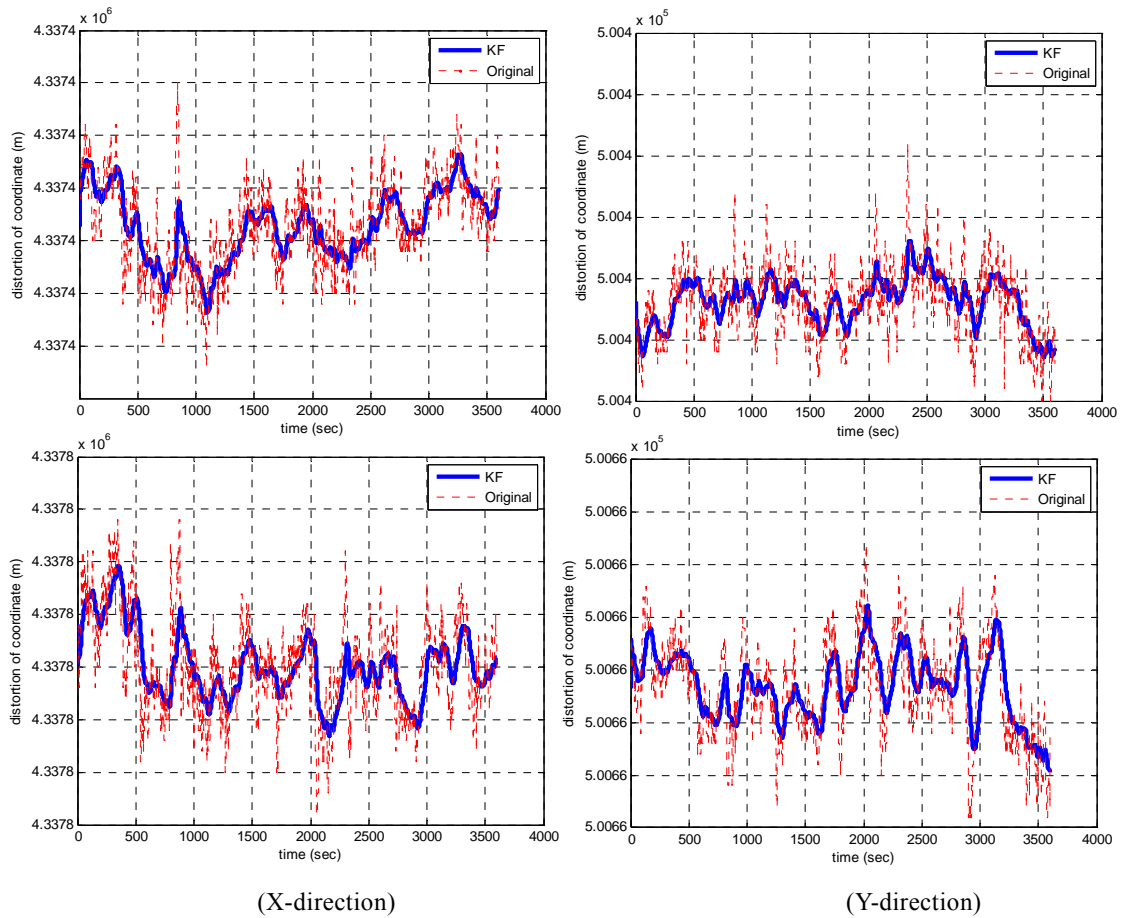


Figure 2.20 The GPS original and KF signals at south (up) and north towers

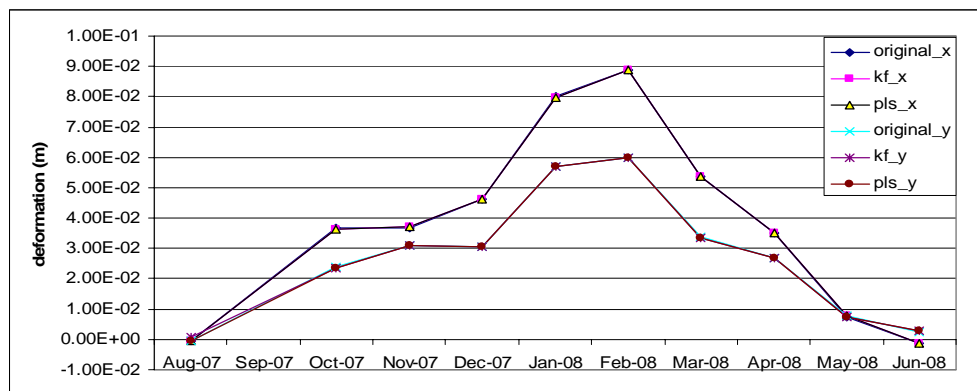


Figure 2.21 The deformation of south tower in two directions

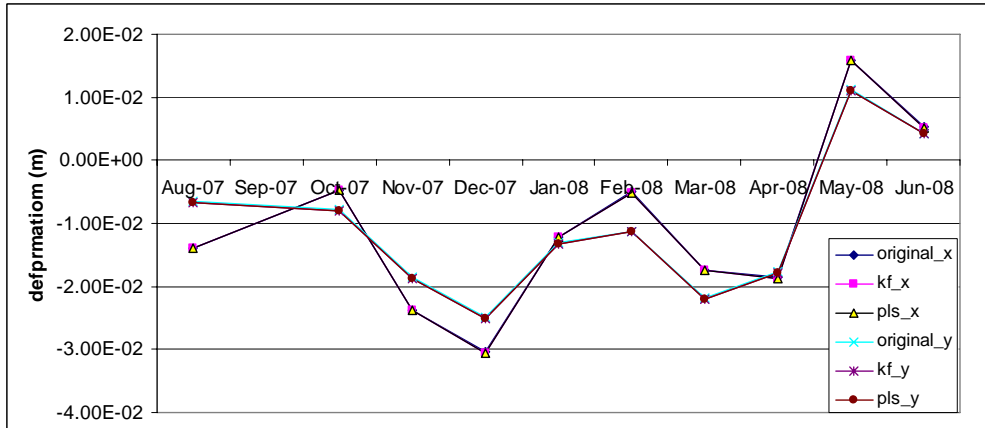


Figure 2.22 The deformation of north tower in two directions

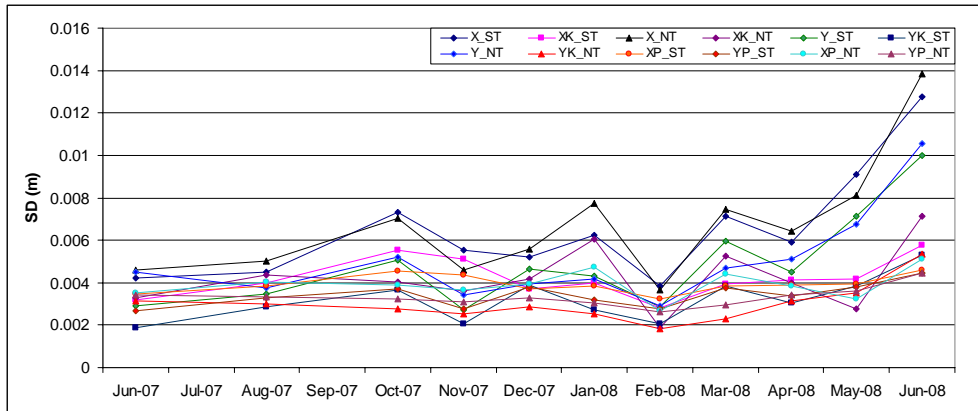


Figure 2.23 The SD of mean original, KF signals and PLS

This reveals that the signals noise is high. Also, it can be seen that the SD of signals after April 2008 is high. This indicates that the cracks had affected tower movement after April 2008 (as shown Figure 2.27). Also, it can be seen that the KF processing had increased the accuracy of signals by approximately 30%. The multi-processing of GPS signals didn't increase the accuracy signals, where the SD of the KF and PLS are so close to each other, as shown in Figure 2.23, also, the deformation calculated from mean GPS signals for original, KF and best position values from PLS are so close to each other, as shown in Figures 2.21 and 2.22. This reveals that the deformation values were not affected by the data processing while their accuracy was affected. Also, it can be seen that the X-

direction movements of the southern tower started to increase from the initial observation until February 2008 (8.87 cm) and later on, a decrease is seen in this movement (Figure 2.20). On the northern tower there are reverse direction movements of the tower (3.05 cm) until December 2007 and a later on, a distortion was seen in this movement (Figure 2.22). However, on this side the maximum increase in the movement becomes significant in December 2007 on the northern tower and as with the southern tower, after February 2008 a decrease was seen. Accordingly, it can be concluded that the X-direction movements of both towers are not similar. The Y-direction movements of the southern tower demonstrate an increase starting from the initial observation until February 2008 (5.98 cm) and later on, a decrease was seen. On the other hand, over similar time duration Y-direction movements of the northern tower are observed in the reverse direction with respect to that of the other tower, the change in movements was 2.51 cm in December 2007. Thus, the X and Y-directions movements of southern tower were observed as the load and velocity of the traffic flow and then in reverse directions as shown in Table 2.5. The reason for the observation of the X-direction movements to be in the same direction and the Y-direction movements under applied loads from December 2007 to March 2008, approximately, and then in a reverse direction for other date monitoring is because the Bridge is almost non-linear movement, the symmetrical in structure and cracks effects.

Table 2.5 the total available vehicle loads and velocity (lane 1 from one side to another side):

Date	Vehicle load (ton)		Vehicle velocity (m/sec)	
	Lane 1	Lane 2	Lane 1	Lane 2
08-2007	9080	71650	2.8e+005	2.0866e+006
10-2007	26141	30296	3.1556e+005	1.7108e+005
12-2007	18781	27335	2.9496e+005	2.6339e+005
01-2008	82593	1.896e+005	1.3946e+006	1.313e+006
07-2008	13837	-----	1.8062e+005	-----

Examining Table 2.5, it can be seen that the load and velocity of traffic increased as the bridge was opened to January 2008. Maximum loads occurred in January 2008. This reveals that traffic loads are the main factor of southern tower movements. Also from Figures, it can be seen that the Y-direction deformation of northern tower is greater than the X-direction from January 2008 to April 2008, and the maximum deformation of southern tower in between October 2007 to April 2008. This reveals that the beginning cracks might occur about these times,

but actually, these cracks affected on the bridge after April 2008. From the calculated deformation and cracks position (see Figure 2.27), it can be concluded that the southern tower movement caused a tension force in the bridge cables, these forces affected the bridge deck by a shearing force. The traffic loads effects were on the mid-span of the bridge, which increased the moment and movement on the girder, and southern tower bridge, respectively. On the other hand towers mostly nonlinear movements, may be the reason behind bridge damage.

After noise elimination from the bridge X&Y-directions time series signals power spectral density (PSD) and short-time Fourier transformation (STFT) components in the series were determined, see sample for those calculation in Figures 2.24, 2.25 and the summary of first peaks values of PSD shown in Figure 2.26.

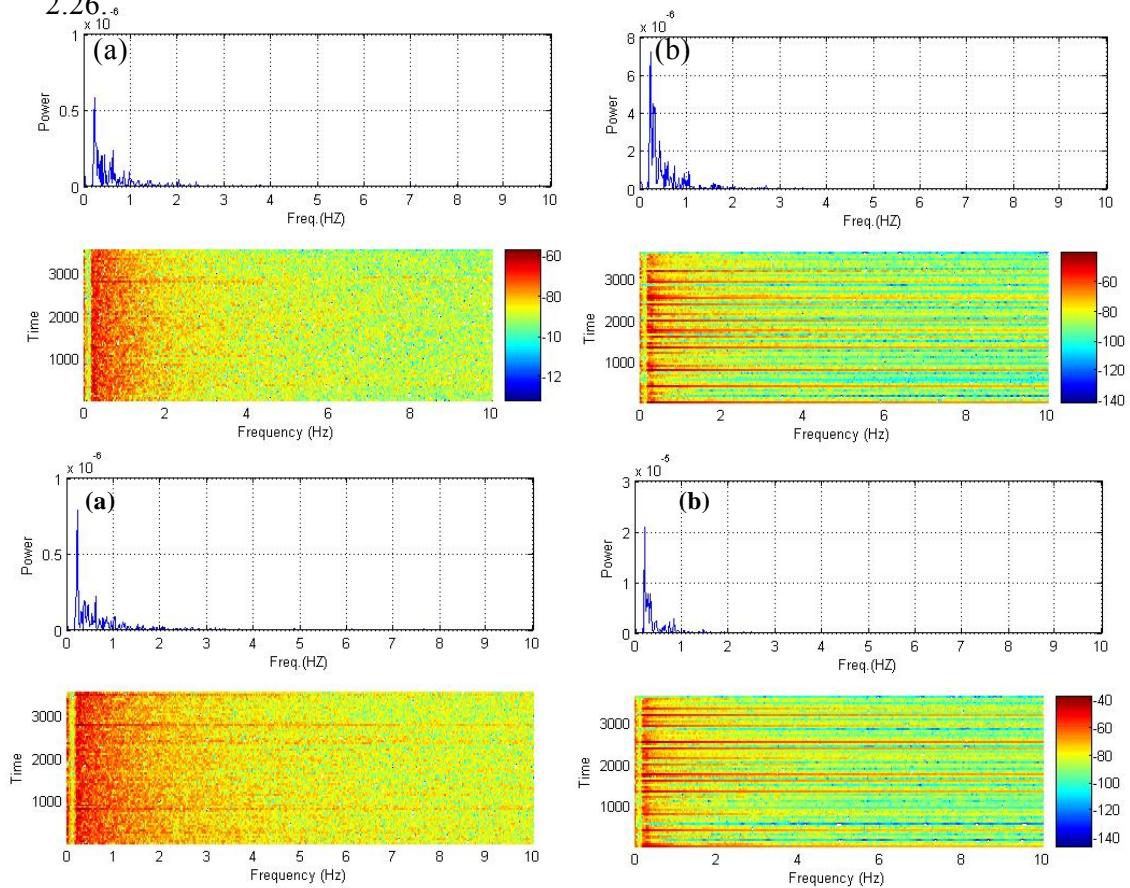


Figure 2.24 The power spectrum signals for south (up) and north X-direction signals (a) June 2007 (b) June 2008

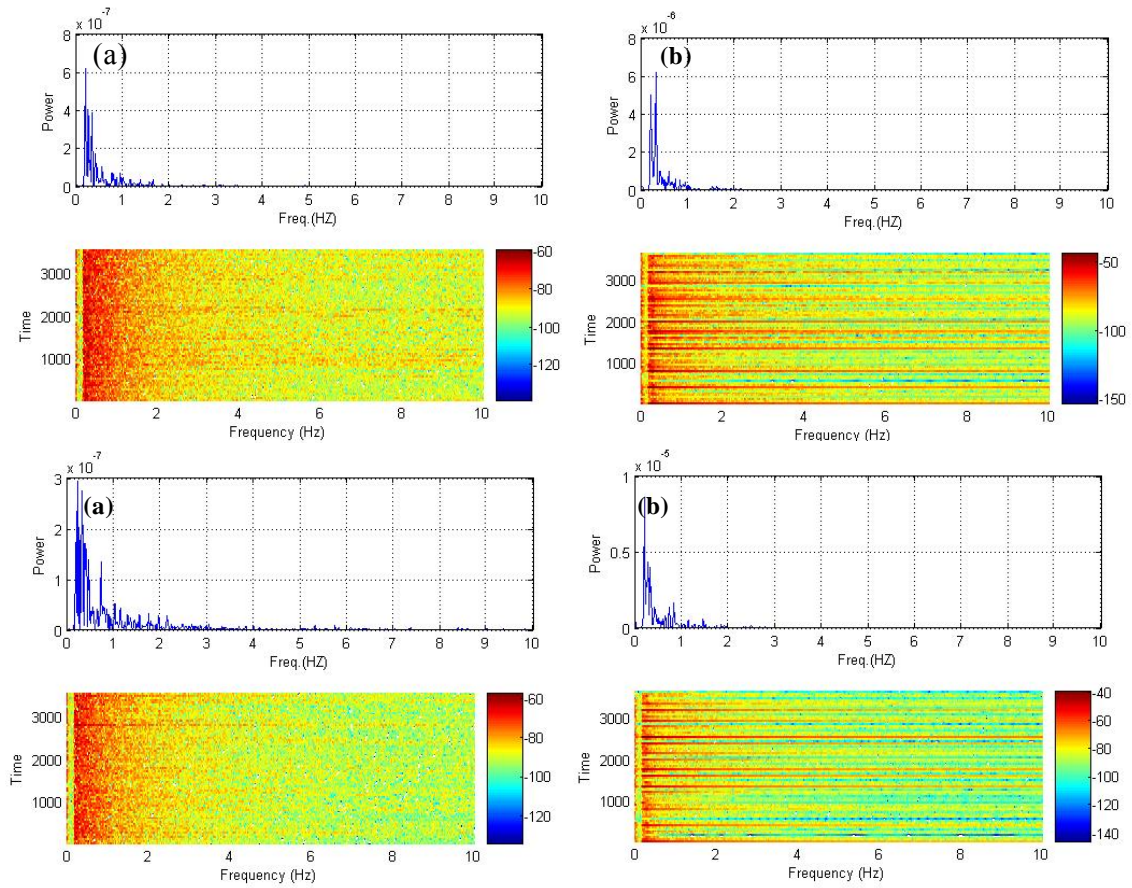


Figure 2.25 The power spectrum signals for south (up) and north Y-direction signals (a) June 2007 (b) June 2008

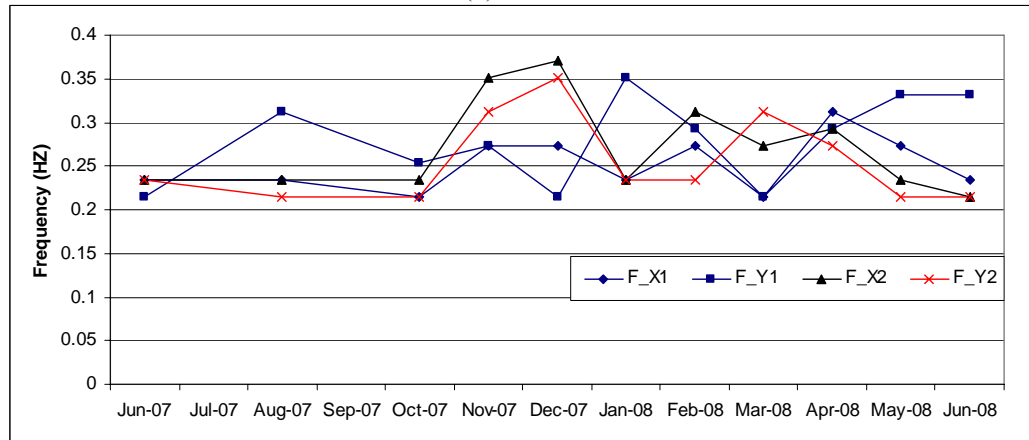


Figure 2.26 The first peak PSD at south (X1, Y1) and north (X2, Y2) bridge towers

These components were examined for high frequency changes, which occur over short-term movements as a result of high frequency, random or instantaneously changing traffic loads and wind speeds affecting the bridge^[104]. Natural frequency is equal approximately $(0.01-0.50) N$, where N is the story number. In this case, the tower height of bridge is 62.50 m. Assuming that, the height of a single story 2.80 m, so the frequency of the tower is approximately in between (0.22 to 11) HZ. However, the frequency components of the bridge towers were calculated at the most as 0.2 Hz. Tenth-order Butterworth Infinite impulse response (IIR) filter was used to design the high pass filter, to reduce the effects of spectral leakage, the Hanning Window^[84] multiplied the series, and the length of FFT is 1024. The periodogram and spectrogram (using Hamming window is a length of FFT data points and 50 data points overlapping in the spectrogram) were used to determine the PSD and STFT, respectively^[77].

From Figures 2.24-2.26, it can be seen that the maximum movements powered high frequencies for X and Y-directions of towers in are not the same, however, frequencies in June 2008 have higher powers. Besides, it can be seen that the towers high distortion frequency in the two directions have happened between October 2007 to and after April 2008. In addition, the high frequency reactions of the southern tower in the X and Y-directions are 0.3125 HZ in April 2008 and 0.3516 HZ in January 2008, whereas the high northern tower frequencies are 0.3711 HZ and 0.3516HZ in December 2007, respectively. This indicates that the high power frequency contributed to the maximum movements of towers and cracks effects. Although, the bridge is symmetrical it was determined that the towers as demonstrated don't have similar movements and frequency under affecting loads, and movements of the southern tower bridge in the X-direction are much large, when compared to X and Y-directions movements of the towers. It also can be seen in Figures 2.24-2.25 that the red frequency is not uniform along the time axis in June 2008. This indicates that the bridge deck cracks bring out the transient characteristics of the bridge towers frequency.

2.4.2.4 Tower Statistical Deformation analysis

Deformation analysis is performed using the certain epoch's results. F-test statistical analysis has been adopted to find out the deformation in the tower^[100]. So in this study, deformations are detected according to the results of unload case, mean KF vector on June 2007 (c), estimation interval onwards. For example, the test value for the X-direction is:

$$T_i = \frac{d_i^2}{\sigma_{d_i}^2} \quad (2.7)$$

$$d_i = X_i - X_c \quad (2.8)$$

$$\sigma_{d_i}^2 = \sigma_i^2 + \sigma_c^2 \quad (2.9)$$

Where

T_i is test value for the X-direction deformation at the i^{th} estimation interval.

d_i is the difference between the mean of the datum group (c) and the next time series groups.

σ_i is the variance in the X or Y-direction at the i^{th} estimation interval.

σ_c is the variance in the X-direction for the estimation interval.

$\sigma_{d_i}^2$ is the variance in the difference vector.

For deformation analysis, the zero and alternative hypotheses are defined as follows:

$$H_0 : E(d_i) = 0 \quad H_a : E(d_i) \neq 0. \quad (2.10)$$

If $T_i \geq F(1-\alpha, 2, df)$, F-test depended on the degree of freedom (df) at the 95% confidence level. It is considered that the difference vector (d_i) is significant and that there is indeed a deformation in the X-dire. the analysis is also applied for the Y-direction components.

From Table 2.6, it was found that the X and Y-directions for the southern tower deformation occurred on October 2007 to April 2008 and October 2007 to May 2008, respectively. On the other hand, for the northern tower the deformation is distorted in the X-direction and it occurred on October 2007 to May 2008 in the Y-direction. It can be also seen, the T values in both directions

for the southern tower are larger than that for the northern tower. From these results, it could be concluded that the movements of the southern and northern towers are abnormal from October 2007 in Y-direction, and the southern tower deformation is greater than that of the northern tower in both directions. For this reason, the deck and tower cracks are shown near from southern tower and no cracks appeared in or near the northern tower.

The crack width happened on Abutment is larger than that located on the mid span and southern tower as shown in Figure 2.27. And the shape and position of abutment crack revealed that the reason behind it is shearing forces.

Table 2.6 The results of statistical test:

Date	Southern Tower				Northern Tower			
	X		Y		X		Y	
	T	F	T	F	T	F	T	F
Aug-07	0.01	2.99	0.03	2.99	6.51	2.99	2.45	2.99
Oct-07	32.39	2.99	33.00	2.99	0.81	2.99	3.57	2.99
Nov-07	37.37	2.99	123.74	2.99	23.73	2.99	21.32	2.99
Dec-07	88.35	2.99	50.52	2.99	32.90	2.99	34.82	2.99
Jan-08	242.07	2.99	298.98	2.99	3.17	2.99	10.84	2.99
Feb-08	429.14	2.99	454.15	2.99	1.79	2.99	9.83	2.99
Mar-08	111.60	2.99	61.90	2.99	7.84	2.99	31.87	2.99
Apr-08	45.00	2.99	56.08	2.99	13.11	2.99	16.30	2.99
May-08	2.10	2.99	3.12	2.99	13.62	2.99	5.45	2.99
Jun-08	0.04	2.99	0.24	2.99	0.44	2.99	0.44	2.99

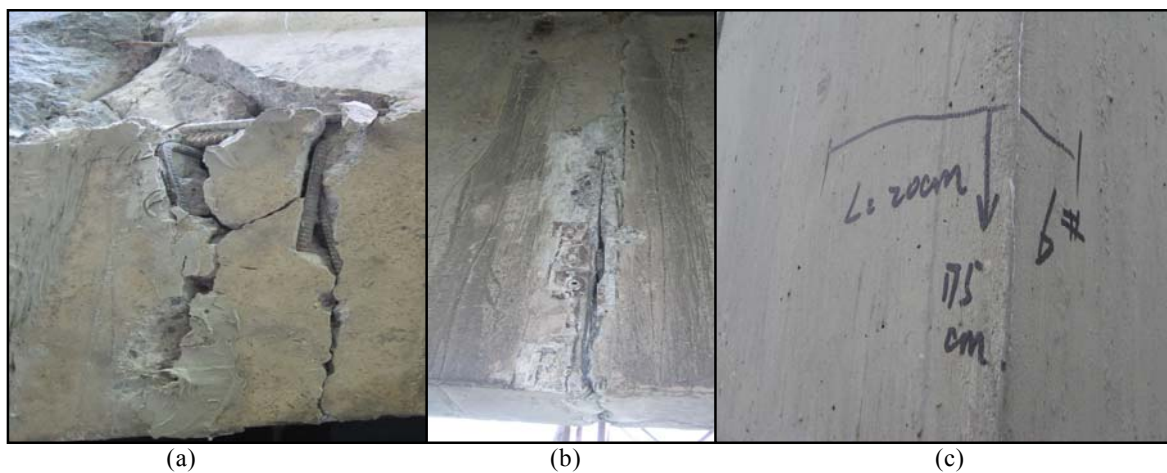


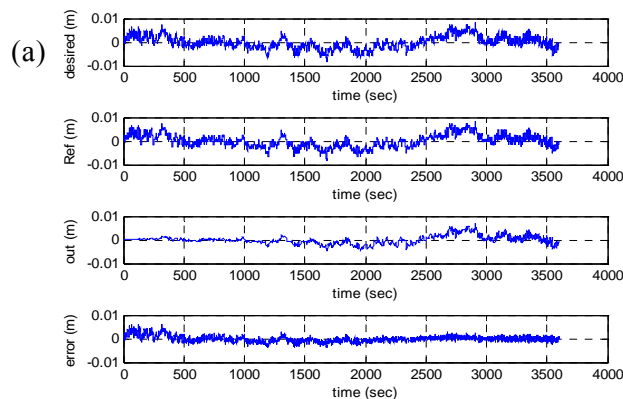
Figure 2.27 The photo of cracks on the (a) south abutment, (b) mid span and (c) south tower

2.4.3 Adaptive filter and analysis of tower movement

In this section, the south tower of Bridge was monitored from June 2007, this was taken as a reference date, and in August, December 2007, March, June, July 2008; these were taken as monitoring dates, based on the local time from 12:00 PM to 1:00 PM. The analysis in this study was based on the data collection in the X and y-directions, since the movement in these directions are greater than in Z-direction, thus the data in Z-direction were declined.

Figure 2.28 show the result of AF for the X and Y-direction June 2007, respectively. The first row on the graph is the relative horizontal positions on the June 6th. The second rows are the measurements reference signals calculated from the June 5th. The third rows are the signals for receiver noise plus tower bridge movements relevant to June 6th observations. The final rows are the isolated multipath series. The horizontal axis of the graphs represents the time, which is one hour, approximately.

From these Figures, it can be seen that the south tower movement is normal at the beginning of the observations, but these movements are opposite with the Finite Element (FE) analysis. It can be also shown that the standard deviations (SD) of the output signals are decreased by 25%. These results indicate that the AF eliminates the noise of the tower real time movement. At the same other dates data was processed. Figure 2.29 shows that the south tower movements relative to the unload case (June 2007) in two directions. The horizontal and vertical axis of the graphs represent the sample number and relative movements (m), respectively.



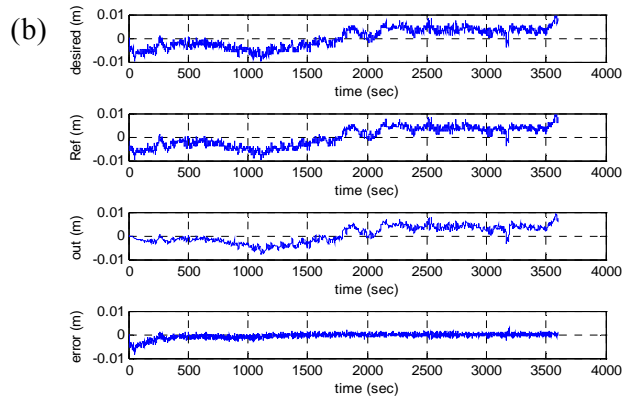


Figure 2.28 AF results of June 2007 signals,(a) X and (b) Y-directions

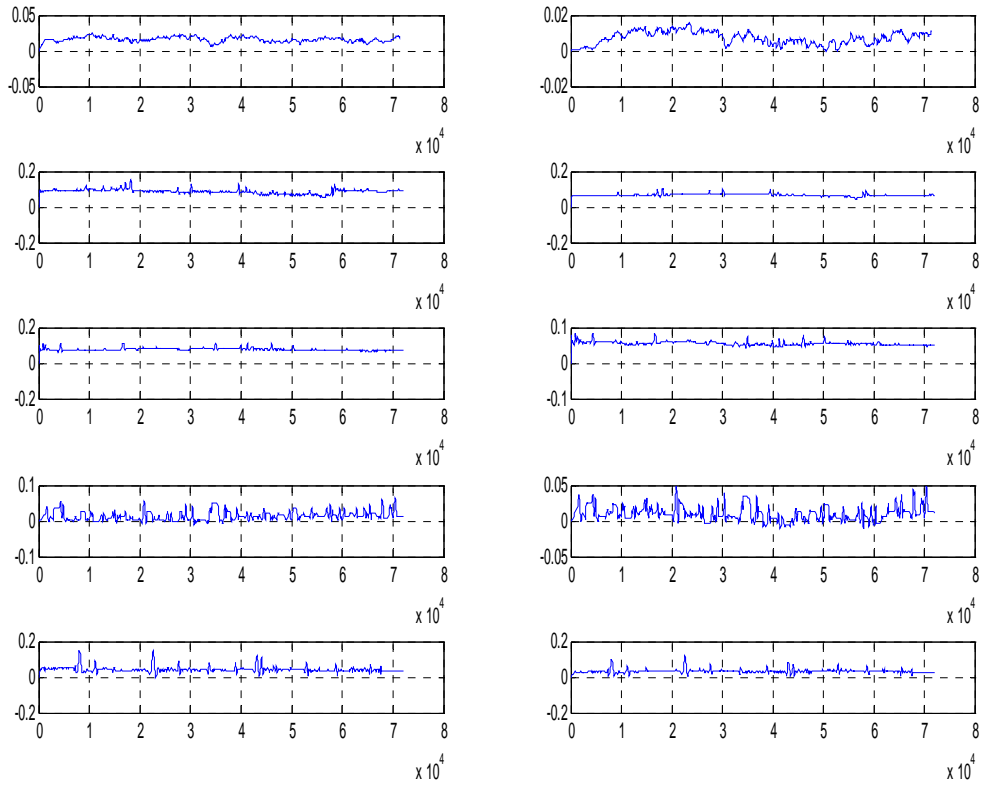


Figure 2.29 The tower movement (X-direction left)(Y-direction right), Aug., Dec. 2007, Mar., Jun., Jul. 2008 (up to down)

From these Figures, it can be seen that the maximum movements of the tower occurred in December 2007, March and July 2008. This indicates that the movement of the tower was affected by the applied load and deck damage. In addition, the signals for the June 2008 are abnormal. This indicates that the deck cracks mostly occurred at this month.

Figure 2.30 shows that the STFT is based on high-pass filter; the results explain that the maximum X and Y-directions high frequencies movements are not the same of the tower.

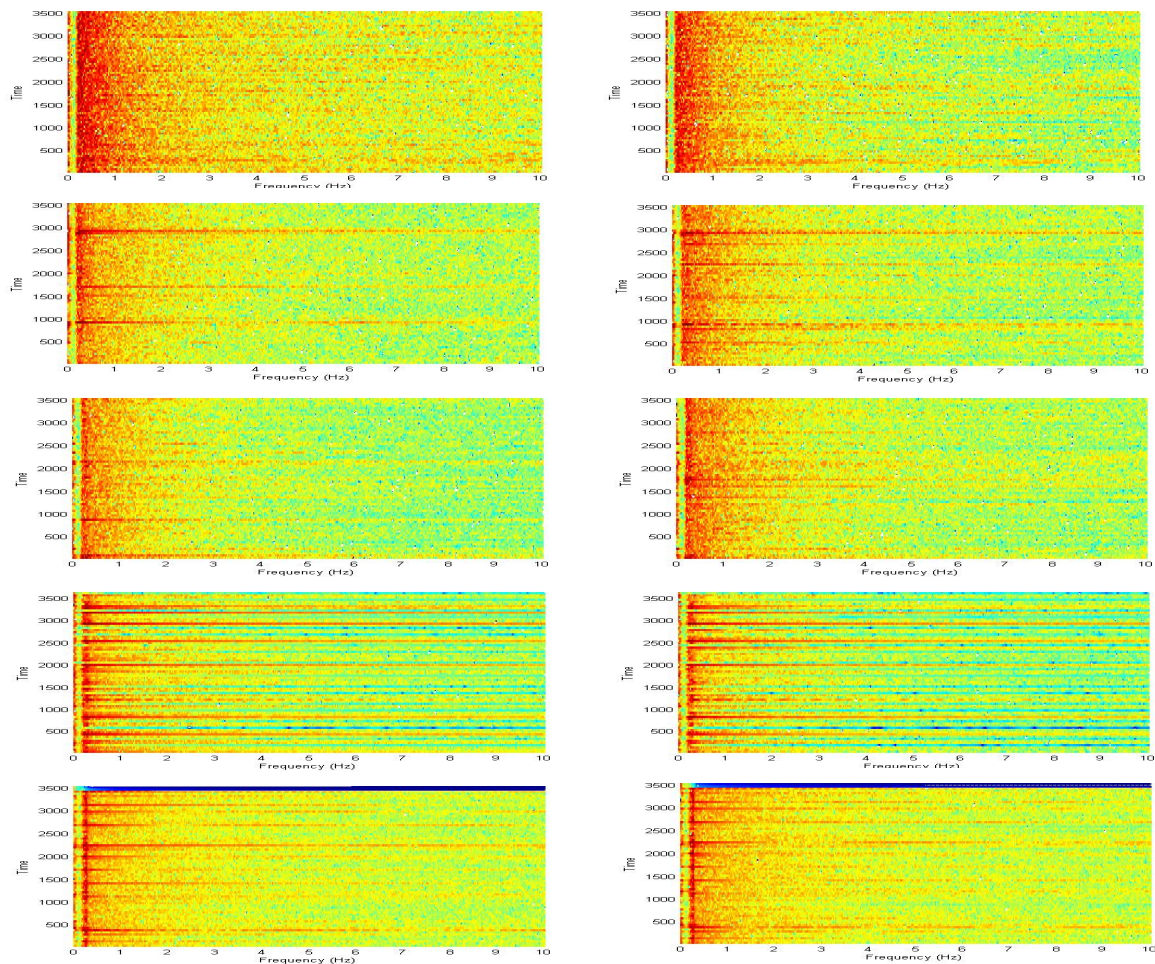


Figure 2.30 Time-Frequency for the tower movement (the continuous red color revealed to the high power), (X-direction left) (Y-direction right), Aug., Dec. 2007, Mar., Jun., Jul. 2008 (up to down)

Besides, it can be seen that the towers high distortion frequency in both directions happened between August 2007 to June 2008 and after it, and high frequency reactions of the south tower in the X and Y-directions are 0.293 HZ and 0.430 HZ in December 2007, respectively. So the high power frequency contribute to the maximum towers movements. Figure 2.30 shows that the red frequency is not uniform along the time axis in June 2008. This indicates that the bridge deck cracks bring out the frequency of the bridge tower movement transient characteristics. In addition, the STFT is a significant step forward from the traditional FFT in terms of structural response analysis.

2.4.4 Sensitivity and statistics of GPS signals based on damage observations and WT analysis

Patsias and Staszewski ^[103] showed the possible use of the WT in developing a damage detection method for optically observed mode shapes. Companion information is produced from the WT of mode shapes: the displacement mode shape comes from the approximation signals and the damage location comes from the detail signals. However, MATLAB DWT tools in have been adopted in this section to analyze the wavelet GPS signals coefficient to detect the bridge displacement and damage.

In addition the phase plane, formed by time and frequency, can display the frequencies on a two-dimensional time-frequency plane that is called STFT plane. It is possible to identify the energy content of the signal at different frequencies. The STFT essentially applies FFT with a short moving time window repeatedly to a short time series to obtain its time-frequency representation. To represent the signal with more detail in the time domain, we have to utilize a smaller time window. If the signal sampling rate remains the same, the method of choosing a smaller time window makes the frequency resolution worse. So a good resolution in the time and frequency domains cannot be achieved at the same time ^[104]. So in this section, the MATLAB code spectrogram was used with smaller Hamming window after pr-processing to analyze the time frequency plane domain.

2.4.4.1 Analysis movement of the Tower Bridge

Structural analysis is required to determine whether significant movements occurred between the monitoring campaigns or not. Geometric modeling is used to analyze spatial displacements. General movement trends are described using a sufficient number of discrete point displacements dn (Δx , Δy , Δz) for n = point number. Comparison of the magnitude of the calculated displacement and its associated accuracy indicates whether the reported movement is more likely due to observations error^[47].

$$|dn| < (en) \quad (2.11)$$

Where, dn is the magnitude of the displacement and en is the maximum dimension of combined 95% confidence ellipse for point (n), It can be calculated as^[14]:

$$e_n = 1.96 \sqrt{\sigma_f^2 + \sigma_i^2} \quad (2.12)$$

Where: σ_f is the standard error in position for the (final) or most recent survey, σ_i is the standard error in position for the (initial) or reference survey. Herein, if $|dn| < (en)$ the point is not moved, else the point is moved.

As the tower in the one side of the Bridge (Southern Tower) is observed in two directions at the same time intervals, it is possible to compare the movements of this tower. The evaluation of observations was performed using BCS and the observation initiation times are shown as reference in the graphs to better interpret the possible changes. The longitudinal movements of the tower on the traffic flow (Y direction) demonstrate an increase starting from the initiation of observation until January 2008 (5.73 cm) and later on, a decrease is seen for movement (Figure 2.31 and Table 2.7). The lateral movements of the tower on the Tianjin side (X direction) demonstrate an increase starting from the initiation of observation until February 2008 and later on, a decrease is noted, the change being 8.44 cm (Table 2.7). Accordingly, it can be concluded that the lateral and longitudinal movements of the towers are approximately similar. This indicates that the both directions tower movements are correlated.

From Table 2.7 and Equations 2.11-2.12, it can be seen that the tower had moved in between October 2007 to May 2008 and moved again after June 2008.

Table 2.7 The movement observations relative to June 2007.

Time index	X-Movement (cm)	Y-Movement (cm)
August 2007	0.291	-0.121
October 2007	2.63	2.37
November 2007	3.25	2.52
December 2007	4.16	2.90
January 2008	7.24	5.73
February 2008	8.44	5.70
March 2008	4.67	3.33
April 2008	3.62	2.61
May 2008	0.689	0.384
June 2008	-0.623	0.395
August 2008	1.81	1.77

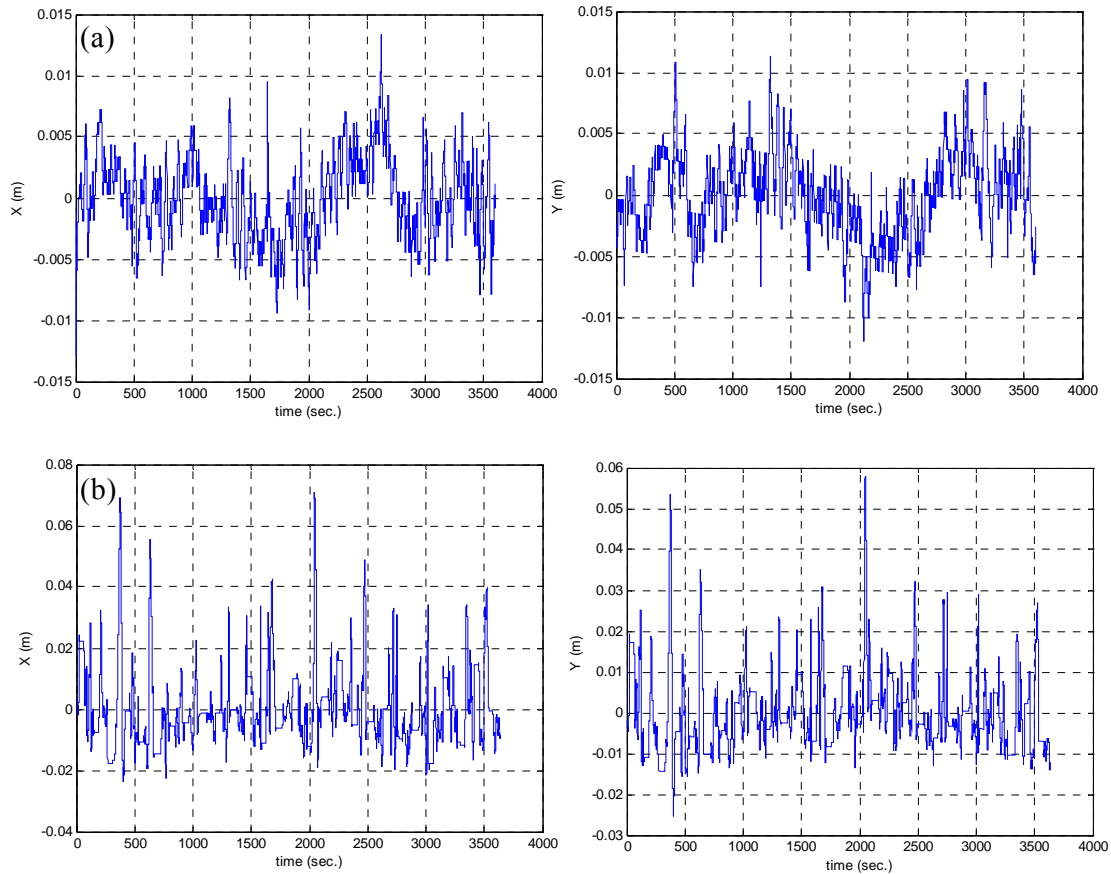
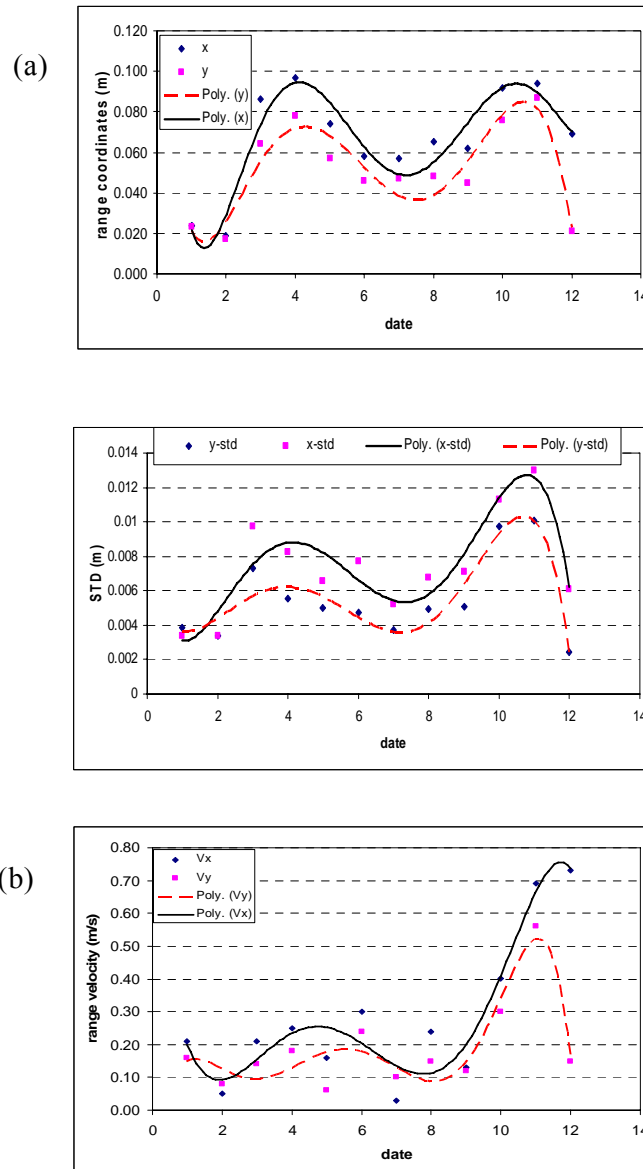


Figure 2.31 Movements of southern tower in X (longitudinal) and Y (lateral) directions (a) unload case (June 2007), and (b) damage case (June 2008).

The following Figures summarize the displacements range of tower and their velocities, acceleration converted range is calculated by movements integration, in addition it also show the observation SD and related converted results.



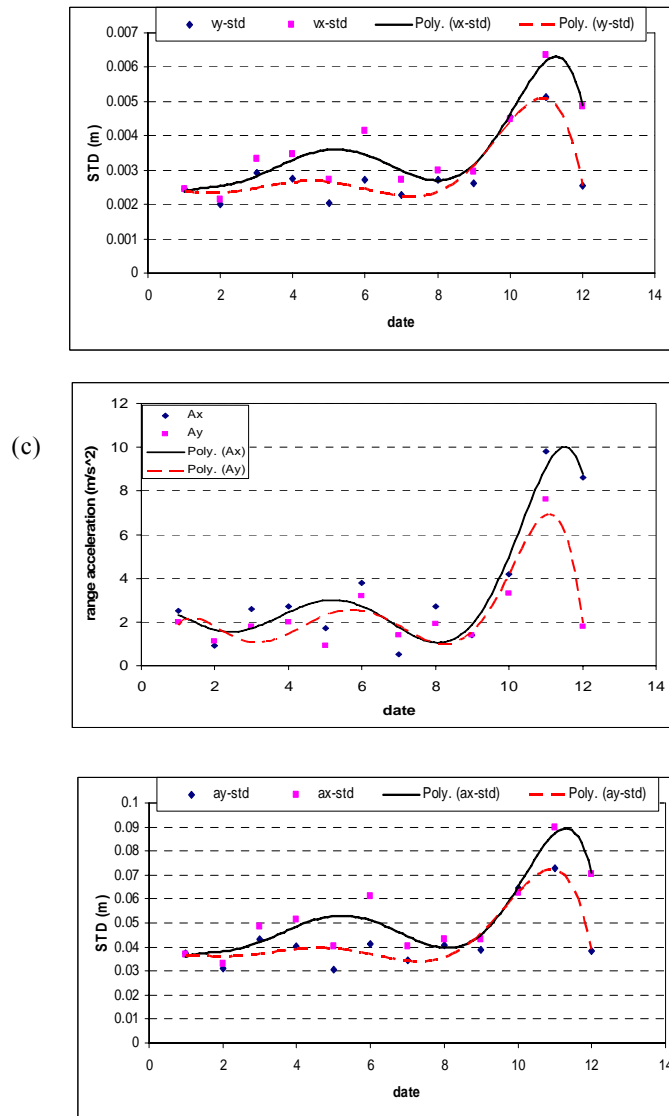


Figure 2.32 Statistical analyses of (a) GPS observation, (b) Velocity converted and (c) Acceleration converted, from GPS signals.

From these figures, it is shown that the velocity and acceleration converted range revealed that the bridge damage may have occurred in between May and July 2008. The GPS displacements range cannot reveal the bridge damage. In addition, the observations SD, velocity and acceleration converted may be near shape of fit polynomial and reveal the bridge damage time.

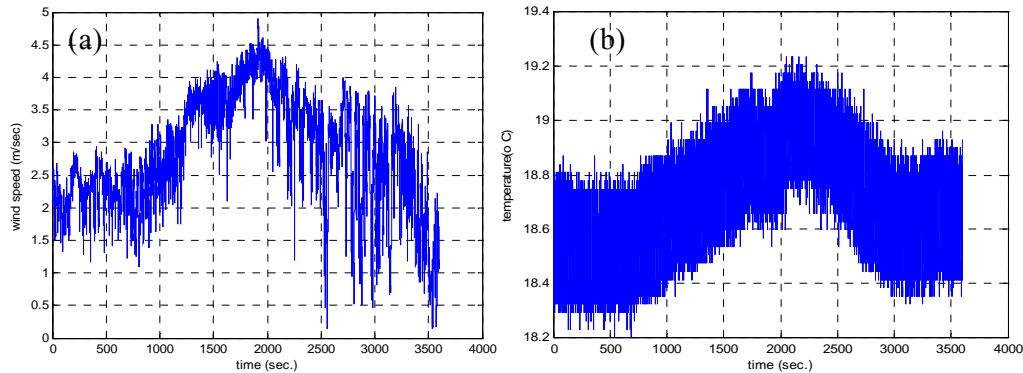


Figure 2.33 Sample environmental observation (a) wind speed, (b) temperature in August 2007.

Wind and temperature effects on the bridge during the period of observations are given in Table 2.8. The deformation bridge tower due to temperature is calculated as Equation 2.2. Where, δ , α , H , ΔT are deformations of tower due to temperature, $(12 \times 10^{-6} / ^\circ\text{C})$ Coefficient of thermal expansion, height of the tower (62.5 m) and change in temperature, respectively.

Table 2.8 Summary of environmental observations with time selections.

Time index	Wind		temperature		
	Mean Speed (m/sec)	Mostly Direction (Deg.)	Max. (°C)	Min. (°C)	δ (mm)
June 2007	-----	-----	-----	-----	-----
August 2007	2.821	150	19.238	18.201	0.778
October 2007	1.471	30-60	9.381	7.825	1.167
November 2007	1.137	250	-1.483	-2.948	1.098
December 2007	0.811	220-260	-0.72	-2.094	1.031
January 2008	4.685	140-160	-6.396	-8.746	1.762
February 2008	3.875	150	-5.908	-8.563	1.991
March 2008	1.113	50-100	1.965	0.836	0.847
April 2008	4.321	20-350	7.397	6.238	0.869
May 2008	3.535	42-48	21.436	19.879	1.168
June 2008	-----	-----	-----	-----	-----
August 2008	-----	-----	21.893	20.612	0.961

During tower observation periods, the deflections due to temperature changed in the bridge tower are not very large. The temperature change decreased between the initiation of observation until January 2008, then there were an increase as shown in Table 2.8. On the other hand, in the same time span

from the commencement of the observations until December 2007 the wind speed decreased significantly, then increased in January 2008, and then changed in-between decreasing and increasing after this date. The wind direction changed as shown in Table 2.8 with the observation period. To study the effect of traffic loads, three days of continuous measurement of GPS and number of vehicles were used, which were from 0:00 of January 10, 2008 to 24:00 of January 12, 2008, whereas the traffic observations are not available on the other observations dates. The averages of all observations in the 20-min segment are plotted in Figures 2.38 (after noising the signals) and 2.39.

From these figures, it can be seen that the correlation between movements of southern tower and the number of vehicles are 0.98 and 0.97 with X and Y-directions, respectively. In addition, it is revealed that the sensitivity of GPS signals increased with the traffic loads movements on the bridge. This revealed that the traffic loads are the main reason of tower movements and damage deck of the bridge. From Tables 2.7, 2.8 and Figures 2.33, 2.40 summarized that the effectiveness of temperature are very low with the time observations. In addition, the wind loads may have some effects on the bridge tower movements but mostly it is not the main reason for tower movements and traffic loads are the main reason of movements and cracks in the tower and bridge deck (Figures 2.14, 2.27).

These photos (Figures 2.14, 2.27) revealed that the cracks are may be due to shear force, cracks b and c may be due to bending moments. So, the movements of towers as shown in Table 2.7 probable tension forces in the bridge cables may have occurred which are may be affected by a shear force on the deck of the bridge. And the increase in traffic loads acting on the bridge with time increased the moments on the bridge mid-span. Herein, we can conclude that the traffic loads are the main reason of bridge cracks, so we recommended that traffic loads should be decreased on the studied bridge.

2.4.4.2 Wavelet Analysis

Figures 2.34 and 2.35 show some of the de-noised time series residuals and the mean and SD of wavelet coefficients at southern original GPS signals deformation. These signals were collected from June 2007 to August 2008.

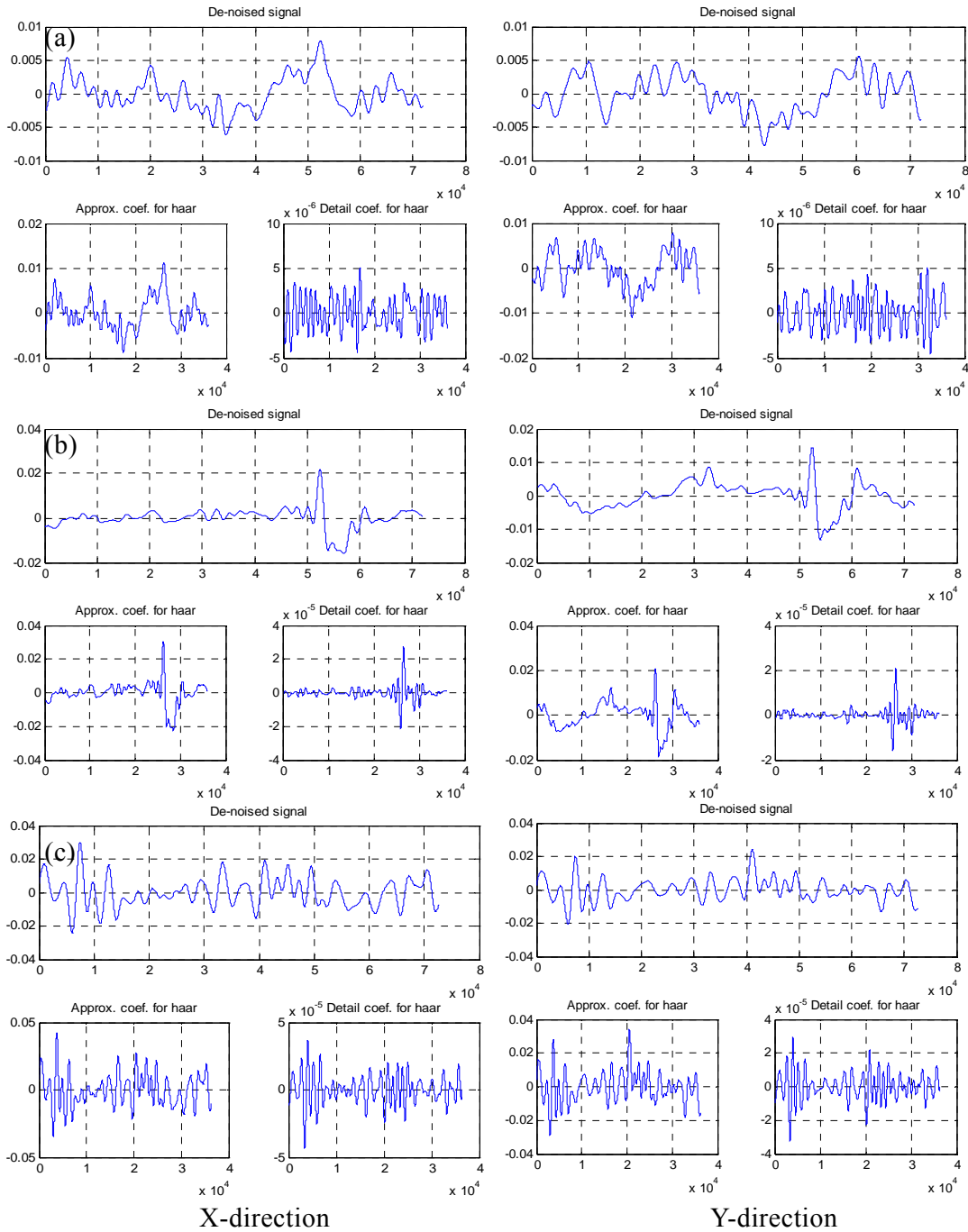
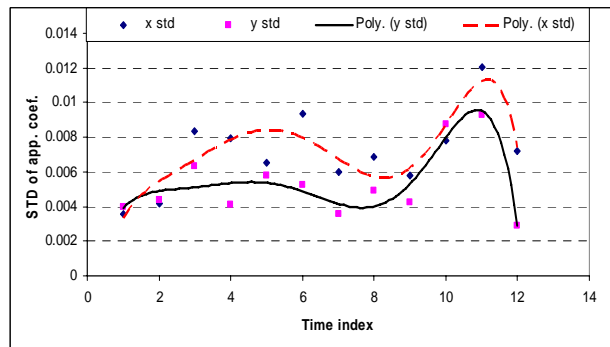
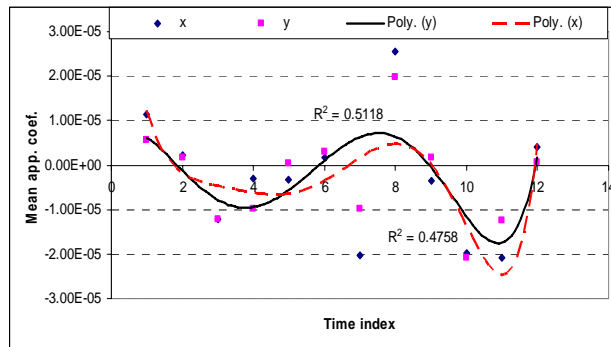


Figure 2.34 The de-noised and coefficient for Haar wavelet analysis in X and Y-directions at (a) unload case (June 2007), (b) load case (December 2007), and (c) damage case (June 2008).

All observation data were collected from 12.00 PM to 1.00 PM for China local time. The residuals are obtained by applying Matlab detrend code of the positioning signals at each monitoring time.

The DWT was computed for each case using MATLAB Wavelet Toolbox. Haar wavelet was used for all the analyses. The DWT Figures show the de-noised results for the considered case. At the top of each figure, the de-noised signal is plotted. Beneath, the low-level approximation signal (a) is displayed. And, the high-level detail signals (d) are shown. In Figure 2.35, a sixth degree polynomial fit.

(a)



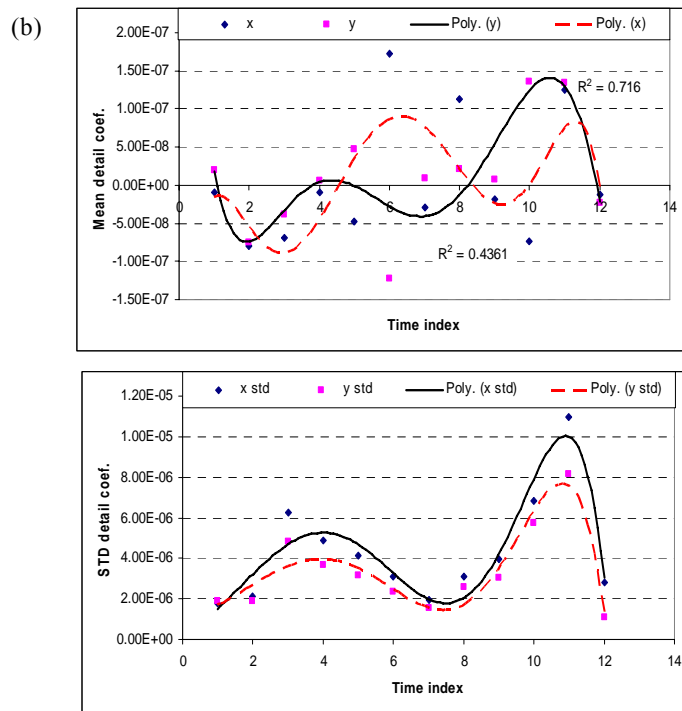


Figure 2.35 Statistical mean and SD of the (a) approximate and (b) detail for the Haar wavelet coefficients with the time monitoring

These Figures can be considered showing the healthy bridge. According from those Figs, clear range oscillations appear in the signals with the shown time index, as the severity of the fault increases to damage case. Figure 2.34(a) shows the high-level signals for the case of an un-loaded bridge. We observe clear oscillations in the signals b and c, as occurred for the loaded bridge. Furthermore, we observe that the pattern created by the eccentricity is totally different from that appearing in the case of damage, which is shown in Figure 2.34(c). These revealed that the sensitivity of the GPS signals does not depend on the position its. Also, the detailed coefficients can refer to traffic loads effects on the bridge, whereas the oscillations in the signals are due to traffic load in Figure (2.34) a, b. while, they were due to traffic loads and damage effects in Figure (2.34) c and the results cited in L. Hui et al. (2009) ^[89]. Figure 2.35 is statistical summary for the wavelet coefficient, from those figs., it can be seen that the maximum mean approximation coefficient at May and June 2008 is (-2×10^{-5}) , Figure 2.35(a), in addition the SD of the approximate coefficient signals are

0.012 and 0.009 in two directions in June 2008.

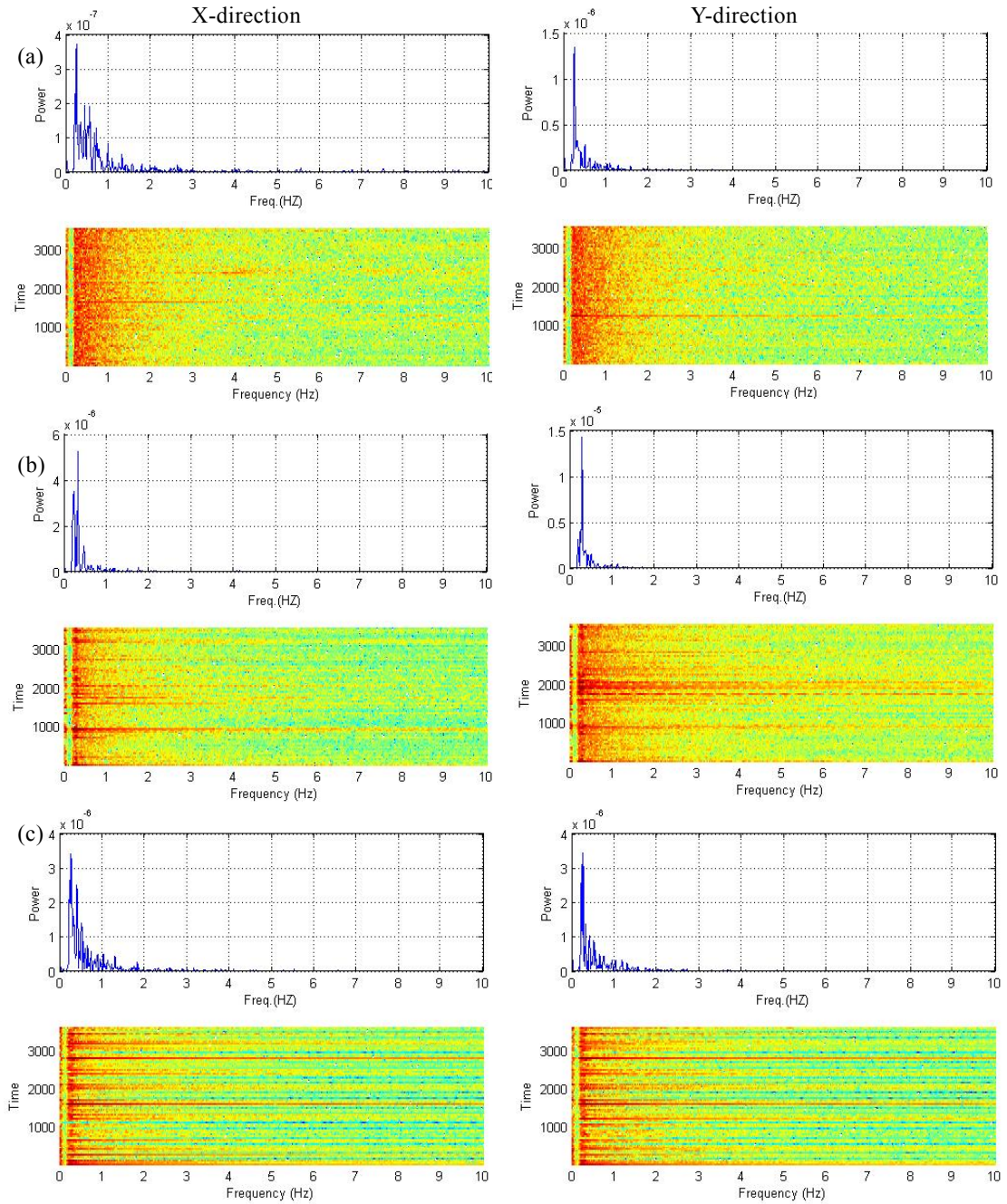


Figure 2.36 one and two D. Frequency for the tower movement in X and Y-direction at (a) June 2007, (b) May 2008 and (c) June 2008 (the continuous red color revealed to the high power).

Also, it can be shown that the same curves shapes in the detailed curves, mean and SD, respectively. In addition, it can be seen that the mean detail coefficient in May and June 2008 at Y-direction is greater than that in the X-direction. These results reveal that the deck damage may have happened in May 2008. Herein, we recommended that the increase of mean or range and SD the detail and approximate coefficients revealed that the damage would occur, so this technique can be used to predict the time damage detection. In addition, these results suggest that the performance of wavelet analysis for structural damage detection depends strongly on the excitation and restoring tower displacements. Clearly, the performance deteriorates as more realistic damage and traffic load happen. Figure 2.36 shows the some results for one and two dimensional frequency domains. Figures 2.37(a) and (b) are summary for the first mode frequency for the GPS signals at the same times above and the maximum power spectral density (PSD) with the time index, respectively.

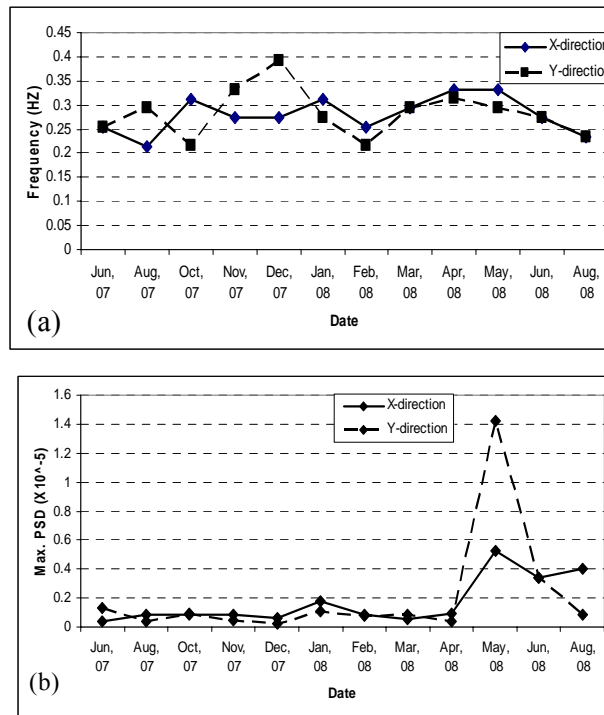


Figure 2.37 (a) The first mode frequency and (b) the maximum PSD of the first mode for the GPS signals

The previous discussed results explain that the maximum high frequencies X and Y-directions tower movements are not the same. Besides, it can be seen that the towers high distortion frequency in both directions happened after August 2007 till June 2008 and after that. The high frequency reactions of the south tower in the X and Y-directions are 0.332 HZ and 0.391 HZ in May 2008 and December 2007, respectively. Figure 2.36 shows that the red frequency is not uniform along the time axis in June 2008. Also, the beginning non-uniform red color is also shown in May 2008, as shown in Figure 2.36(b). Beside that, from the results, it is shown that the red color returns are uniform in August 2008. In addition, from Figure 2.37(a), it can be seen that the correlation between the frequencies in both directions as caused by traffic load is very low which have little effects to the occurred damage. Also, Figure 2.37(b) revealed that the maximum X and Y-direction PSDs at May 2008 are 0.49 and 1.42, whereas, it can be shown that the maximum X-direction PSD is greater than the PSD for the Y-direction, Figure 2.37(b). These results reveals that the beginning of damage may have happened in May 2008 and has increased up to June 2008. In addition, the STFT is a significant step forward from the traditional FFT in terms of structural response analysis. It is also found that the low frequency obtained from power spectrums reflected the bridge expected time damage.

2.4.5 Geometrical Models Analysis

In this section the data were collected between June 2007 and June 2008 every months based on the local time from 11:00 AM to 2:00 PM. The analysis in this study was based on the data collection in the X and y-directions, since the movement in these directions are greater than in Z-direction, thus the data in Z-direction were declined. Figure 2.38 shows one sample of GPS signals and the KF results in X and Y directions, respectively.

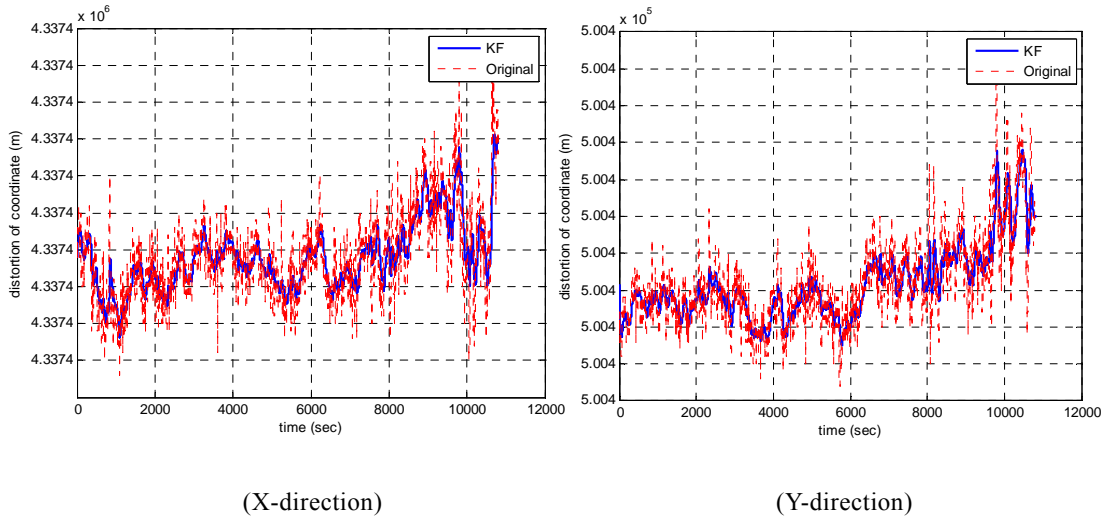


Figure 2.38 A subset of the GPS results for the south tower site with the model kalman filter superimposed (6 June 2007)

From the KF obtained results sited in Figure 2.39, it can be seen that the different between the SD for GPS and KF coordinates is very clear. This indicates that the random noise of GPS signals is too high. The results also revealed that the percentage increase in residuals on May and June 2008 for X and Y coordinates are 90 %, 50% and 173 %, 100% respectively. This is related to the effects of deck cracks. Also, it can be seen that the SD values for KF are less than those obtained by GPS (i.e. the KF decreased the noise of signals by 28 %). This indicates that the KF is accurately one of the methodologies to eliminate the noise of dynamic signals.

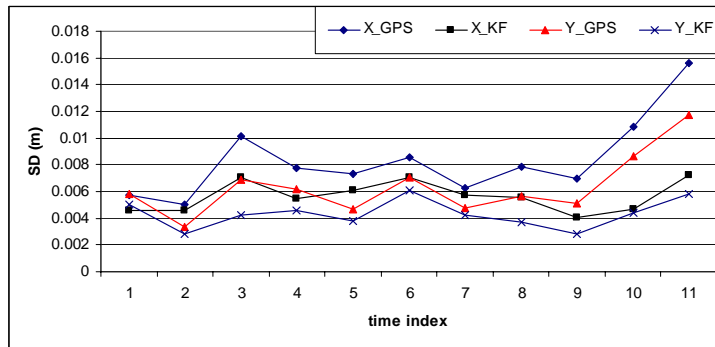


Figure 2.39 The SD of KF and GPS signals for the X and Y coordinate

The south and north towers mean filters Cartesian coordinates, the long-monitoring time selection and time index are shown in Figures 2.40 and 2.41, respectively. From these Figures, it can be seen that the maximum deformation of the south tower measured on February 2008 and of the north tower measured on December 2007 are 10.50 cm and 3.80 cm, respectively. These indicate that the load have much effects on the bridge that opened on August 2007. In addition, it is found that the movements of these towers happened on December 2007 to March 2008 are non-linear, which indicates the instability of the bridge. Figure 2.40, also indicates that the maximum deformation of the coordinates pronounced on January and February 2008 and the upper point of the south tower is returned to its original position after 10 months. This can be attributed to the tower elasticity that absorbed the applied loads. Hence, it should be mentioned that the bridge GPS collection data under unload state on 6 June, 2007 are considered as a reference for the other monitoring date.

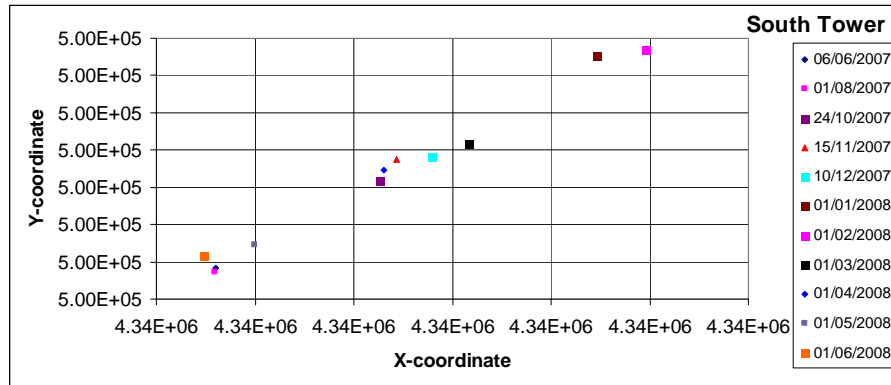


Figure 2.40 The mean values of filters values for the south tower coordinates with the time monitoring

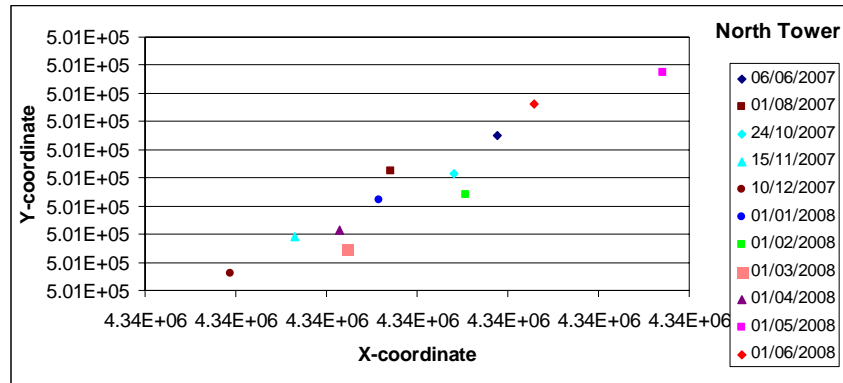


Figure 2.41 The mean values of filters values for the north tower coordinates with the time monitoring

2.4.5.1 Plane analysis

In order to determine the south tower deformation, two fixed points (2 and 3) and one movement point (1) are assumed to create the geometrical plane shown in Figure 1.8. In this figure, the planes 2 and 1 are used in the deformation monitoring in X&Y-directions, respectively. The deformation in Y-direction is determined based on the assumptions that the fixed points coordinates in X direction are equal to any values and in Y-direction to be the same value of unloaded tower for the same direction, and vice versa is assumed for determining the deformation in X-direction. For the Z-direction, the coordinates of the fixed points are assumed to be any equal values and the upper point of the tower is assumed to be the tower height.

Table 2.9 points out the obtained parameters from Equation 1.21 and generally shows that the assumed coordinate's values have an effect on the parameters never on the deformation values.

Table 2.9 The parameters of two assumed planes at south tower:

	Parameters	A	b	c	d
X direction	South tower	5050.000	0	0	-2.19E+10
Y direction	South tower	0	100.000	0	-5.00E+07

From Table 2.9, it is found that the values of c parameter equal to zero for X and Y - directions due to the free errors in Z -direction. The values of b parameter are found to be zero in X -direction and for a parameter equal to zero in Y -direction, which indicates that the monitoring direction has an effect on the parameters values. For this model the mean Cartesian coordinate filtered from KF is used. Figure 2.42 shows the calculated deformation values in X and Y -directions using Equation (1.22). From this Figure, it can be seen that the deformation of the upper tower point is very clear. Also, it can be seen that the maximum deformation in X & Y -directions are 0.087 m and 0.058 m, respectively. The statistical analysis of deformation in X and Y -directions at 5% level of significant indicates that the tower deformation was happened between August 2007 and June 2008. From this analysis, it can be concluded that the designed geometrical plane model can be used to determine the structural deformation.

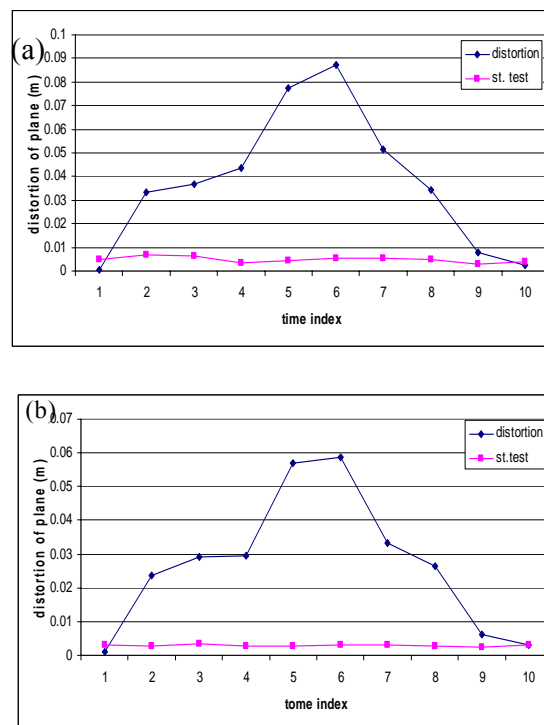


Figure 2.42 The distortion of plane in (a) X -direction and (b) Y -direction respectively for the south tower

2.4.5.2 PC analysis

In this analysis the unload cases data that collected on 6 June 2007 is predicted (smooth line) and used as a reference for other mentoring date. Figure 2.43 shows the distance and angle of PC analysis for both prediction and signal.

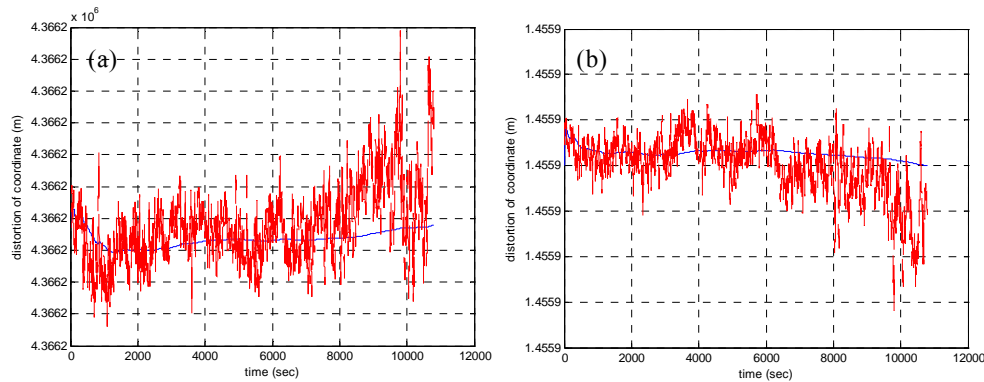


Figure 2.43 The main signal and prediction signal (smooth) (a) distance PC and (b) angle PC

From this Figure and the calculation error signals using Equations (1.26) and (1.27), it can be seen that the deformation between the reference case and the other cases are significant, which indicates that the applied loads have more effect on the bridge since August 2008. Figures 2.44 and 2.45 show that the maximum, minimum and mean values of PC parameters (i.e. distortions of distance and angle). From these Figures, it is found that the movement and angle of the tower to be 8.7 cm and, -1.015×10^{-8} radian respectively on February 2008, which indicate that the tower is moved towards NE direction due to the traffic load effects at the mid span. Figure 2.46 shows the statistical analysis of the tower movement. From this Figure, it is found that the maximum deformation in the distance and angle that happened between December 2007 and March 2008. Also, Figure 2.46 indicates that deformation in the distance is happened between August 2007 and May 2008 and the SD of signals on May and June 2008 is greater than the other date due to the cracks. This means that the cracks are happened on April 2008.

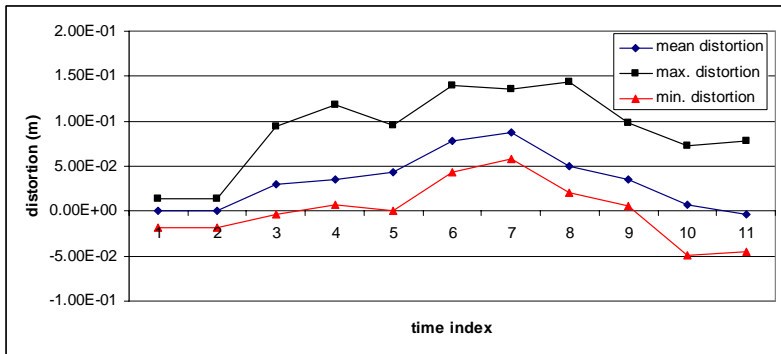


Figure 2.44 The Maximum, Minimum and mean for the distance PC distortion

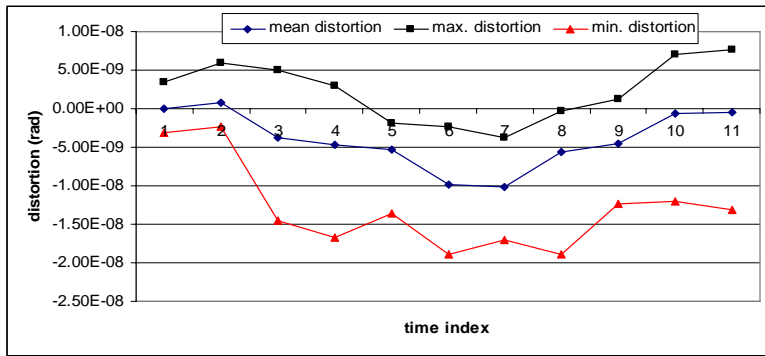


Figure 2.45 The Maximum, Minimum and mean for the angle PC distortion

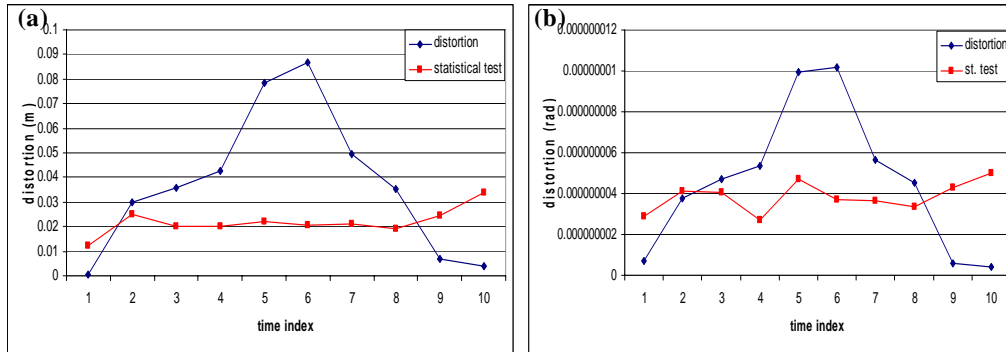


Figure 2.46 The statistical test of the (a) distance and (b) angle for PC

2.4.5.3 Span Length analysis

This analysis is calculated using Equation (1.28) to monitor the bridge span length as shown in Figure 2.47. From this Figure, it is found that the span length has significantly changed with the monitoring time. The mean of the span length predicted is decreased by 0.023 % in between June 2007 and February 2008. This indicates that the towers are moved towards the bridge between this period and its return to the original position after the cracks happened.

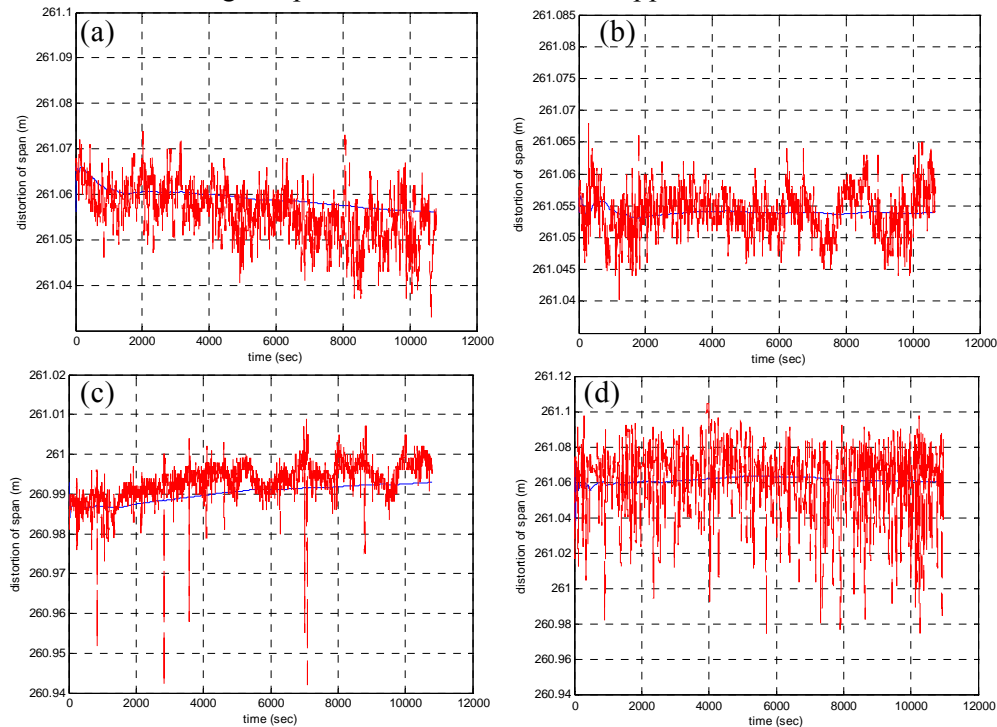


Figure 2.47 A subset of the span length calculated with the model kalman predictions, smooth, a- June 2007, b- August 2007, c- February 2008 and d- June 2008

Figure 2.48 shows the mean distortion of the span length predicted with its statistically analysis. From this Figure, it can be seen that after six months of bridge opening the deformation in span length is 6.9 cm due to the increased in traffic loads at mid span. From statistical analysis, it is found that the deformation is happened from August 2007 to May 2008. These results are close to that obtained in Figure 2.42 and at the same time reflect that the cracks happened in the bridge deck caused by south tower deformation. Hence, it should

be mentioned that this method can be applied if the direction of the movement for two towers are known.

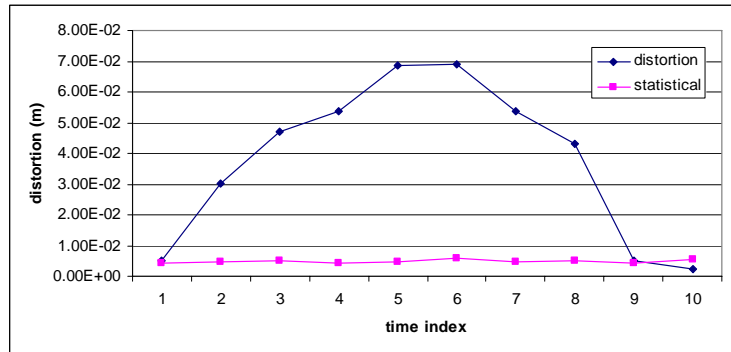


Figure 2.48 Statistical test of the span length distortion

2.5 Summary

Based on the signal processing and movements analysis, the analysis of the result leads to the following findings:

It was found that the calculated coordinates from PLS and KF analysis methods are much close, the KF increased the accuracy of the signals by approximately 30%, so the KF is better to filtering dynamic GPS signals.

Based on the time series analysis of the environmental and traffic loads observation, it was found that the bridge tower movements happened due to the traffic loads effect.

Based on the time series movement analysis, it was found that the bridge cracks are mainly caused by the shear force due to movement of the south tower and the bridge non-linear movements due to traffic loads, The SD obtained from AF processing analyses of GPS data increased significantly. The two-dimension frequency obtained from STFT reflects the expected movements and damage to the bridge.

The designed plane and PC geometrical analysis models prove to calculate the long-time structural deformation monitoring easily. GPS signals noise contains complex errors, and the signals accuracy obtained from the wavelet analysis (de-noised process) increased by 24%.

Chapter 3 Multi input / Single Output Model Identification of Bridge Tower Movements Using GPS Monitoring System

3.1 Introduction

A convenient way of describing a dynamic system is by use mathematical models. These models can be represented in continuous time either as differential equation systems or discrete-time as difference equation systems. There are in general two ways to construct mathematical models, which are physical modeling and system identification [107-112; 129].

The system models can be simulating the effects of the physical laws pertaining to the system when available with the help of input-output quantities [114]. In addition, when there is little information on the physical laws pertaining to the system or when the system is too complex, identification methods such as parametric identification are used to define the model of the system. In this case, preliminary assumptions are made on the order of complexity, input and output parameters of the system. The model is then expressed as the relationship between the selected system inputs and outputs [115-116]. However, in this section, two identification models namely; Multi Input-Single Output (MISO) robust fit regression and Neural Network Auto-Regression Moving Average with eXogenous input (NNARMAX) models were used for the identification of these data.

3.2 Robust fitted regression

The most common general method of robust regression is, introduced by [74]. Consider the fitted model:

$$y = a + b_1x_{i1} + b_2x_{i2} + \dots + b_kx_{ik} + e_i \quad (i = 1, 2, \dots, n) \quad (3.1)$$

where y_i are the observed output quantities or signals, $x_{i1}, x_{i2}, \dots, x_{ik}$ are the observed input quantities or signals, a, b_1, b_2, \dots, b_k are unknown

parameters, the number of unknowns $u=k+1$, k is the number of input quantities, n is the number of observations and e_i is the random error with $E(e_i)=0$; $\text{var}(e_i)=\sigma^2$. The unknowns form a vector of unknowns, U , i.e. $U^T=[a,b_1,\dots,b_k]^T$. Unknown parameters U in Equation 3.2 can be estimated and tested for statistical significance using the least squares method. The estimation process should be repeated after removing the insignificant parameters from the model (Equation 3.1).

$$U = (A^T P A)^{-1} A^T P y \quad (3.2)$$

$$V = y - AU \quad (3.3)$$

Where, A is the design matrix, y is the vector of the n observed output quantities, V is the vector of the n residuals ($V^T=[v_1,\dots,v_n]^T$) and P is the weight matrix ($P=\text{diag}(w_1,\dots,w_n)$, w_i is the chosen weight function in Equation 3.4).

It is usually assumed that the response errors follow a normal distribution, and that extreme values are rare. Still, extreme values called outliers do occur. The main disadvantage of Least Square (LS) fitting is its sensitivity to outliers. Outliers have a large influence on the fit because squaring the residuals magnifies the effects of these extreme observation points. Bi-square weighted robust predictors were used in the regression analysis to minimize the influence of outliers. Bi-square weights; minimize a weighted sum of squares, where the weight given to each observation point depends on how far the point is from the fitted line. Points near the line get full weight. Points farther from the line get a reduced weight. Robust fitting with bi-square weights uses an iteratively re weighted LS algorithm, and follow the weight function.

$$w_i = \begin{cases} [1 - (\frac{v_i}{r})^2]^2 & \text{for } |v_i| \leq r \\ 0 & \text{for } |v_i| > r \end{cases} \quad (r = 4.685) \quad (3.4)$$

Solving the robust model (Equation 3.1) is a weighted least-squares problem, minimizing $\sum w_i^2 v_i^2$. The weights, however, depend upon the

residuals; the residuals depend upon the estimated coefficients, and the estimated coefficients depend upon the weights. An iterative solution is therefore required:

1. Select initial estimates U , such as the LS estimates.
2. At each iteration t , calculate residuals $e_i(t-1)$ and associated weights from Equation 3.4 from the previous iteration.
3. Solve for new weighted-least-squares estimates using Equation 3.1.
4. The procedure is completed when the fit converges. Otherwise, next iteration of the fitting procedure should be performed by returning to the first step [77].

3.3 The NNARMAX model

The general input-output model structure (Figure 3.1) used for modeling of nonlinear and time invariant dynamic systems excited by deterministic input is Auto-Regressive Moving Average with eXternal input (ARMAX), assuming unit sampling interval, there are an input and output quantity or signals $u(t)$ and $y(t)$ respectively, $t=1,2,\dots,n$. the input-output relationship can be written as [93] :

$$A(q^{-1}, \theta)y(t) = G(q^{-1}, \theta)u(t) + H(q^{-1}, \theta)e(t) \quad (3.5)$$

Where

$$A(q, \theta) = 1 + a_1q^{-1} + \dots + a_{n_y}q^{-n_y}$$

$$G(q, \theta) = b_1q^{-1} + \dots + b_{n_u}q^{-n_u}$$

$$H(q, \theta) = 1 + c_1q^{-1} + \dots + c_{n_e}q^{-n_e}$$

$$\theta = [a_1 \dots a_{n_y} \quad b_1 \dots b_{n_u} \quad c_1 \dots c_{n_e}]$$

are the parameter vector, $y(t)$ the output at time t ($t=1,2,\dots$), $u(t)$ the input and $e(t)$ The stochastic input $e(t)$ are innovations, which is an equivalent process of the noise and prediction error.

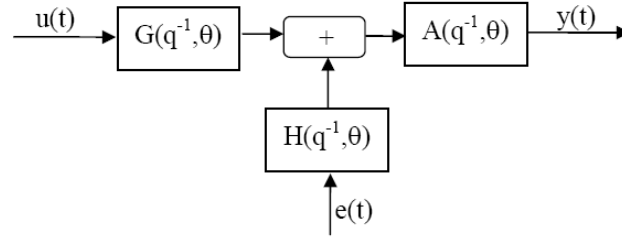


Figure 3.1 ARMAX Model Structure

To identify a neural network ARMAX (NNARAX) model, the nonlinear model is determined as follows:

$$\hat{y}(t|\theta) = g(y(t-1), \dots, y(t-n_a), u(t-n_k), \dots, u(t-n_b-n_k+1), e(t-1), \dots, e(t-n_c)) \quad (3.6)$$

In the statements presented above, $\hat{y}(t|\theta)$ is the output neural network (prediction vector), n_a is the past output used for determining the prediction, n_b is the past input, n_k is the time delay, and n_c is the past residuals.

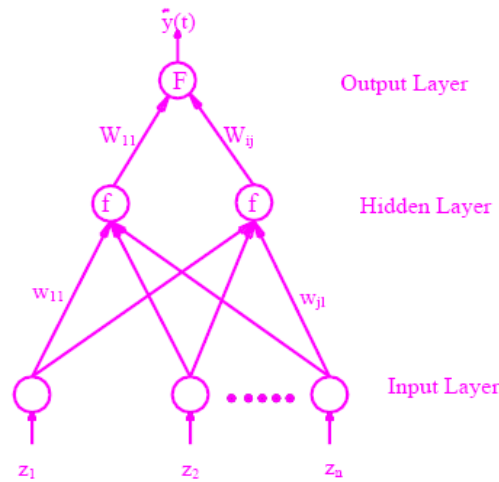


Figure 3.2 MLP-network scheme

$$\hat{y}_i(w, W) = F_i \left(\sum_{j=0}^q W_{ij} f_j \left(\sum_{l=1}^m w_{jl} z_l + w_{j0} \right) + W_{i0} \right) \quad (3.7)$$

Here, w_{j0} and W_{i0} are the bias parameters; m is the number of input

units; and q is the number of hidden units. The function $f(\cdot)$ that is implemented in this paper is tangent function and $F(\cdot)$ is linear function output. The weight (alternatively by the matrices w and W) are the adjustable parameters of the network, and they are determined from through the process called training. The training data are a set of input $u(t)$, and corresponding desired outputs $y(t)$. Specify the training set by:

$$z_n = [u(t), y(t)] \quad t = 1, 2, \dots, n \quad (3.8)$$

The objective of training is then to determine a mapping from the set of training data to the set of possible weights, so that the networks will predictions $\hat{y}(t)$, which are close to the true. The prediction error approach is based on the introduction of measure of closeness in terms of a mean of mean square error criterion ^[87-88]:

$$V_n(\theta, z_n) = \frac{1}{2n} \sum_{t=1}^n [y(t) - \hat{y}(t|\theta)]^T [y(t) - \hat{y}(t|\theta)] \quad (3.9)$$

The weights are then found:

$$\hat{\theta} = \arg \min V_n(\theta, z_n) \quad (3.10)$$

The NN model (shown in Figure 3.2) for ARMAX consists of three layers, i.e. one input layer (y, u, e), one hidden layers and one output layer \hat{y} . Note that to achieve the universal fitting property, exactly one layer of tangent nodes and two layers of weighted connections are require. The hidden layer is considered to be the number of tangent assumed. Increasing the number of hidden neurons can realize modeling of more complicated system ^[103]. If the network training finds an acceptable solution, tangent layer may force the hidden units to capture the significant features in modal parameters. The identification method for the NNARMAX model is the Levenberg-Marquardt method, which provides a numerical solution to the problem of minimizing a function, generally nonlinear, over a space of parameters of the model. These minimization problems arise especially in least squares curve fitting and nonlinear programming. In addition, it does not only provide an estimate of the NNARMAX model parameters, but also, of the covariance matrix of the parameters. The square roots of the diagonal elements of this

matrix are estimates of the standard deviations of individual model parameters. With this covariance matrix, it is also possible to estimate the standard deviations of a new observation. The standard deviations can be used to establish confidence intervals around the predicted values ^[88-89]. If a new observation lies outside the confidence intervals on the prediction, it is likely that the system is damaged ^[89].

3.4 Criterion of parameters and prediction

Many different models can be fitted to the observation. The following criteria can be used to assess and compare the quality of models.

A) The first criterion: Model parameters have to be tested whether or not the deviations at the “0” expected values are significant. In order to do this, \hat{t} test values are calculated for each parameter, as follows:

$$\hat{t} = \frac{\text{parameter}}{\text{standart deviation of parameter}} \quad (3.11)$$

These testing values are compared with pre-determined $1-\alpha$ confidence levels and $t_{f,1-\alpha/2}$ confidence limit of t distribution dependent on the f order of freedom. As results of the test, insignificant parameters are excluded from the function and this procedure is continued till all parameters become significant ^[85].

B) The second criterion: is the value of the loss function, defined as:

$$\lambda_0 = \frac{1}{n} \sum_{t=1}^n e^2(t) \quad (3.12)$$

where $e(t)$ is a residual of the observation and the predicted model ($e(t)=y(t)-\hat{y}(t)$).

C) The third criterion includes penalties for model complexity similar to the Akaike’s Final Prediction Error (FPE) criterion which is defined as,

$$\text{FPE} = \lambda_0 \left(1 + \frac{2k}{n-k}\right) \quad (3.13)$$

λ_0 is the loss function and k defines the number of parameters in the model. The FPE represents a balance between the number of parameters and

the explained variation.

D) The fourth quality criterion for a model is provided by the Auto-Correlation Function (ACF) of the residuals. The lag m Auto-Correlation (AC) is defined as

$$\lambda(m) = \frac{1}{n} \sum_{t=1}^n e(t-m)e(t) \quad (3.14)$$

Ideally, the residual is white noise, and therefore, the AC $\lambda(m)$ is zero when k is nonzero. A large AC when k is nonzero indicates that the residual is not zero-mean white noise and also implies that the model structure is not relevant to the system or that there might be a need to increase the model order. In real world applications, AC $\lambda(m)$ cannot be zero when m is nonzero because of limited length of observation points. If the value of AC falls within 95% of the confidence interval, the AC value is insignificant and this value is considered to be equal to zero^[87].

E) The fifth quality criterion for a prediction model is R-square, which is defined as:

$$R^2 = \frac{\sum_{i=1}^n (\hat{y}_i - \bar{f})^2}{\sum_{i=1}^n (y_i - \bar{y})^2} \quad (3.15)$$

In the above, \bar{y} and \bar{f} are the means of the observed data and predicted values respectively. The R-square represents a balance between the old and the predicted data variation.

3.5 Identification of Tower bridge movements

3.5.1 Tower displacements

Three continuous days of GPS, temperature, humidity, number of vehicle and wind velocity measurements, which were recorded from 0:00 January 10th, 2008 to 24:00 January 12th, 2008, are used for study. The averages of all

observations in 20-min segments are plotted in Figures 3.4 (after de-noising the signals in Figure 3.3) and 3.5. The original displacement history measurements in X and Y directions (BCS) for the tower were extracted using the de-noising process are presented in Figure 3.3.

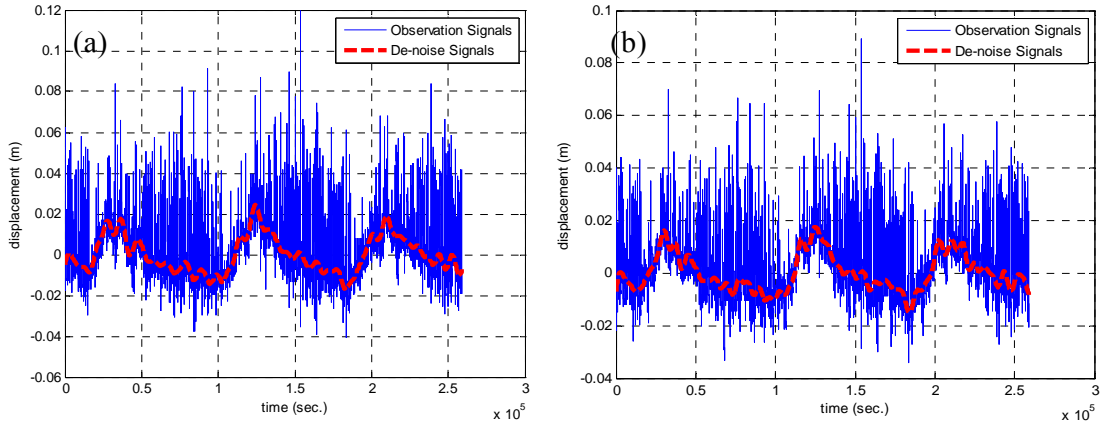


Figure 3.3 Observation, de-noised signals of tower displacements in (a) X and (b) Y-directions

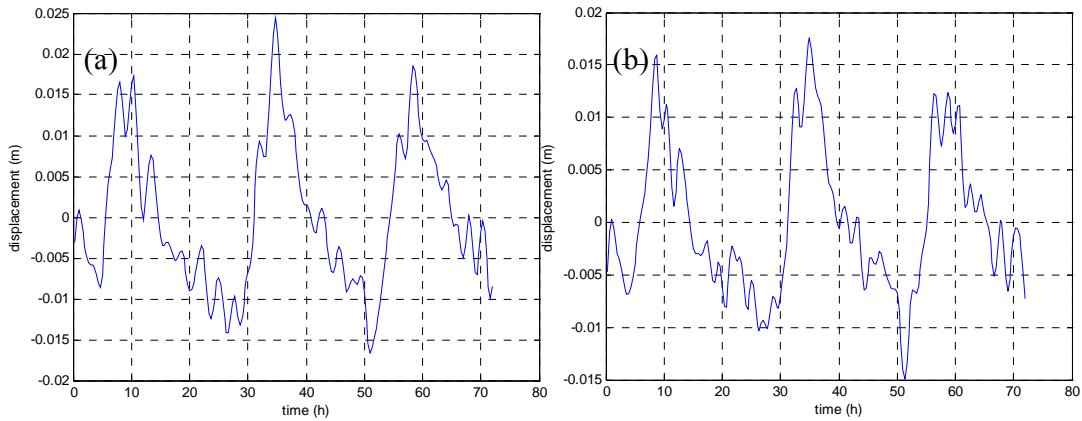


Figure 3.4 mean 20-min. displacement of de-noised signals for southern tower in (a) X and (b) Y-directions

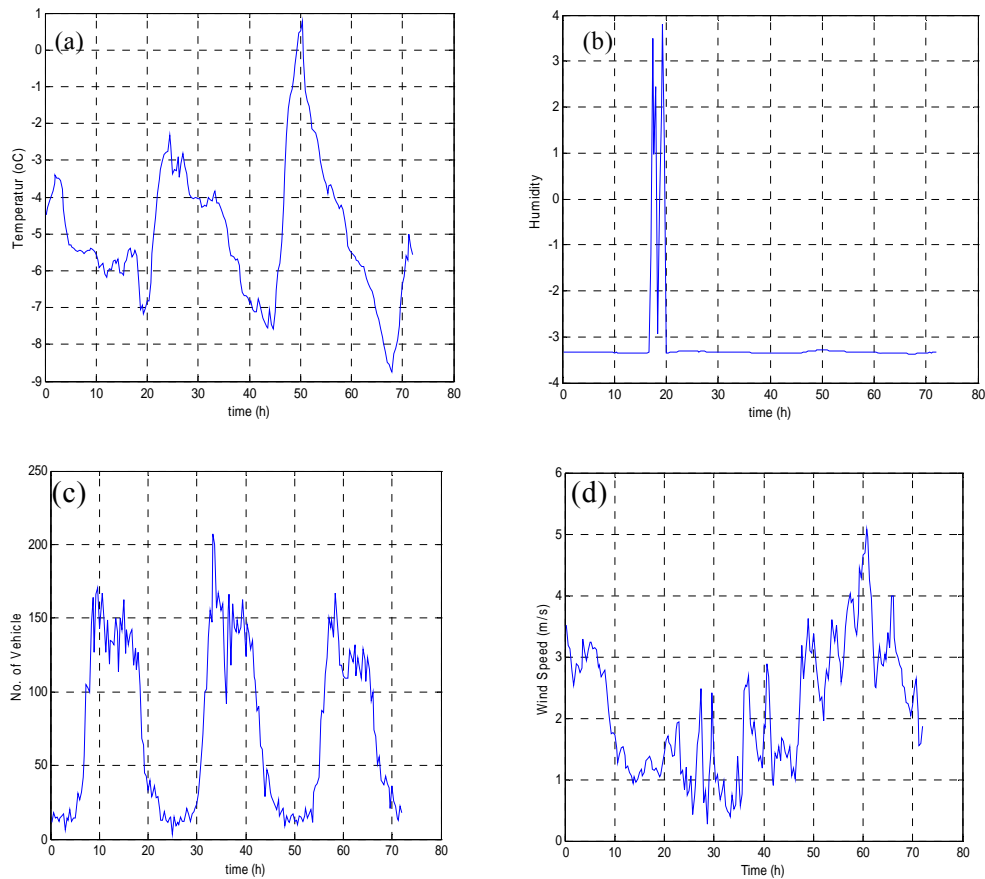


Figure 3.5 Variation in (a) Temperature, (b) Humidity, (c) Number of vehicle, and (d) Wind speed during the observation

The trend components in the series were investigated from the obtained data within de-noising process analysis. The trend component in the series represents the long-term changes related to time and it can be defined by a polynomial function in the time domain. From Figure 3.3, it was found that the maximum and minimum residuals between the original and de-noised signals are 11.86 cm and -3.63 cm, respectively. This indicated that the Multipath errors of GPS signals are high. This error due to the base station is near to building, which contains the process monitoring system.

As well as, it can be seen that the de-noising processing caused an increased

in the signals accuracy by 24%. The results have shown that noises can effectively be removed and the useful signals can be extracted from original signals with wavelet analysis as Figure 3.3.

From Figure 3.4, it can be seen that the X and Y-directions displacement of the tower show increase from starting the measurements at 0.00 (January, 10, 2008) to 10.00 (1.73, 1.60 cm) then decrease at 1.00 (January, 11, 2008) (-1.41,-1.04 cm). The same cycles were shows in another days 11 and 12 January 2008. In addition the maximum displacement becomes significant at 11.00 (January, 11, 2008) in X and Y-directions, 2.44, 1.76 cm, respectively, whereas, the minimum displacements are -1.66 and -1.50 cm in X and Y-directions respectively. Accordingly, it can be assumed that the tower displacement in two directions change in a similar manner. However, it can be concluded that the correlation between two directions are strongly influenced. It can be seen from Figure 3.5 that the temperature increased and decreased random with the time, whereas, it can be show the maximum and minimum temperature are 0.80 °C and -8.76 °C at 2.00 and 20.00 (January, 12, 2008), respectively (Figure 3.5 (a)). In addition, the humidity can be assumed constant with the time observations, whereas shows increased at (18.00 to 20.00) in January 10 (Figure 3.5 (b)). On the other hand, wind speed decreased from the starting to 11.00 (January, 11) then increased significantly till 12.00 January, 12 and decreased afterwards, as shown in Figure 3.5 (d). Wind direction was between South East and North West during the observation period (150-350°) and mostly direction is South West (250°). The vehicle number, as shown in Figure 3.5 (c), increased and decreased significantly with the displacement of tower in X and Y-directions. In addition, the time intervals for changes in the number of vehicles also coincided with the time intervals for the changes in the displacement X and Y- directions of the tower. However, it can be concluded that the main factor of displacements in X and Y-directions are the number of vehicle. Also, the wind may be affects on the displacement of two directions in the last day of observations.

3.5.2 Identified Models

The Bridge will hereafter be referred to as "the system" in the identification study and the tower will be considered as the components of the system. Temperature (T), the number of vehicle on the bridge (V), the wind speed (W) and humidity (H) were chosen as the input quantities of the input signal, and the displacements in the X and Y-directions were chosen as the output quantities of the system. Robust fit regression and NNARMAX models were considered in the development of the transfer functions describing the relationship between the input and output quantities observed at tower. Transfer functions considered in expressing the relationship between the observed input and output quantities of the tower are illustrated in Figure 3.6.

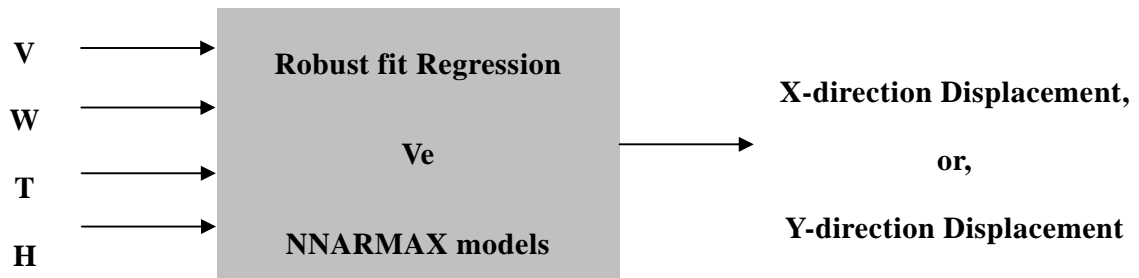


Figure 3.6 Input-output quantities and models considered in the development of transfer functions for the bridge tower

The bridge tower models have to be accurate and reliable and this depends on the accuracy and reliability of the observations used to define the model. The accuracy of the observations was checked with the instruments used. The accuracy of the instruments used can be shown in section 2.3. The observations needed to be checked for outliers, where they increase the difficulty of defining the inherently complex NNARMAX models. So, the existence of outliers in the X and Y-directions were investigated in the definition phase of the robust fit regression model. The trend of the displacements recorded in the X and Y-directions were calculated in the initial phase of the model definition. Afterwards, the unknown parameters U^T of the robust regression model and the covariance matrices of these parameters were predicted using LS method. However, due to the sensitivity of the LS method to incompatible measurements, the existence of

outliers was checked with bi-square weighted robust predictors. As a result of the investigation, w_i bi-square weights were found to be close, or near to “1” which showed that there were no outliers in the observations for the X and Y-directions. Therefore, model parameters for the tower displacements for X and Y-directions and their respective covariance matrices were predicted with bi-square weighted robust predictors. The results of this model were shown in Tables 3.1 and Figures 3.7.

In addition, the model evaluation criteria; loss function λ_0 , FPE and R-square values were calculated. The statistical significance of the model coefficients presented in Table 3.1 were tested by comparing them with the confidence boundary of the t-distribution related to the degree of freedom “f” at a confidence level of 95%, $t_{f,1-\alpha/2}$. Test results revealed that the coefficient pertaining to the temperature and humidity in the model 1 representing the displacements of the tower in the X and Y-directions were statistically insignificant since $t_{T,H} < 1.96$. Hence, the effect of temperature and humidity on the tower displacements in the X and Y-directions were ignored. Therefore, the models, model 2, used for calculating the tower displacements in the X and Y-direction were defined with respect to the variations in wind speed and the number of vehicles on the bridge (Table 3.1).

Table 3.1 Robust fit model of the displacement of tower in X and Y directions with respect to the number of vehicle (V), wind speed (W), temperature (T), and humidity (H)

Model	Dis= $b_0+b_1V+b_2W+b_3T+b_4H$	t (V,W,T,H)	λ_0	FPE	R ²
1	X= $-0.0168+0.00012V+0.0018W-6.4e-5T-0.0010H$	18.08,5.35 0.31,-2.80	2.6e-5	2.7e-5	0.63
	Y= $-0.0112+9.8e-5V+0.0011W+0.00016T-0.00069H$	17.45,3.89,0.93,- 2.26	1.7e-5	1.8e-5	0.62
2	X= $-0.0136+0.00012V+0.0019W$	19.43,5.85	2.6e-5	2.7e-5	0.62
	Y= $-0.0099+9.5e-5V+0.0012W$	18.33,4.45	1.7e-5	1.8e-5	0.61

It can be seen in Table 3.1 that the λ_0 , FPE and R-square values of the models describing the displacements of the tower in the two directions are nearly the same. This confirms that temperature and humidity has a negligible effect on the tower displacements in the two directions. As a result, the models used for

calculating the tower displacements in the two directions were defined with respect to the number of vehicles on the bridge (V) and wind speed change (W) (model 2).

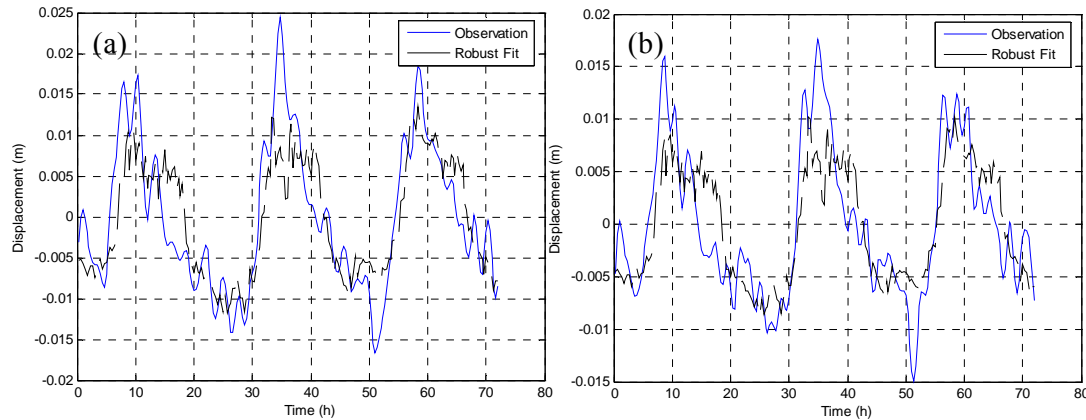


Figure 3.7 Observation displacement and output produced by Robust fit regression of southern tower in (a) X and (b) Y-directions

Robust predictors were used to check the existence of possible outliers in the observations and to identify the significant input parameters in the definition of multiple regression models for the X and Y displacements. In this type of models, there are no time lag between the inputs and outputs. Therefore, tower responds synchronously to the input quantity which is typical for static systems. Thus, it would not be incorrect to rephrase the robust multiple regression models as “static” robust multiple regression models. Furthermore, the values of the previous system inputs and outputs are not taken into account in this model. Static robust multiple regression models derived in this manner can be expressed with the n_a ; n_b ; n_c and n_k parameters of the NNARMAX model. Static robust multiple regression models used to define the displacements of the tower in this manner can be expressed with the NNARMAX [0 1 0 0] model of $[n_a; n_b; n_c; n_k]=[0;1;0;0]$. In this situation, robust static multiple regression models used to define the X and Y displacements of the tower have exogenous orders of $n_b=[1 1]$, the past error $n_c=[0 0]$ and time lags of $n_k=[0 0]$ for auto-regressive order of $n_a=0$ and the number of input variables of $n_u=2$ (number of vehicles and wind speed).

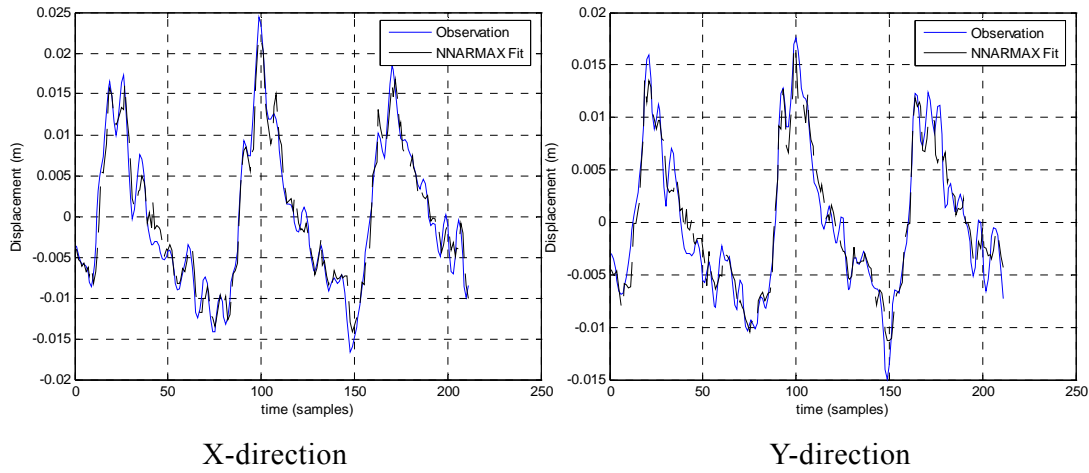


Figure 3.8 Displacements output of the NNARMAX models for the tower displacements

Table 3.2 Parameters of NNARMAX models of the towers displacements in the X and Y-directions

Displacement direction	NNARMAX [na,nb,nc,nk]	λ_0	FPE	R ²
X	NNARMAX[4 ,4 2,1 2,1 4]	1.83e-6	2.93e-6	0.90
Y	NNARMAX[5 ,4 1,1 1,5 3]	1.67e-6	2.59e-6	0.86

NNARMAX models with the capability of taking into account the previous input–output and stochastic quantities and the time lag of the system were used to define the transfer functions of the tower displacements. These models can be quite difficult to set up when there is more than one input quantity. Insignificant input parameters and outliers in the observations significantly increase the difficulty of setting up the NNARMAX models. For this reason, results of the robust fit regression analysis were used to facilitate the definition of NNARMAX models of the tower displacements in Equation 3.6. A number of NNARMAX models with different orders of complexity and time lags were considered in the selection of the proper order of complexity and time lag. Parameters of these models were predicted with the least square method. NNARMAX models with the minimum λ_0 , FPE and maximum R-square values were selected as the proper models to express the tower displacements (Table 3.2).

Each of the models presented in Table 3.1 have different orders and time

lags. In the selection process for the proper model for the tower, the residuals predictions of the models were tested to see whether they are within the ACF confidence interval. It was seen that the model corrections are within the ACF $\lambda(m)(-u_{1-\alpha/2} \text{ srm} < \lambda(m) < u_{1+\alpha/2} \text{ srm})$ confidence interval (Figure 3.9). ACF (for $m > 0$) has a normal distribution with an average value of zero and a standard deviation of $\text{srm} \approx 1/\sqrt{n} \cdot \alpha$ assumed significance level, $u_{1-\alpha/2}$ is the standard normal variable in the $1-\alpha/2$ probability. The ACF confidence interval for $\alpha=0.05$ is $\pm 1.96/\sqrt{n}$. Here, n is the number of observations.

The displacement outputs of the NNARMAX models (Table 3.2) and the field observations of the tower displacements are presented in Figure 3.8. It can be seen from these figures that the model outputs are very conformity with the field observations. ACF and 95% confidence intervals of the model residuals of NNARMAX describing the X and Y displacements of the towers are also presented in Figure 3.9.

In the definition of the tower displacements of the Bridge with NNARMAX models, time lags were taken into account as well as the previous input and output quantities. These types of models reflect the definition of dynamic systems as “systems that store energy and release it over a time span”. Hence, the tower displacements of the bridge were modeled with NNARMAX models shown in Table 3.1 which have the capability of modeling dynamic response^[87].

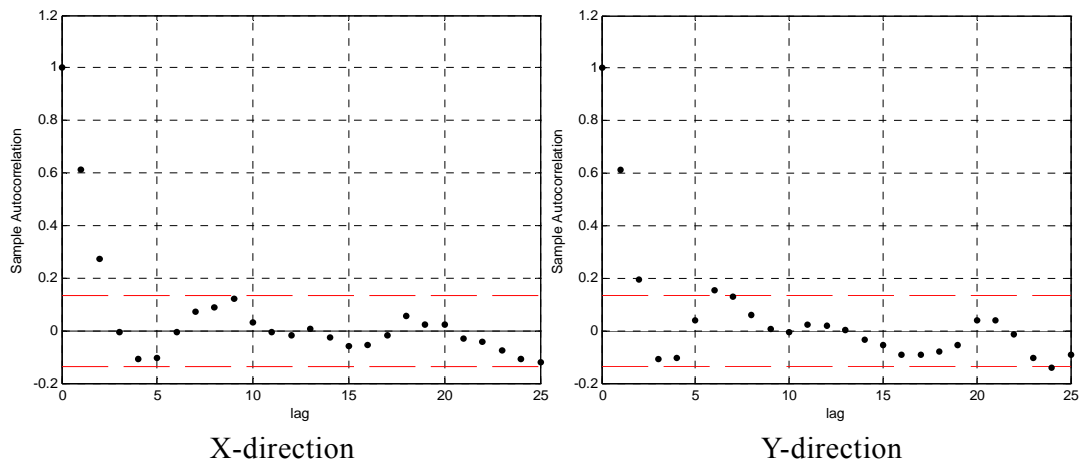


Figure 3.9 ACF and 95% confidence intervals of NNARMAX models describing the displacements of the tower (time lag (h))

The ACF and 95% confidence intervals of the residuals for the NNARMAX models for two directions, which presented in Table 3.2 and the static robust multiple regression NNARMAX [0100] models used to describe to the displacements of the tower in the two directions, were presented in Figures 3.9–3.10. There were a loss of information in the static models describing the tower displacements in the two directions which can be seen in Figure 3.10 as the residuals of ACF of static NNARMAX [0100] models for the X and Y tower displacements were out of the confidence interval $\pm 1.96/\sqrt{n}$ for $\alpha=0.05$. Residuals for the NNARMAX [4411] and [5415] models, however, remained in the boundaries of the ACF confidence interval and there was no loss of information in the description of the X and Y tower displacements as can be seen in Figure 3.9.

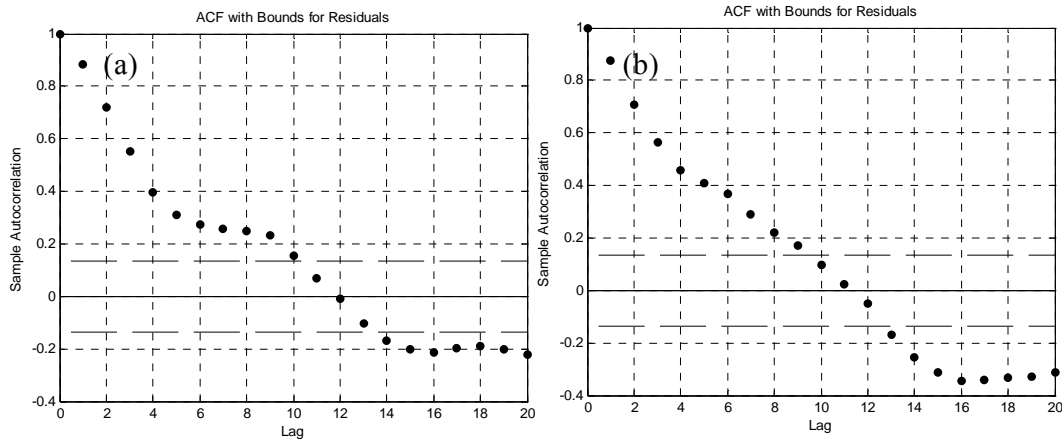


Figure 3.10 ACF and 95% confidence intervals of the residuals for the static multiple regression NNARMAX0100 model used to describe the displacements of the tower in the X (a) and Y (b) directions (time lag (h)).

The fact that, λ_0 , FPE and R-square values (Table 3.1) of the robust fit regression models are higher and less, respectively, than those of the NNARMAX models (Table 3.2), confirms the selection of NNARMAX for modeling the displacements response of the bridge towers.

3.6 Summary

The robust fit regression models have good capacities for mapping the relationship between the applied loads effects factors and displacements of the tower. Temperature and humidity effects on the entire model shapes are insignificant.

The predicted models reflect the behavior of the bridge tower displacements were a general increase in the number of vehicle on the bridge, and the traffic loads are the main factor for the tower displacements, and NNARMAX [4411] and [5415] models were found to be suitable for obtaining the tower displacements.

Chapter 4 Bridge Deformation Monitoring Based on GPS/ Accelerometer Integration Technique

4.1 Introduction

Global Positioning System (GPS) with 10–20 Hz sampling rates has become a useful tool for measuring and monitoring static, quasi-static and dynamic responses in long-period civil engineering structures exposed to gust-winds, traffic, earthquakes or temperature variation.

Accelerometers have been used extensively for bridge dynamic monitoring using the force measurements directly. These sensors are used to sense accelerations. Compared with other surveying systems such as a surveying total station, accelerometers have some special advantages when they are used for bridge monitoring. The sampling rate of an accelerometer can reach several hundred Hz or even higher depending upon application requirements, which is a very important characteristic when monitoring a bridge with high dynamics^[83]. However, this chapter analyzes movement and damage to the Bridge based on data collections from GPS and Accelerometer instruments.

4.2 Bridge Deformation Monitoring Based on GPS and Accelerometer background

Due to the severe environments encountered in the bridge deflection monitoring, the instruments used must be lightweight, portable, reliable, and easy to install. The results must be easy to interpret. These are of great importance under extreme loading scenarios such as strong wind, volcanic eruption, and earthquake shock. At the same time, for correctly interpreting the dynamics of monitored bridges, the measurements should meet accuracy specification requirements. This means the deflections of the bridge should be measurable with available surveying instruments. For instance, in order to measure centimetre level deflections the internal accuracy of a GPS receiver should be better than a few millimetres level, and multipath and other error sources should be

appropriately mitigated or modelled.

Conventional surveying methods such as levelling have been used in the past to monitor static displacements of engineered structures with millimetre level or higher accuracy, and will certainly continue to be used in the future. Modern leveling sensing stations could provide one-dimensional 2-millimetre accuracy at a sampling rate of 2.56 Hz ^[28]. Surveying robots, EDM, Theodolites, surveying total stations, photogrammetry, and other surveying instruments could be employed to monitor structural deformation. However, the inherent disadvantages of these terrestrial surveying systems have greatly limited their applications. The main disadvantages of these surveying approaches are as follows:

- A) Long-term intervals between measurements (days or even months)
- B) Averaging of data over a relatively long time span (often some hours are smoothed which leads to smoothing effects that could hide real movements of the stations)
- C) Relatively low data sampling rate and a poor level of automation
- D) Batch mode analysis (data is collected, transmitted to a computer and evaluated a few hours later).

Due to the above limitations of terrestrial surveying methods, they cannot be employed to monitor structures with dynamic structural deflection and semistatic movements at the same time. Accelerometers have been used extensively for bridge dynamic monitoring. These sensors are used to sense accelerations, and triaxial accelerometers could measure three orthogonal accelerations simultaneously. Compared with other surveying systems, triaxial accelerometers have some special advantages when they are used for bridge monitoring. The sampling rate can be 1000 Hz depending upon application requirements, which is a very important characteristic when monitoring a bridge with high dynamic. Triaxial accelerometers are superior to other sensors since they are not dependent on propagation of electromagnetic waves, and therefore avoid the problems of refraction, line of sight connections to the terrestrial or space objects, and do not have visibility problems caused by weather. An accelerometer could form a completely self-contained system, utilising only measurements of accelerations to infer the positions of the system, through integration based on the laws of

motion.

However, the positional drift of an accelerometer grows extremely rapid with time and can reach hundreds of meters after intervals of several hours^[49]. The main error sources come from the instrumental biases and scale factor offsets and the unknown gravity of the earth. In normal applications, continuous updating is used to avoid error accumulation. These are operations, which allow the errors either to be directly measured or to be modelled. The most common update is the Zero Velocity Update (ZUPT). Another method is the Coordinates Update (CUPT). It is the need to update that has severely restricted the widespread applications of accelerometer technology as a standalone positioning method in surveying. In bridge deflection monitoring, it is impossible to conduct ZUPT. Only CUPT aided with GPS fixes could be a realistic option to overcome drift problem of accelerometer^[34].

Like accelerometers, tiltmeters, strain gauges, and other sensors are used to measure deflections and displacements in bridge inspection. These instruments are high cost, complex to install and maintain, and need frequent re-calibration. They are also very vulnerable to the environments. The collected raw data need to be interpreted to obtain direct geometric results, which in many ways is a very complicated procedure. For instance, the vibration periods are very low on long span suspension bridges, and there exist both semistatic and dynamic displacements. It is very difficult for accelerometers to accurately detect these very slow movements of 0.1~0.3 Hz vibration frequencies^[32, 66]. Measurability of the instruments used for bridge monitoring is another issue. The lateral movements are usually activated by the wind loads and the vertical displacements are mainly caused by the change of ambient temperature and traffic loads. These loads will introduce relative small movements in the longitudinal direction. The mean lateral movements of the Akashi Kaikyo Bridge monitored by GPS could reach 5.13m with vibration amplitude of 0.78 m but the longitudinal movements are only several centimeters^[43]. Interferometric synthetic aperture radar (InSAR) could provide dense spatial coverage of the deformation body in a cost-effective manner. It can be used to detect deformation with sub-millimetre accuracy. However, its temporal coverage is limited by the repeat periods of the satellites, which are 35 days for ERS-1 and 44 days for

JERS-1 ^[40]. It is apparent that InSAR techniques could not be used to monitor bridge deformations with high resolutions both temporally and spatially.

Ground-based laser scanning techniques can be used to collect a large amount of precise 3D points of the monitored objects over a range of 5~350m ^[41]. This emerging technique could also be employed to detect surface deformations. However, the technique is limited by range of operation, a low sampling rate, a requirement of semistatic status of the monitored targets, and the long time spent in image processing. All these limitations exclude these techniques from the instrumentation list for long span suspension bridges. Whilst terrestrial surveying methods require line of sight between stations, GPS can conduct unattended, continuous field operations with high sampling rates, and an integrated communications network technique. Reduction of GPS data gathered at a high sampling rate is more complex than it is for conventional surveying methods. Robust automation of highly precise GPS data collection, quality control, data processing, and analysis, are all now reasonable routine. GPS does not have range limitation and it is explicitly connected to an absolute reference frame. Hyzak (1997) summarized some advantages of GPS for structural deflection monitoring ^[61],

- 1) All weather observations
- 2) Various levels of accuracy to meet different application requirements, for instance GPS could provide 1 cm (instantaneous) to 1 mm (with averaging) positioning accuracy
- 3) 3D positions in a uniformly defined world reference (WGS84)
- 4) Continuous monitoring with data rates up to 20 Hz
- 5) Automated operation with less human intervention, and near real-time capability
- 6) Kinematic methods for efficient data collection
- 7) No long-term sensor drifts (in fact, the accuracy of a GPS observable can be increased over time).

GPS observations can also serve as the spatial reference frame for other types of measurements such as those from accelerometers and strain gauges. GPS can be integrated with other sensors to form a totally automated and continuously operating system. As an increasingly developing technology, GPS has its own

limitations aforementioned when it is used to monitor long flexible structures. In general, GPS accuracy depends on a geometric distribution of the satellites. It could be very difficult to obtain ideal DOP values for precise real-time GPS positioning all the time, depending on the location, because of the deficiency of the design of satellite sky distribution. GPS has limited measurement redundancy in real-time kinematic positioning mode. With pure GPS techniques, the level of redundancy is insufficient to monitor the quality of the observations. Loss of lock to satellite signals due to the signal blockages by surroundings and the changes of satellite geometry, and also bridge deformations, is another major problem for kinematic GPS bridge monitoring. It will introduce new ambiguities to be solved. For instance the mean lateral movements at midspan of the Akashi Kaikyo Bridge could be larger than 5m with over 2m vibration in the typhoon seasons ^[42], exhibiting itself a typical deformation behavior of such type of bridges. Signal recapturing usually takes time, depending on the receiver quality and observation conditions, and will cause discontinuous observations. Relatively low data rate (maximum 20 Hz currently) could not meet the requirement to monitor higher structural dynamics. For example, this sampling rate is insufficient to monitor the vibration frequency higher than 10 Hz (Nyquist frequency $> 10\text{Hz}$).

Multipath signature is still the bottleneck for the highly precise bridge monitoring, even though many efforts have been put into this field at the very beginning of GPS positioning, practical and efficient approaches to mitigate the impacts of multipath are needed to be further investigated. Tropospheric delay could cause problems as well when GPS is used for flexible structure monitoring in a real-time kinematic mode. The difference in tropospheric delay patterns on two ends of a baseline could introduce several centimetre position errors due to the unequally distributed water vapor between rover and reference stations, and temperature or humidity. This will produce a varying time series of relative tropospheric delay into the kinematic positioning solutions, which will distort the reasonable interpretation of bridge deflection. To cope with this, meteorological parameters can be employed. Since averaging techniques cannot be used, it will be very difficult to maintain the positioning accuracy on each epoch basis in the kinematic mode. It has been found that there are significant interferences that come from ambient environmental factors. Examples are dense cables and

passing vehicles obstructing the GPS signals, which will cause cycle slips and multipath. Roberts et al reported outliers of several decimeters in the Humber Bridge positioning solutions, which might have been introduced by the cycle slips^[32]. A lot of other studies have also revealed that the special observation environments and particular characteristics of multipath signatures make the mitigation techniques a restriction for GPS engineering applications^[16].

GPS receivers integrated with triaxial accelerometers could provide an improved overall system in terms of productivity and reliability. The sensor integration and data fusion techniques need to be further studied. Interpretation and comparison of GPS positioning solutions with the results predicted by models or measured by other techniques are important in GPS/accelerometer based BDMS. The methodologies, algorithms, and visualisations of the results need to be developed. The findings and conclusions from these studies are based on the author's initiatives. Suspension bridges are capable of movements from a few decimetres to metres at the middle spans, under wind and traffic loadings or dead loadings from earthquake shocks. With the above endeavours, the use of kinematic on the fly (OTF) GPS positioning technique aided by triaxial accelerometers at strategic points upon the bridge decks should enable accurate and detailed monitoring of the bridge's dynamic responses. Such real-time system could be used to monitor the performance of the bridge at different loadings and warn of potentially dangerous bridges. Moreover, future bridge designs and traffic management schemes could also benefit from such a deformation monitoring system through more detailed understanding of the relationship between loading and response.

4.3 GPS/Acceleration integration analysis Tower bridge movement

In this section, the data of south tower of Bridge was collected in January 17 2008 from 12:00 PM to 13:00 PM. The analysis was based on the data collection in the X and y-directions, since the movement in these directions are greater than in Z-direction, thus the data in Z-direction were declined.

4.3.1 Wden Matlab Function (WMF)

Function `wden` is exploited to eliminate noises of one dimension time series in MATLAB wavelet analysis packet automatically. There are four kinds of method of selecting the threshold, and “soft”, “hard” threshold eliminating noises. Furthermore, there are global or decomposed layers threshold available for selecting also. The trend components in the series were investigated from the obtained data within `Wden` analysis. However, function `Wden` is a more common processing method for eliminating one/two dimension signal noises or compressing disposal, which is a numbered threshold processing of wavelet decomposed coefficients. One can select one processing method for his special objects. The four processing choices are as follows [74, 77].

1. “`rigsure`” is an adaptive threshold choice based on unbiased probability estimating principle of quadratic equations, which defines a threshold ε , and obtains its probability estimators; then minimizes ε to get the threshold (selected). It’s a soft threshold estimator.

2. “`sqtwolog`” uses a fixed form of threshold, and its value is equal to $\sqrt{2 \cdot \log(\text{length}(X))}$.

3. “`heursure`” is a integrated one by the former two choices, optimal predicting variable threshold. When Signal-to-Noise ratio (SNR) is very small, and “`rigsure`” estimating comes into being very big noises. In this case, one can uses “`sqtwolog`” choice with a fixed threshold.

4. “`minimaxi`” uses also a form of fixed threshold, and comes into being a maximum value of minimized mean square errors. In statistics, the maximum value principle is exploited to design an estimator, and can minimize maximum mean square errors in the given function groups

4.3.2 GPS Displacement

For analyzing the signals of GPS measurements, a preprocessing should be done first. That is to delete noises and extract useful signals. Wavelet analysis is a strong tool to eliminate noises according to the noise characteristics. Function `wden` is exploited to eliminate noises of one dimension time series in Matlab

wavelet analysis packet automatically. There are four kinds of method to select the threshold, and “soft”, “hard” threshold eliminating noises. Furthermore, there are global or decomposed layers threshold available for selecting also. In this study, within the wden function, heursure is used to eliminate and compact the noises [77]. Displacement measurements were performed on January 17, 2008 from 12.00 PM to 1.00 PM. The original displacement history measurements in X and Y directions (local coordinates) on the tower were extracted using Wden function as presented in Figure 4.1.

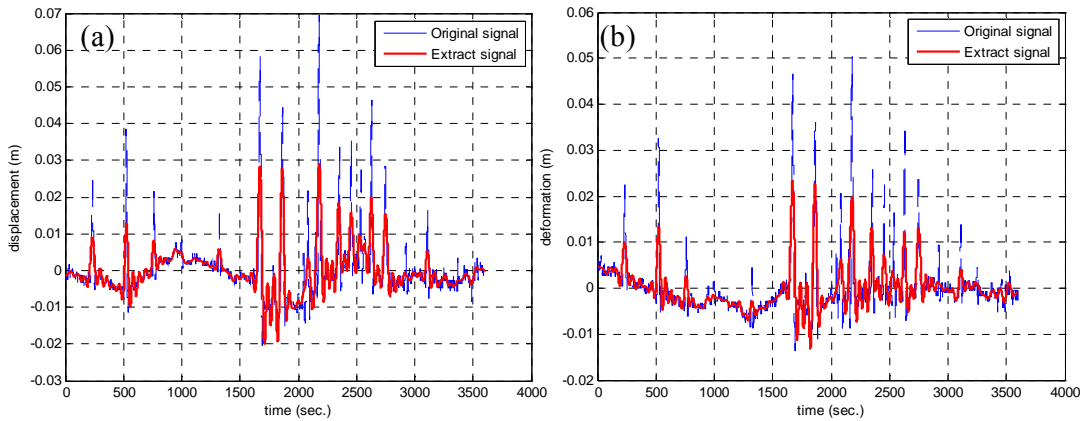


Figure 4.1 Time history of movement of a southern tower bridge in (a) X and (b) Y-directions

The trend components in the series were investigated from the obtained data within wden analysis. The trend component in the series represents the long-term changes related to time and it can be defined by a polynomial function in the time domain. The transformation of the series without trend components from time domain to frequency domain is performed using Fast Fourier Transform (FFT) which is not different from Discrete Fourier Transform (DFT). It is an effective and excellent algorithm for the calculation of DFT. Yet as DFT has periodic characters, it is assumed that the final sample of the signal is followed by an initial sample of the signal in the spectrum calculation. In this case, a spectral leakage occurs as a result of the signal energy leakage to other frequencies.

In order to minimize this effect, it is proposed to multiply the signal by window function as expressed in Equation 4.1. This function characterizes with amplitude slowly approaches zero at the edges before the transformation is

performed.

$$w(i+1) = 0.54 - 0.46 \cos\left(2\pi \frac{i}{n-1}\right) \quad (4.1)$$

FFT is applied to $Y(t_{ip}) = Y(t_i) * w(i)$ windowed observations, $X(n)$ FFT coefficients in Equation 4.2 are obtained.

$$X(n) = \sum_{t_i=0}^{N-1} Y(t_{ip}) e^{-jn \frac{2\pi}{N} t_i} \quad (4.2)$$

For $0 \leq n \leq N - 1$, the calculation of $X(n)$ in Equation 4.2 requires N complex multiplications and $N - 1$ complex sums. Computing all the N of the $X(n)$ values demands N^2 complex multiplications and $N^2 - N$ complex additions. The FFT coefficients $X(n)$ are in the complex plane but this representation does not aid interpretation. Therefore, the power of the FFT signal is:

$$P_{XX}(n) = |X(n)|^2 \quad (4.3)$$

$P_{XX}(n)$ values are calculated with the use of Equation 4.3 and dominant frequencies in the series are determined by the density frequencies of the signal.

The natural frequency ranged from $0.01N$ to $0.50N$, where N is the number of story ^[105]. In this case, the tower height of Bridge is 62.50 m. approximately; it was assumed that, the height of story equal to 2.80 m and the tower frequency is between 0.22 to 11HZ. In addition, the frequency components of the bridge towers were calculated to be not more than 0.2 Hz. The first mode natural frequencies of the southern tower bridge were shown in Figures 4.3. From these Figures, it was found that the GPS and accelerometer values in the X-direction are 0.32 Hz and 0.41Hz, respectively, whereas these values were found to be 0.31 Hz and 1.1 Hz, respectively in the Y-direction.

As shown in Figure 4.1, the displacement in the X-direction is found to be between -20.02 and 28.91 mm with average value of 1mm, whereas it was found to be between -13.02 and 23.38 mm with an average value of 0.80 mm in the Y-

direction. Figure 4.1 also revealed that the average directional displacement can be construed as a static component of the displacement while its dynamic component can be verified to be approximately 1mm. The average wind speed during the observation period of the tower displacement measurements using the GPS was 2.50 m/s with the prevalent wind direction of 25° (Figure 4.2).

These results revealed that the loads and traffic velocities affect the towers movements, and the tower was moved in the opposite direction of the wind since the wind speed is equal to 2.50 m/s (normal speed). In addition, it can be seen that the temperature has lower effects on the deformation, since the difference in temperature was found to be 1.75°C (see Figure 4.2c).

From Figure 4.1, it was found that the residuals between the original and the extracted signals are 5.97 cm. This suggests that the GPS signals noise is high. As well as, it can be seen that the Wden function processing caused an increased in the signals accuracy by 20%. Therefore, it's recommended to use wden function for GPS signals extraction.

The obtained data from wavelet analysis were used to plot the power spectral density in X and Y directions as shown Figures 4.3 and 4.5. From these Figs, it can be seen that the power in the X direction is greater than that in the Y direction. This indicates that the power spectral density is a good parameter to detect the tower movements and this observation complies with the results obtained by ^[106].

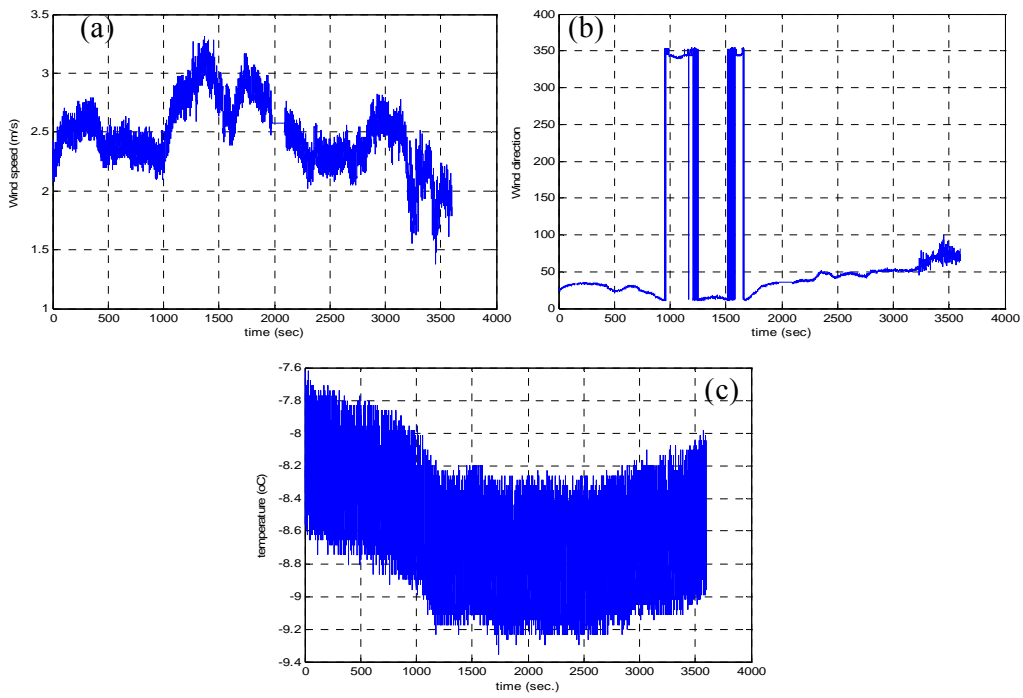


Figure 4.2 Time history of wind and temperature for the bridge (a) speed, (b) direction and (c) Temperature.

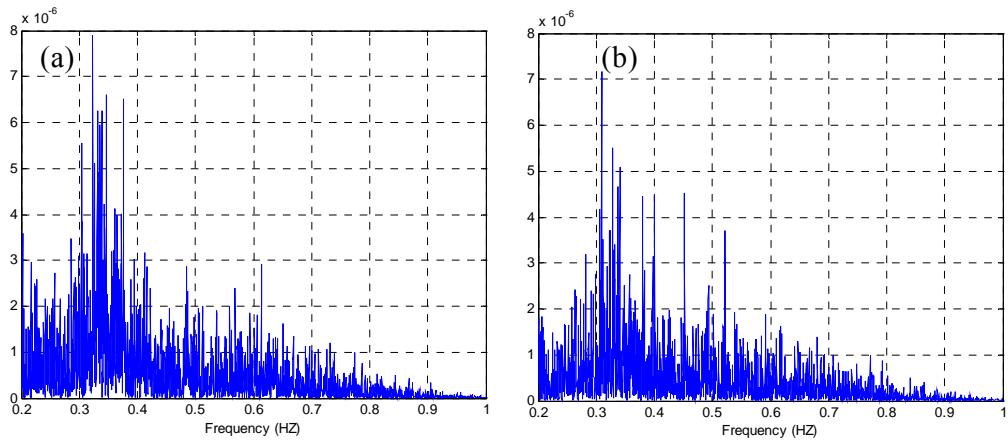


Figure 4.3 Fundamental natural GPS signal frequency plot: (a) X-axis frequency; (b) Y-axis frequency

4.3.3 Acceleration measurements

Figure 4.4 shows the values registered by the accelerometer at a 100 Hz-data rate on the same time of GPS observation. It is possible to note that the output is quite noisy. In spite of that, the accelerometer values obtained have an absolute range variation of 2.42 m/s^2 and 0.14 m/s^2 with average 0.01 m/s^2 and 0.00 m/s^2 in X and Y-directions, respectively.

The FFT was applied to a 2×10^{16} sample of accelerometer data and the frequency spectrum results are shown in Figure 4.5.

From Figure 4.4, it can be seen that the range and the acceleration average in the X direction are too high, which indicates that the tower movements in X-direction are critical. In addition, it can be seen that there is a difference between the calculated frequency from GPS signals and that calculated from Accelerometer signals. This reveals that the GPS system can be used to measure the deformation. Due to its signals errors, GPS can not used to measure the high frequency for the dynamic behavior of the tower. Thus, an accelerometer must be added to the monitoring systems for measuring the high frequency of such a structure.

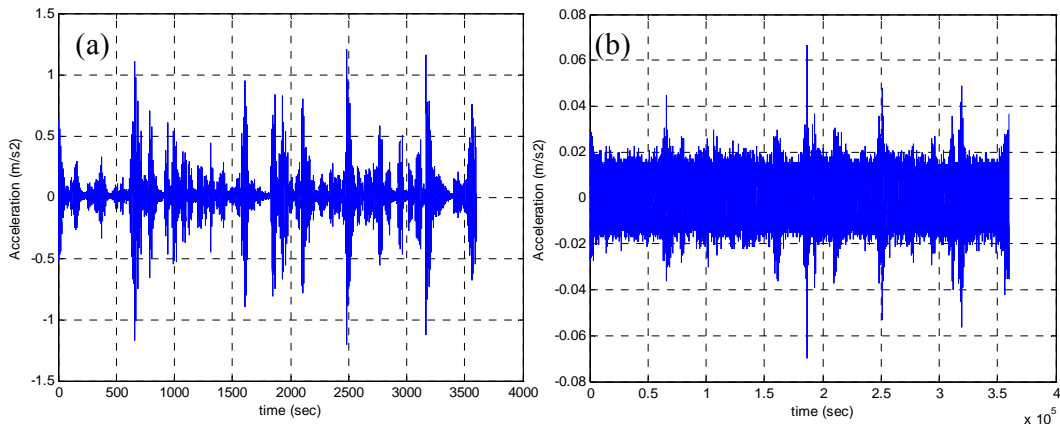


Figure 4.4 Time history of accelerometer the southern tower bridge (a) X and (b) Y-directions

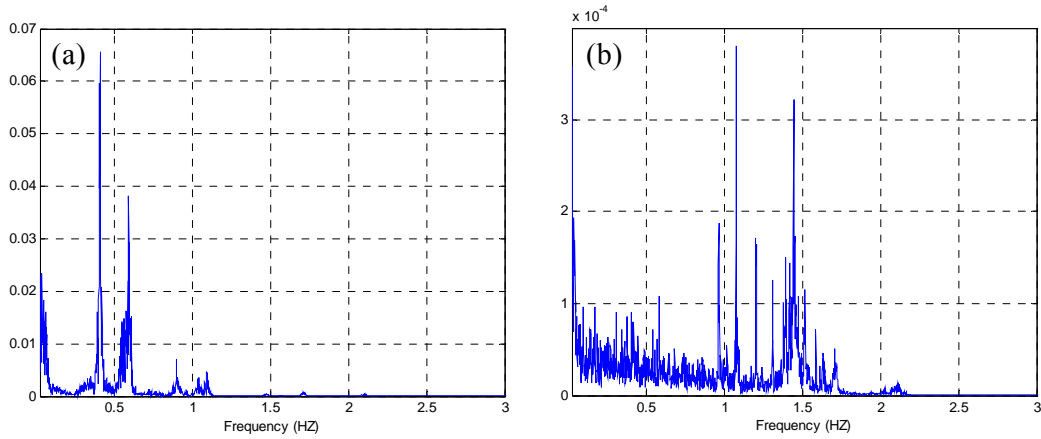


Figure 4.5 Fundamental natural Accelerometer signal frequency plot: (a) X-axis frequency; (b) Y-axis frequency

4.3.4 Torsional displacement

The tower displacements consist of horizontal displacement in the X and Y-axis as well as torsional displacement. For this reason it is assumed that the first coordinates observed denote GPS₁ coordinates as (X₁, Y₁) and next observations are GPS_i coordinates as (X_i, Y_i), so the torsion displacements T(t) are measured from the first coordinates observed. The T(t) and the coordinates values at time t are computed as:

$$T(t) = \tan^{-1}\left(\frac{\Delta Y(t)}{\Delta X(t)}\right) = \tan^{-1}\left(\frac{Y_i(t) - Y_1(t)}{X_i(t) - X_1(t)}\right) \quad (4.4)$$

The computed T(t) values of the tower are shown in Figure 4.6a. In general, a tower bridge is assumed to be as a rigid diaphragm with infinite stiffness. Therefore, the distance between two GPS stations (i.e. GPS coordinates) may maintain zero m during the measurement periods.

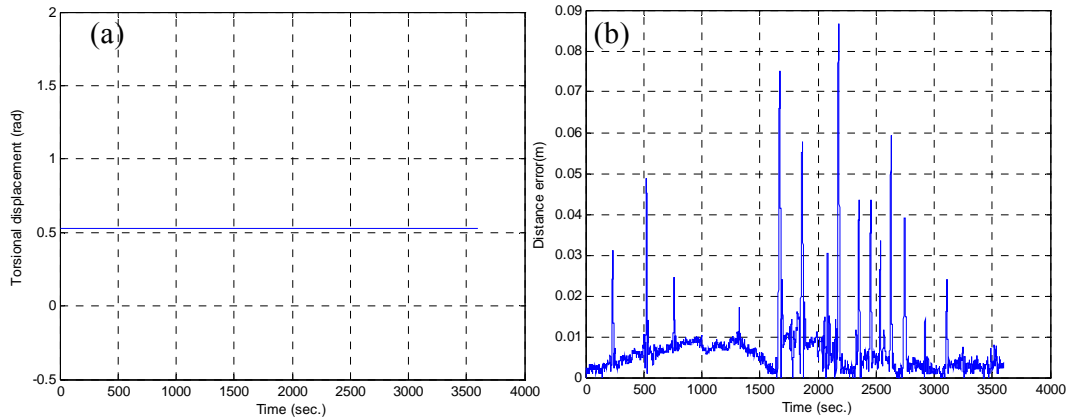


Figure 4.6 (a) Torsion displacement; (b) the distance error between the first and series positions

The distance error between two GPS stations during the measurement periods can be computed as follows:

$$\Delta S = \sqrt{(\Delta X)^2 + (\Delta Y)^2} \quad (4.5)$$

Using this distance error we can indirectly evaluate the accuracy of the GPS displacement measurement system. The computed distance error between two GPS stations measurements as shown in Figure 4.6b are maintained with on 8 cm range.

Figure 4.6a shows that the $T(t)$ is equal to 0.51 radian and the distance errors in almost of all the observation period didn't exceed 1cm, which indicates that the tower movements are affected by the traffic loads. In addition, this Figure indicates that the GPS signals contain a complex error, which affects the accuracy of the calculated deformation values.

4.3.5 Deformation analysis

Deformation analysis is performed using the certain epoch's results. F-test statistical analysis is adopted to find out the deformation in the tower. In this study, the statistical analysis of the deformations obtained from wden Matlab function is based on the first observation group as shown in Figure 4.7 (i.e. this group is considered as a datum group and consists of the first 3 sec observations).

The time series of the next groups in X-direction are related to the first group and are calculated as shown in Equations: 2.7-2.9.

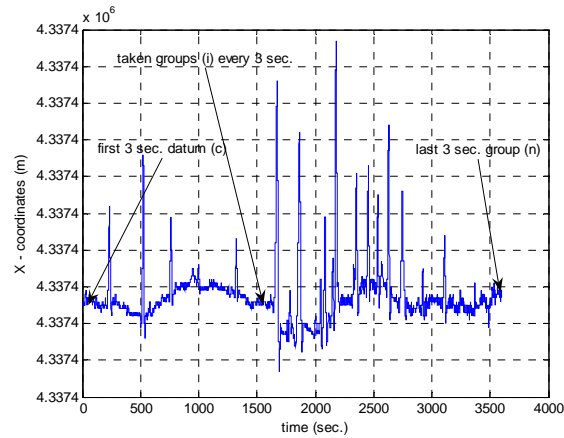


Figure 4.7 continuous deformation analyses Scheme

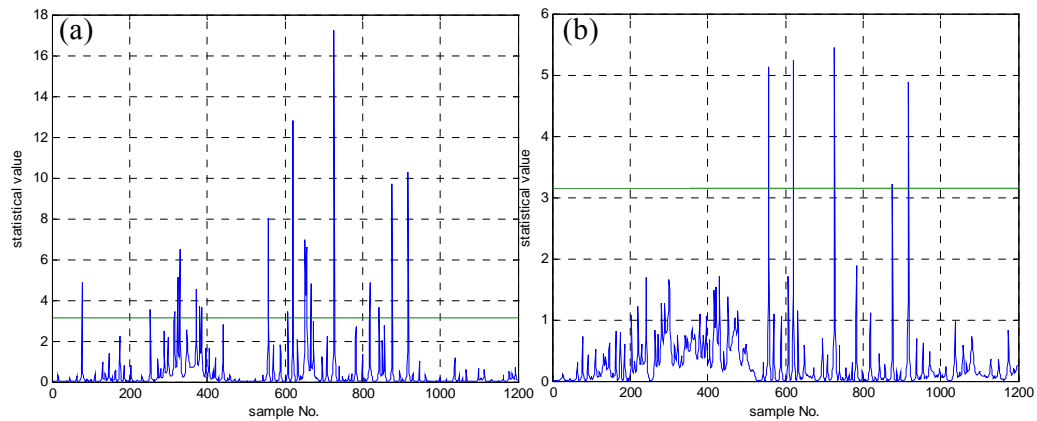


Figure 4.8 continuous deformation statistical tests (a) X-direction; (b) Y-direction

From statistical analysis (Figure 4.8), it can be seen that the tower movements are very clear in time periods from 400 to 900 sec in X-direction and 1600 to 2600 sec in both directions (i.e. X and Y-directions). These indicate that the movements of tower are not susceptible to the environmental effects and the results cited in L. Hui et al ^[89] prove this fact.

4.4 Summary

Based on the GPS/Accelerometer integration study, the analysis of the results leads to the following findings:

Matlab Wden function increases signals accuracy by 20%. It is recommended to use the Wden function for GPS signals extraction.

Due to the GPS signals errors, it is not recommended to use the GPS analysis methods for high frequency dynamic behavior of bridge towers. Thus, an accelerometer should be added to the monitoring systems for measuring the high frequency movements of the structures, and GPS can be used as a trustworthy tool for characterizing the dynamic behavior of the low frequency bridges.

Conclusions and Recommendations

Concluding Remarks

Based on the Kalman prediction analysis with parametric least square processing study, Kalman and Adaptive filtering process, analysis of the result leads to the following findings:

- 1- The proposed surveying techniques using DGPS and RTK can provide valuable deformation data of the structural members.
- 2- It was found that the calculated coordinates from PLS and KF analysis methods are much close.
- 3- The SD obtained from multiple processing analyses of GPS data was increased significantly. This indicates that more accurate deformation value can be captured, whereas the KF increased the accuracy of the signals by approximately 30%.
- 4- After six months of bridge opening, the maximum deformation was pronounced 48.2 m far from the beginning abutment.
- 5- It was observed that the S-tower was returned to its original case after ten months of traffic opening.
- 6- Based on time series frequency analysis, it was found that the peak frequency values deviate from a constant value along the time axis when non-stationary displacement responses arise, and as an effect of cracks. The unstability of higher power frequency reveals the movements of bridge towers.
- 7- Based on the time series movement analysis, It was found that the bridge cracks are mainly caused by the shear force due to movement of the south tower and the bridge non-linear movements due to traffic loads.
- 8- The SD obtained from AF processing analyses of GPS data increased significantly.

Following are the used environmental, GPS observations and wavelet analysis to propose and analyze the movements and damage detection of the Bridge:

- 1- GPS signals sensitivity is very high to the movements and damage of structures.
- 2- The low frequency analysis results obtained from the power spectrum density reflected the expected damage time of the Bridge.
- 3- The effectiveness damage of the bridge happened in May 2008 and continued in June 2008 with the increasing traffic loads.
- 4- The cracks of the bridge deck bring out the frequency of the bridge tower movement transient characteristics.
- 5- The STFT is a significant step forward from the traditional FFT in terms of structural response analysis.
- 6- The increase of mean or range and SD the detail and approximate coefficients revealed that the damage would occur, so this technique can be used to predict the damage time detection.
- 7- The range of converted acceleration and velocity and its SD revealed that the damage of the bridge might have occurred in between May and July 2008.

Based the geometrical study, results analysis leads to the following findings:

1. Non-linearity between the movement and frequency for the two towers is clearly pronounced in the one period between December 2007 and March 2008.
2. The designed plane and PC geometrical analysis models prove to calculate the long-time structural deformation monitoring easily.
3. Traffic loads, non-linearity movements of the bridge and the south tower movement are the main factors that affect the expected bridge life.
4. Based on the statistical analysis herein. It is recommended to use the plane model for structural monitoring.

In the identification study, we have proposed and analyzed two MISO identification model, the robust fit multiple regression and the neural network ARMAX model. Based on this limited study, the analysis of the results leads to the following findings:

- 1- GPS signals noise contains complex errors, and the signals accuracy obtained from the wavelet analysis (de-noised process) increased by 24%. So, it is recommended to use wavelet analysis in the de-noised process of

GPS signals.

- 2- The robust fit regression models have good capacities for mapping the relationship between the applied loads effects factors and displacements of the tower. Temperature and humidity effects on the entire model shapes are insignificant.
- 3- It has been noted that the robust fit multiple regressions or NNARMAX [0100] behave in a static manner, which can lead to a loss of information used in calculating the tower displacements.
- 4- NNARMAX [4411] and [5415] models were found to be suitable for obtaining the tower displacements. In addition, no loss of information was observed since the residuals of these models stayed within the confidence intervals of the auto-correlation functions.

Based on the GPS/Accelerometer integration study, the analysis of the results leads to the following findings:

1. Matlab Wden function increases signals accuracy by 20%. It is recommended to use the Wden function for GPS signals extraction.
2. Due to the GPS signals errors, it is not recommended to use the GPS analysis methods for high frequency dynamic behavior of bridge towers. Thus, an accelerometer should be added to the monitoring systems for measuring the high frequency movements of the structures.
3. GPS can be used as a trustworthy tool for characterizing the dynamic behavior of the low frequency bridges. With the advancements of the GPS frequency-sampling rate, the dynamic behavior of the bridges in high frequency can be measured.

Recommendations and Future works

Based on the theoretical and analytical study results described in this thesis, the following recommendations are made for further research work.

Theoretical simulations reveal that it is possible to improve the accuracy of the positioning solutions. It needs to be further validated in the actual bridge monitoring. Whilst GLONASS demonstrated its potential by providing

positioning solutions of uniformed accuracy, the integration of GPS with the Galileo satellites to improve satellite geometry for bridge deformation purpose need to be explored.

Augmented GPS systems under development may provide enhanced deformation monitoring capabilities to further improve the accuracy and precision of monitoring results attainable in area similar to those tested within this research. Such systems include Wide Area Augmentation Systems (WAAS), Galileo, and the use of ground based GPS transmitters (pseudolites). Research into these augmentation systems will enhance the robustness of the deformation monitoring system, while also improving the error detection and mitigation capabilities of the deformation monitoring systems.

As adaptive filtering approach has been successfully used to isolate the components from the time series with high level correlation, its capability to process the time series with large deformation is required to be further studied. In this case, the multipath signature will be buried by actual bridge movements but still contaminates the quality of the measurements.

The integrity monitoring model should be further optimized to take into account the fact that multiple rovers can be biased at the same time. In the present study only two rovers have been used on the towers, whereas no rover was setup on the bridge deck, so we recommended a support for RTK-GPS data input from a larger number of rover stations on the deck with the supported sensors options in future.

References

1. R. Farrar, W. Keith. An introduction to structural health monitoring. *Philosophical Transactions of the Royal Society A* (London: Royal Society Publishing), 2006, 365(1851): 303–315. Doi: 10.1098.
2. J. Cooper. World's Longest Suspension Bridge Opens in Japan. *Public Roads*, 1998, 62(1): 32.
3. C. Farrar, S. Doebling, D. Nix. Vibration-Based Structural Damage Identification. *Philosophical Transactions of the Royal Society: Mathematical, Physical & Engineering Sciences*, 2001, 359(1778):131–149. Doi:10.1098/rsta.2000.0717.
4. S. Kashima, Y. Yanaka, K. Mori. Monitoring the Akashi Kaikyo Bridge: First Experiences. *Structural Engineering International*, 2001, 11(2): 120-123.
5. Y. Fujino, M. Murata, S. Okano, M. Takeguchi. Monitoring System of the Akashi Kaikyo Bridge and Displacement Measurement Using GPS. In: A.E. Aktan and S.R. Gosselin (Editors), *Nondestructive Evaluation of Highways, Utilities, and Pipelines IV*, Proceedings of SPIE, 2000.
6. P. Thompson. *Bridge Management 2: PONTIS: the Maturing of Bridge Management Systems in the USA*. Thomas Telford, London, 1993.
7. P. Cross. Prospects for GPS - New Systems, New Applications, New Techniques. *Engineering Surveying Showcase*, 2000, 1:10-14.
8. C. Rizos, S. Han, A. Roberts. Permanent Automatic Low-cost GPS Deformation Monitoring Systems: Error Mitigation Strategies and System Architecture, ION GPS'97, 10th Int. Tech. Meeting of the Sat. Div. of the U.S. Inst. of Navigation, Kansas City, USA, September 1997: 909-917.
9. V. Fairweather. Measuring Bridge Movement. *Civil Engineering*, ASCE, 1996, 66(6): 48.
10. P. Norgard. Deformation Survey of the Storebaelt Bridge: GPS Shows Its Merits. *Geomatics Info*, 1996, 10(4):37-39.
11. V. Ashkenazi., A. Dodson, T. Moore, G. Roberts. Monitoring the

- Movements of Bridges by GPS, ION GPS'97, 10th Int. Tech. Meeting of the Sat. Div. of the U.S. Inst. of Navigation, Kansas City, USA, 1997: 1165-1172.
12. A. El-Rabbany. Introduction to GPS The Global Positioning System. Artech House, Boston. London, 2002.
 13. J. Leva. An alternative closed-form solution to the GPS pseudo-range equations. Aerospace and Electronic Systems, IEEE Transactions, 1996, 32(4):1430 – 1439.
 14. Javad navigation systems inc. <http://www.javad.com/index.html?/jns/gpstutorial/Chapter3.html>.
 15. M. Meo, E. Luliano, A. Morris. Health Monitoring of Large Scale Civil Structures, Cranfield University, 2002.
 16. G. Roberts, A. Dodson, V. Ashkenazi. Twist and Deflection: Monitoring Motion of Humber Bridge. GPS World, 1999,10(10):24-34.
 17. Y. Xu, D. Sun, J. Ko, J. Lin. Fully Coupled Buffeting Analysis of Tsing Ma Suspension Bridge. Journal of Wind Engineering and Industrial Aerodynamics, 2000, 85:97-117.
 18. C. Rizos, S. Han, L. Ge, H. Chen, Y. Hatanaka, K. Abe. Low-cost Densification of Permanent GPS Networks for Natural Hazard Mitigation: First Tests on GSI's GEONET Network. Earth Planets Space, 2000, 52:867-871.
 19. K. Hudnut, Y. Bock, J. Galetza, F. Webb, W. Young. The Southern California Intergrated GPS Network (SCIGN). Deformation Measurements and Analysis, 10th International Symposium on Deformation Measurements, March 2001, Orange, California, USA, 2001:129-148.
 20. F. Teferle, R. Bingley, A. Dodson, N. Penna, T. Baker. Using GPS to Separate Crustal Movements and Sea Level Changes at Tide Gauges in the UK. In: H. Drewes (Editor), Vertical Reference Systems. International Association of Geodesy Symposium, Springer-Verlag, 2001.
 21. F. Brunner, H. Hartinger, B. Richter. Continuous Monitoring of Landslides Using GPS: a Progress Report. In: S.J. Bauer and F.K. Weber

- (Editors), Proc. Geophys. Aspects of Mass Movements, Austrian Academy of Sciences, Vienna,2000:75-88.
22. T. Forward, M. Stewart, N. Penna, M. Tsakiri. Steep Wall Monitoring Using Switched Antenna Arrays and Permanent GPS Network. Deformation Measurements and Analysis, 10th International Symposium on Deformation Measurements, March 2001, Orange, California, USA, 2001:33-41.
 23. K. Hudnut, T. Behr. Continuous GPS Monitoring of Structural Deformation at Pacoima Dam, California. Seismological Research Letter, 1998, 69(4):299-308.
 24. J. Lovse, W. Teskey, G. Lachepelle, and M. Cannon. Dynamic Deformation Monitoring of Tall Structure Using GPS Technology, Journal of Surveying Engineering, 1995, 121(1):35-40.
 25. J. Guo, S. Ge. Research of Displacement and Frequency of Tall Building under Wind Load Using GPS, ION GPS'97, 10th Int. Tech. Meeting of the Sat. Div. of the U.S. Inst. of Navigation, Kansas City, USA, September 1997:1385-1388.
 26. Y. Fujino, M. Murata, S. Okano, M. Takeguchi. Monitoring System of the Akashi Kaikyo Bridge and Displacement Measurement Using GPS. In: A.E. Aktan and S.R. Gosselin (Editors), Nondestructive Evaluation of Highways, Utilities, and Pipelines IV, Proceedings of SPIE, 2000.
 27. G. Roberts. Kinematic GPS. PhD Thesis, The University of Nottingham, 1997.
 28. K. Wong, K. Man, W. Chan. Monitoring Hong Kong's Bridges: Real-Time Kinematic Spans the Gap. GPS World, 2001, 12(7):10-18.
 29. B. Harvey. Transformation of 3D coordinates. The Australian Surveyor, 1986, 33(2):105-125.
 30. R. Bingley, A. Dodson, N. Penna, N. Teferle, T. Baker. Monitoring the Vertical Land Movement Component of Changes in Mean Sea Level Using GPS: Results from Tide Gauges in the UK. J. of Spatial Engineering,2001, 3(1):9-20.
 31. C. Young. Single Frequency OTF Kinematic GPS Bridge Deflection Monitoring. MSc Thesis, The University of Nottingham, 1998.

32. G. Roberts, X. Meng, A. Dodson. Using Adaptive Filtering to Detect Multipath and Cycle Slips in GPS/Accelerometer Bridge Deflection Monitoring Data, FIG XXII International Congress, Washington, D.C. USA, April 19-26, 2002.
33. G. Roberts, X. Meng, A. Dodson, E. Cosser. Geodetic Signal Diagnosis and its Applications to Structural Deformation. 2nd Symposium on Geodesy for Geotechnical and Structural Engineering, Berlin, 2002.
34. G. Roberts, X. Meng, A. Dodson. Structural Dynamic and Deflection Monitoring Using Integrated GPS and Tri-axial Accelerometers, ION GPS'2000, 13th Int. Tech. Meeting of the Sat. Div. of the U.S. Inst. Of Navigation, Salt Lake City, USA, 2000:59-68.
35. G. Roberts, X. Meng, C. Brown. The Use of GPS for the Measurement of Bridge Movements: A Viability Study, The University of Nottingham, Brunel University, 2000.
36. G. Roberts, X. Meng, A. Dodson. The Use of Kinematic GPS and Triaxial Accelerometers to Monitor the Deflections of Large Bridges. Deformation Measurements and Analysis, 10th International Symposium on Deformation Measurements, Orange, California, USA, 2001:268-275.
37. G. Roberts, X. Meng, A. Dodson. Data Processing and Multipath Mitigation for GPS/Accelerometer Based Hybrid Structural Deflection Monitoring System, ION GPS'2001, 14th Int. Tech. Meeting of the Sat. Div. of the U.S. Inst. of Navigation, Salt Lake City, USA, 2001:473-481
38. X. Meng, G. Roberts, A. Dodson, E. Cosser, C. Noakes. Simulation of the Effects of Introducing Pseudolite Data into Bridge Deflection Monitoring Data. 2nd Symposium on Geodesy for Geotechnical and Structural Engineering, Berlin, 2002.
39. W. Chen. Integration of GPS and INS for Precise Surveying Applications. PhD Thesis, The University of Newcastle Upon Tyne, 1992.
40. L. Ge, S. Han, C. Rizos. The Double Interpolation and Double Prediction (DIDP) Approach for InSAR and GPS Integration, The International Archives of Photogrammetry and Remote Sensing (IAPRS), XXIII, Amsterdam, Holland, 2000:205-212.

41. S. Gordon, D. Lichti, M. Stewart. Application of High-Resolution, Ground-Based Laser Scanner for Deformation Measurements. Deformation Measurements and Analysis, 10th International Symposium on Deformation Measurements, Orange, California, USA, 2001:23-32.
42. S. Kashima, Y. Yanaka, K. Mori. Monitoring the Akashi Kaikyo Bridge: First Experiences. Structural Engineering International, 2001, 11(2):120-123.
43. A. Lowry, R. Macleod. PMoSTM - A Real Time Precise DGPS Continuous Deformation Monitoring System, ION GPS'97, 10th Int. Tech. Meeting of the Sat. Div. of the U.S. Inst. of Navigation, Kansas City, USA, 1997:923-927.
44. L. Oliver, C. Stephen. Dynamic load testing of Seiss bridges. <http://ibeton.epfl.ch/publications/199x/burdet95.pdf>, (1995), 1995.
45. W. EL-Dakakhni. Theory of Structures. Assiut University, Egypt, 1995.
46. Joseph S. Engineering and Design- Structural Deformation surveying . U.S Army Corps of Engineering, U.S.A, 2002.
47. L. Robert. Engineering and Design-Deformation Monitoring and Control Surveying . U.S Army Corps of Engineering, U.S, 1994
48. G. Roberts, A. Dodson, V. Ashkenazi. Comparison of GPS Measurements and Finite Element Modeling for Deformation Measurements of the Humber Bridge. Institute of Engineering Surveying and Space Geodesy, U.K, 2000.
49. A. Leick. GPS satellite surveying. Wiley and Sons, New York. U.S, 1990.
50. H. Park, H. Sohn, I. Kim, J. Park. Application of GPS to monitoring wind-induced responses of high-rise buildings. J. Struct. Design Tall Spec. Build. 2008,17:117–132.
51. X. Guochang. GPS Theory, Algorithms and Applications; Second Edition. Springer-Verlag Berlin Heidelberg New York, 2007.
52. B. Hofmann, H. Lichtenegger, J. Collins. Global positioning system: theory and practice, 5th edition, Springer-Verlag, Berlin Heidelberg New York, 2001.
53. R. Hatch. Dynamic differential GPS at the centimeter level. 4th inter.

-
- Geodetic symp. On satellite positioning, Austin, Texas, 1986:1287-1298.
54. D. Rutledge, J. Gnipp, J. Kramer. Advances in real-time GPS deformation monitoring for landslides, volcanoes and structures, 10th FIG int. symp. On deformation measurements, Orange, California, 2001: 110-121.
 55. B. Remondi, G. Brown. Triple differencing with Kalman filtering: making it works. *GPS Solution*, 2000, 3(3):58-64.
 56. J. Behr, K. Hudnut, N. King. Monitoring structural deformation at Pacoima dam, California, using continuous GPS. *Proc. of ION-GPS98*, Nashville TN, USA, 1998:59-68.
 57. J. Van. *GPS for land surveyors*. Ann Arbor Press, Chelsea, Michigan, 1996.
 58. S. Mike, T. Maria. *Long-term Dam Surface Monitoring Using the Global Positioning System*. School of Spatial Sciences, Curtin University of Technology, Australia, 1987.
 59. B. Tolman, B. Craig. An Integrated GPS/Accelerometer System for Low Dynamics, *International Symposium on Kinematic Systems in Geodesy, Geomatics and Navigation*, Banff, Alberta, Canada, 1997.
 60. M. Hyzak, M. Leach. *Bridge Monitoring by GPS*. *Surveying World*, 1995, 3(3):8-11.
 61. M. Hyzak. *Practical Application of GPS to Bridge Deformation Monitoring*, the 64th FIG Permanent Committee Meeting and Symposium, Washington D.C, 1997.
 62. US Coast Guard news release. *Global Positioning System Fully Operational*.
 63. K. Duff. *Deformation Monitoring with GPS, Part 1: System Design and Performance*, *Symposium on Surveying of Large Bridge and Tunnel Projects (FIG)*, 1997.
 64. K. Duff. *Structural Deformation Monitoring with GPS: Operational Issues*, *Conference on Structural Materials Technology*. Texas Department of Transportation, 1998.
 65. USACE. *Engineering Manual (EM 1110-1-1004): Deformation monitoring and control surveying*, Department of the Army, U.S. Army

- Crops of engineers (USACE), Washington, DC 20314-1000, 1994.
66. X. Meng, A. Dodson, G. Roberts. Detecting bridge dynamics with GPS and triaxial accelerometers, *Journal Engineering Structures*, 2007, 29:3178–3184. doi:10.1016/j.engstruct.2007.03.012
 67. Q. Li, J. Wu. Time–frequency analysis of typhoon effects on a 79-storey tall building. *Journal of Wind Engineering and Industrial Aerodynamics*, 2007, 95:1648–1666
 68. M. Filipe, C. Elsa, C. Alvaro. Operational modal analysis and finite element model correlation of the Braga Stadium suspended roof, *Journal Engineering Structures*, 2008, 30:1688–1698
 69. L. Ruben., O. Maria, S. Mauricio. Dynamic characteristics of a long span seismic isolated bridge. *Journal Engineering Structures*, 2003, 25:1479–1490
 70. N. Elsheimy. ENGO 361 Course of least square estimation, Department of Geomatics Engineering, University of Calgary, Canada, 2001. <http://www.wcm2.ucalgary.ca/engo/node/36>
 71. J. Fox. *An R and S-PLUS Companion to Applied Regression*, Thousand Oaks CA: Sage, USA, 2002.
 72. J. Dunnycliff. *Geotechnical instrumentation for monitoring field performance*, 1st Edition, John Wiley&Sons, New York, ISBN 0471096148, 1988.
 73. M. Kaloop. *Leveling by using global positioning system*. M.Sc. Thesis, Mansoura University, Public Works Department, faculty of Engineering, El-Mansoura, Egypt, 2006.
 74. M. Yu, H. Guo, C. Zou. Application of wavelet analysis to GPS deformation monitoring. *Proc. of IEEE/ION PLANS 2006*, San Diego, California, 2006:670-676.
 75. M. Rabah. *Enhancing Kinematic GPS-Ambiguity resolution for medium baselines using a regional ionosphere model in real-time.*, Egypt, 1998.
 76. EMR. *GPS positioning guid.* the department of Energy, Mines, and Resources, Canada, 1995.
 77. Mathworks. *Matlab*, Release 12, The Mathworks, Inc, 2000.
 78. A. Beshr. *Accurate Surveying Measurements for Smart Structural*

-
- Members. M.Sc. Thesis, Mansoura University, Public Works Department, faculty of Engineering, El-Mansoura, Egypt, 2004.
79. C. Goad. Precise positioning with the GPS, In applied Geodesy. Lecturer notes in earth science, Edited by Turner, Springer-Verlag, Berlin, 1987, 12:17-30.
80. S. Han. Quality control issues relating to instantaneous ambiguity resolution for real-time GPS kinematic positioning. *J. of Geodesy*, 1997, 71:315-361.
81. R. Hatch, H. Euler. Comparison of several AROF kinematic techniques. 7th international technical meeting of the satellite division of the institute of navigation, Sat Lake City, Utah, 1994:363-370.
82. RTCM. Recommended standard for differential navstar GPS service, Ver. 2.1, RTCM SC-104, Washington, D.C, 1994.
83. R. Langley. RTK GPS. *GPS world*, 1998, 9(9):70-76.
84. N. Talbot. Centimeter in the field, a users perspective of real-time kinematic positioning in a production environment. 6th international technical meeting of the satellite division of the institute of navigation, Salt Lake city, Utah, 1993:1049-1057.
85. H. Martin. *Matlab recipes for earth sciences*, 2nd Ed. Springer Berlin Heidelberg, New York, 2007.
86. H. Jinglu, H. Kotaro, K. Kousuke. A homotopy approach to improving PEM identification of ARMAX models. *Automatica*, 2001, 37:1323-1334. Doi: 0 0 0 5 - 1 0 9 8 (0 1) 0 0 0 8 1 - 4
87. M. Norgaard. Neural network based system identification toolbox, version2. Tech. Report. 00-E-891, Department of Automation, Technical Un. Of Denmark, 2000.
88. H. Christiaan, R. André, S. Freek. *Introduction to Mathematical Systems Theory Linear Systems, Identification and Control*. Birkhauser Verlag, Basel, Switzerland, 2007.
89. L. Hui, L. Shunlong, J. Ou, L. Hongwei. Modal identification of bridges under varying environmental conditions: Temperature and wind effects. *Struct. Control Health Monit*, 2009 . Doi: 10.1002/stc.319
90. A. Zainal, S. Halim, N. Khairul. A Geodetic Deformation Survey to

- Monitor the Behavior of a Concrete Slab During Its Axial Compression Testing. Proc., 1st FIG International Symposium on Engineering Surveys for Construction Works and Structural Engineering, Nottingham, United Kingdom, 2004. <http://eprints.utm.my/1207/>.
91. R. Kalman. A new approach to linear filtering and prediction problems. Transactions of the ASME, Ser. D, Journal of Basic Engineering, 1960, 82:34–45.
 92. M. Grewal, A. Andrews. Kalman Filtering: Theory and Practice. Englewood Cliffs, NJ: Prentice-Hall, 1993.
 93. W. Gethin, X. Meng, A. Dason. Using Adaptive Filtering to Detect Multipath and Cycle Slips in GPS/Accelerometer Bridge Deflection Monitoring Data. FIG XXII International Congress, Washington, D.C. USA, 2002
 94. L. Hui, Y. Bao, J. Ou. Structural Damage Identification Based on Integration of Information Fusion and Shannon Entropy. Mechanical Systems and Signal Processing, 2008, 22:1424-1440.
 95. L. Hongwei, J. Ou. A remote deformation monitoring system for a cable-stayed bridge using wireless internet-based GPS technology. Proc. 3rd IAG / 12th FIG Symposium conference, Baden, 2006.
 96. J. Ko, Y. Ni. Technology developments in structural health monitoring of large-scale bridges. J. Engineering Structures, 2005, 27:1715–1725.
 97. D. Hearn, M. Baker. Computer Graphics (2nd Edition). Prentice-Hall International Ltd, London, 1994.
 98. C. Armenakis. Displacement monitoring by integrating on-line photogrammetric observations with dynamic. PhD thesis, Department of surveying engineering, University of New Brunswick, Canada, 1987.
 99. R. Azar, H. Shafri. Mass structure deformation monitoring using low cost differential global positioning system device. J. Applied Sciences, ASCE, 2009, 6(1):152-156.
 100. Y. Chen. Analysis of deformation surveys - A generalized method. Department of Surveying Engineering, Technical Report No. 94, University of New Brunswick, Fredericton, N.B, 1983.
 101. M. Acar, M. Özlüdemir, O. Akyilmaz, R. Çelik, T. Ayan. Deformation

- analysis with total least squares. *J. Nat. Hazards Earth Syst. Sci.*, EGU, 2006, 6(4):663-669.
102. V. Janssen. A mixed-mode GPS network processing approach for volcano deformation monitoring. PhD thesis, University of NSW, 2003.
103. S. Patsias, W. Staszewski. Damage detection using optical measurements and wavelets. *Structural Health Monitoring*, 2002,1:5–22.
104. L. Xu, J. Guo, J. Juang. Time-frequency analysis of a suspension bridge based on GPS. *Journal of Sound and vibration*, 2002,254:105-116.
105. R. Nayeri, S. Masri, R. Ghanem, R. Nigbor. A novel approach for the structural identification and monitoring of a full-scale 17-story building based on ambient vibration measurements. *J. smart materials and structures*, 2008, 17:025006(19pp). DOI: 10.1088/0964-1726/17/2/025006
106. H. Erdogan, E. Gulal. The application of time series analysis to describe the dynamic movements of suspension bridges. *J. Nonlinear Analysis: Real World Applications*, 2009,10:910-927. DOI: 10.1016/j.nonrwa.2007.11.013.
107. G. Hart, J. Yao. System identification in structural dynamic. *Journal of the engineering mechanics division, proceedings of the ASME*, 1977,103(66):1089-1104.
108. M. Filipe, C. Elsa, C. Álvaro. Challenges in the Application of Stochastic Modal Identification Methods to a Cable-Stayed Bridge. *Journal of bridge engineering*, ASCE, 2007, 12(6):746-754.
109. L. Ingela. Regressor and Structure Selection Uses of ANOVA in System Identification. PhD-thesis, Department of Electrical Engineering Linköpings universitet, SE–581 83, Sweden, 2006.
110. Y. Pi, N. Mickleborough. Modal identification of vibrating structures using ARMA models. *Jornal of engineering mechanics*, ASCE, 1989, 115(10):2232-2250.
111. J. Weng, C. Loh, J. Lynch, K. Lu, P. Lin, Y. Wang. Output-only modal identification of a cable-stayed bridge using wireless monitoring systems. *Journal of Engineering Structures*, 2008,30:1820-1830.
112. H. Gwanghee, J. Joonryong. A Smart Monitoring System Based on

- Ubiquitous Computing Technique for Infra-structural System: Centering on Identification of Dynamic Characteristics of Self-Anchored Suspension Bridge. *KSCE Journal of Civil Engineering*, 2009, 13(5):333-337
113. S. Doebling, C. Farrar, M. Prime, D. Shevitz. Damage identification and health monitoring of structural and mechanical systems from changes in their vibration characteristics: a literature review. Los Alamos National Laboratory Report LA-13070-MS, 1996.
 114. C. Shane, J. Ratneshwar. Structural damage detection using AR-ARX models, Department of Mechanical and Aeronautical Engineering, Clarkson University, 2005.
 115. M. Gevers, L. Miskovic, D. Bonvin, A. Karimi. Identification of multi-input systems: variance analysis and input design issues , *Automatica*, 2006,42:559 – 572
 116. K. Kuhlman. Importance of autocorrelation for parameter estimation in regression models, theory and deformation analysis, in: *The 10th International Symposium on Deformation Measurements*, California, 2001.
 117. C. Ince, M. Sahin. Real-time deformation monitoring with GPS and Kalman Filter. *J. Earth, Planets Space*, 2000, 52(10):837-840.
 118. W. Helmut. *Health Monitoring of Bridges*. John Wiley & Sons Ltd, The Atrium, Southern Gate, Chichester, West Sussex, PO19 8SQ, U K, 2009.
 119. G. Armer. *Monitoring and assessment of structures*. Taylor& Francis, London and New York, 2001.
 120. E. Douglas. *Health Monitoring of Structural Materials and Components Methods with Applications*. John Wiley & Sons Inc., Hoboken, USA, 2007.
 121. E. Kaplan, C. Hegarty. *Understanding GPS Principles and Applications*. Second Edition, ARTECH HOUSE, INC. Norwood, 2006.
 122. http://en.wikipedia.org/wiki/Global_Positioning_System
 123. A. Quinquis. *Digital signal processing using Matlab*. John Wiley&Sons,Inc, Hoboken, USA and ISTE Ltd, London, UK, 2008.
 124. J. He, Z. Fu. *Modal analysis*. Planta Tree, Oxford Auckland Boston

- Johannesburg Melbourne New Delhi, 2001.
125. D. Inman, C. Farrar; et al. Damage prognosis for aerospace, civil and mechanical systems. John Wiley&Sons,Inc, Hoboken, USA, 2005.
 126. E. Simu, R. Scanlan. Wind effects on structures; fundamentals and applications to design. third edition; A wiley-interscience; John Wiley&Sons,inc; New York, USA, 1996.
 127. S. Utku. Theory of adaptive structures; incorporating intelligence into engineered products. CRC; Boca Raton Boston London; UK, 1998.
 128. R. Shouresh, S. Lim. Sensor informatics and advanced vibration control of civil structures. prss. Of 3rd international conference on earthquake engineering; Nanjing; China, 2004.
 129. P. Anderson. Identification of civil engineering structures using vector ARMA models. Department of building technology and structural engineering; Aalborg University; Denmark, 1997.
 130. L. Hui, J. Ou, et al. Structural Health Monitoring System for the Shandong Binzhou Yellow River Highway Bridge. Computer-Aided Civil and Infrastructure Engineering , 2006, 21:306–317.
 131. S. Haykin. Kalman filter and neural networks. John wiley&Sons,Inc. New Work, USA, 2001.
 132. SPSS (1999). Inc. Version 10.0.5, Chicago, Illinois.

Appendix (A): Some used MATLAB programs

A-1) Kalman Prediction Process

```

%%initial values
A=1; , F=1; Ql=1 , Qw=0;
%%loading the observation vector
X=Original(:,3);
[n,m]=size(X);
%%initial state
for i=1:1
x(i)=mean(X);
Qx(i)=1;
end
%%prediction of state vector
for i=2:n
    x(i)=F*x(i-1);
    Qx(i)=F*Qx(i-1)*F'+Qw;    %variance covariance matrix of
prediction state
    Px(i)=inv(Qx(i));    %weight of prediction state
    Pl(i)=inv(Ql);    %weight of observation vector
    K(i)=Qx(i)*A'*inv(A*Qx(i)*A'+Ql);    %kalman gain value
    x(i)=x(i)+K(i)*(X(i,1)-x(i));    %the filtered estimate
vector
    Qx(i)=(1-K(i)*A)*Qx(i)*(1-K(i)*A)'+K(i)*Ql*K(i)';    %the
variance covariance matrix of estimation vector
    Qv(i)=Ql-(A*Qx(i)*A');    %the variance covariance matrix of
residuals
end
t=1/20:1/20:1/20*n;

```

A-2) Kalman Filter Process

```

%%initial values
A=1; , F=1; Ql=1 , Qw=10^-6;

```



```

%%loading the observation vector
X=Original(:,3);
[n,m]=size(X);
%initial state
for i=1:1
x(i)=mean(X);
Qx(i)=1;
end
%%prediction of state vector
for i=2:n
    x(i)=F*x(i-1);
    Qx(i)=F*Qx(i-1)*F'+Qw;    %variance covariance matrix of
prediction state
    Px(i)=inv(Qx(i));        %weight of prediction state
    Pl(i)=inv(Ql);          %weight of observation vector
    K(i)=Qx(i)*A'*inv(A*Qx(i)*A'+Ql);    %kalman gain value
    x(i)=x(i)+K(i)*(X(i,1)-x(i));        %the filtered estimate
vector
    Qx(i)=(1-K(i)*A)*Qx(i)*(1-K(i)*A)'+K(i)*Ql*K(i)';    %the
variance covariance matrix of estimation vector
    Qv(i)=Ql-(A*Qx(i)*A');    %the variance covariance matrix of
residuals
end
t=1/20:1/20:1/20*n;

```

A-3) Adaptive Filter Process

```

data=load('p3.txt');
x=data(:,2);
x=detrend(x);
y=data(:,3);
y2=detrend(y);
figure
plot(x,y2)
n=10;

```

```

wn=.99;
b=fir1(n,[.2/10 9.9/10]);
d=filter(b,1,x);
d1=filter(b,1,y2);
%l=kron(d,d');
%mu=1/max(eig(l));
mu=1;
ha=adaptfilt.lms(10,mu);
[y,e]=filter(ha,x,d);
[y1,e1]=filter(ha,y2,d1);
figure
plot(y,y1)
[k,m]=size(x);
t=1/20:1/20:1/20*k;

```

A-4) Polar Coordinate Model

```

Load data
[n,m]=size(data);
x1=data(:,2);
y1=data(:,3);
%x2=data(:,4);
%y2=data(:,5);
r1=sqrt(x1.^2+y1.^2);
%r2=sqrt(x2.^2+y2.^2);
t=1/20:1/20:1/20*n;
for i=1:n
    set1(i)=atan(x1(i)/y1(i));
    % set2(i)=atan(x2(i)/y2(i));
end
load('matlab.mat')
d1=r1-x11;
load('angle.mat')
d2=set1'-set11;

```

A-5) Tortion GPS Coordinates

```

data=Original;
x1=data(:,2);
y1=data(:,3);
x2=data(:,4);
y2=data(:,5);
dx=x2-x1;
dx=dx';
dy=y2-y1;
dy=dy';
n=length(data);
i=1:n;
    ds(i)=dy(i)/dx(i);
    se=atan(ds);
t=1/20:1/20:1/20*n;
dl=dy-261.0706805657;

```

A-6) Convert GPS to Acceleration

```

clc; clear all; format long
data=load('p2.txt');
x=data(:,2);
y=data(:,3);
n=length(x);
dt=1/20;
t1=dt:dt:dt*n;
i=2:n-1;
    vx(i)=0.50*((x(i+1)-x(i))/dt+(x(i)-x(i-1))/dt);
    vy(i)=0.50*((y(i+1)-y(i))/dt+(y(i)-y(i-1))/dt);
m=length(vx);
t=dt:dt:dt*m;
i=2:m-1;
    ax(i)=0.50*((vx(i+1)-vx(i))/dt+(vx(i)-vx(i-1))/dt);
    ay(i)=0.50*((vy(i+1)-vy(i))/dt+(vy(i)-vy(i-1))/dt);
c=length(ax);
ta=dt:dt:dt*c;

```

A-7) Robust Fit

```
load mean_20min_ys_weden %mm
load mean_20min_tempr %tmm
load mean_20min_wind %wmm
load mean_20min_him %hmm
load traffic_no %traf

vmm=traf';
y=mm;
x=[vmm;wmm];
y=y';
x=x';

[b,stats] = robustfit(x,y,'bisquare',4.685,'on');
yhat=b(1)+b(2)*vmm+b(3)*wmm;
yhat=yhat';
e=y-yhat;
t=1/3:1/3:1/3*length(yhat);
h = legend('Observation','Robust Fit',1);
sum=0;
for i=1:length(e)
    sum=sum+e(i)^2;
end
lam=sum/length(e);
FEP=lam*(1+(2*length(b))/(length(e)-length(b)));
sum1=0;
sum2=0;
for i=1:length(yhat);
    sum1=sum1+(yhat(i)-mean(yhat))^2;
    sum2=sum2+(y(i)-mean(y))^2;
end
R=(sum1/sum2);
figure
autocorr(e)
title('ACF with Bounds for Residuals')
```

Appendix (B): Some Observations Movements Results

These Tables show that the deformation of Southern tower (DX1,DY1) and Northern tower (DX2,DY2) relative to mean of June 2007 observations. All dimensions by meters.

B-1) June 2007

DX1	DY1	DX2	DY2
0.003660	-0.002122	0.003883	0.003722
0.003660	-0.002122	0.003883	0.004722
0.003660	-0.002122	0.003883	0.004722
0.002660	-0.001122	0.003883	0.004722
0.002660	-0.001122	0.003883	0.004722
0.002660	-0.001122	0.003883	0.004722
0.002660	-0.001122	0.003883	0.004722
0.002660	-0.001122	0.003883	0.004722
0.002660	-0.001122	0.003883	0.004722
0.002660	-0.001122	0.003883	0.004722
0.002660	-0.001122	0.003883	0.004722
0.002660	-0.001122	0.003883	0.004722
0.002660	-0.001122	0.003883	0.004722
0.002660	-0.001122	0.003883	0.004722
0.002660	-0.001122	0.003883	0.004722

B-2) August 2007

DX1	DY1	DX2	DY2
-0.00234	-0.00512	-0.01712	-0.01128
-0.00234	-0.00512	-0.01712	-0.01128
-0.00234	-0.00512	-0.01712	-0.01128
-0.00234	-0.00512	-0.01712	-0.01128
-0.00234	-0.00512	-0.01712	-0.01128
-0.00234	-0.00512	-0.01712	-0.01128
-0.00234	-0.00512	-0.01712	-0.01128
-0.00234	-0.00512	-0.01712	-0.01128
-0.00234	-0.00512	-0.01712	-0.01128
-0.00234	-0.00512	-0.01712	-0.01128
-0.00234	-0.00512	-0.01712	-0.01128
-0.00234	-0.00512	-0.01712	-0.01128
-0.00234	-0.00512	-0.01712	-0.01128
-0.00234	-0.00512	-0.01712	-0.01128
-0.00234	-0.00512	-0.01712	-0.01128

B-3) October 2007

DX1	DY1	DX2	DY2
0.02366	0.014878	-0.00612	-0.00828
0.02366	0.014878	-0.00612	-0.00828
0.02366	0.014878	-0.00612	-0.00828
0.02466	0.014878	-0.00612	-0.00828
0.02466	0.014878	-0.00712	-0.00828
0.02466	0.014878	-0.00712	-0.00828
0.02466	0.014878	-0.00712	-0.00828
0.02466	0.014878	-0.00712	-0.00828
0.02466	0.014878	-0.00712	-0.00828
0.02466	0.015878	-0.00712	-0.00828
0.02466	0.015878	-0.00712	-0.00828
0.02466	0.015878	-0.00712	-0.00828
0.02466	0.015878	-0.00712	-0.00928
0.02466	0.015878	-0.00712	-0.00928
0.02466	0.015878	-0.00712	-0.00928
0.02466	0.015878	-0.00712	-0.00928
0.02466	0.015878	-0.00712	-0.00928
0.02466	0.015878	-0.00712	-0.00928
0.02466	0.015878	-0.00712	-0.00928
0.02466	0.015878	-0.00712	-0.00928
0.02466	0.015878	-0.00712	-0.00928

B-4) January 2008

DX1	DY1	DX2	DY2
0.08266	0.059878	-0.00812	-0.00928
0.08266	0.059878	-0.00812	-0.00928
0.08266	0.059878	-0.00812	-0.00928
0.08266	0.059878	-0.00912	-0.00928
0.08266	0.059878	-0.00912	-0.00928
0.08266	0.059878	-0.00912	-0.01028
0.08266	0.059878	-0.00912	-0.01028
0.08266	0.059878	-0.00912	-0.01028
0.08266	0.059878	-0.00912	-0.01028
0.08266	0.059878	-0.00912	-0.01028
0.08266	0.059878	-0.00912	-0.01028
0.08266	0.059878	-0.00912	-0.01028
0.08266	0.059878	-0.00912	-0.01028
0.08266	0.059878	-0.00912	-0.01028
0.08266	0.059878	-0.00912	-0.01028
0.08266	0.059878	-0.00912	-0.01028
0.08266	0.059878	-0.00912	-0.01028
0.08266	0.059878	-0.00912	-0.01028
0.08266	0.059878	-0.00912	-0.01028
0.08266	0.059878	-0.01012	-0.01028
0.08366	0.059878	-0.01012	-0.01028
0.08366	0.059878	-0.01012	-0.01028

B-5) Febraury 2008

DX1	DY1	DX2	DY2
0.08766	0.058878	-0.00712	-0.01428
0.08766	0.058878	-0.00712	-0.01428
0.08766	0.058878	-0.00712	-0.01428
0.08766	0.058878	-0.00712	-0.01428
0.08766	0.058878	-0.00712	-0.01428
0.08766	0.058878	-0.00712	-0.01428
0.08766	0.058878	-0.00712	-0.01428
0.08766	0.058878	-0.00712	-0.01428
0.08866	0.058878	-0.00712	-0.01428
0.08866	0.058878	-0.00712	-0.01428
0.08866	0.058878	-0.00712	-0.01428
0.08866	0.058878	-0.00712	-0.01428
0.08866	0.058878	-0.00712	-0.01428
0.08866	0.058878	-0.00712	-0.01428
0.08866	0.058878	-0.00712	-0.01428
0.08866	0.058878	-0.00712	-0.01428
0.08866	0.059878	-0.00712	-0.01428
0.08866	0.059878	-0.00712	-0.01428
0.08866	0.059878	-0.00712	-0.01428
0.08866	0.059878	-0.00712	-0.01428
0.08866	0.058878	-0.00712	-0.01428
0.08866	0.058878	-0.00712	-0.01428

B-6) April 2008

DX1	DY1	DX2	DY2
0.05366	0.047878	-0.04312	-0.03028
0.05366	0.047878	-0.04312	-0.03028
0.05366	0.047878	-0.04312	-0.03028
0.05366	0.047878	-0.04312	-0.03028
0.05366	0.047878	-0.04212	-0.02928
0.05366	0.047878	-0.04212	-0.02928
0.05366	0.047878	-0.04212	-0.02928
0.05366	0.047878	-0.04212	-0.02928
0.05366	0.047878	-0.04212	-0.02928
0.05366	0.047878	-0.04212	-0.02928
0.05366	0.047878	-0.04112	-0.02928
0.05366	0.047878	-0.04112	-0.02928
0.05366	0.047878	-0.04112	-0.02928
0.05366	0.047878	-0.04112	-0.02928
0.05366	0.047878	-0.04112	-0.02828
0.05366	0.047878	-0.04112	-0.02828
0.05366	0.047878	-0.04112	-0.02828
0.05366	0.047878	-0.04112	-0.02828
0.05366	0.047878	-0.04112	-0.02828
0.05366	0.047878	-0.04012	-0.02828
0.05366	0.047878	-0.04012	-0.02828
0.05366	0.047878	-0.04012	-0.02828

B-7) June 2008

DX1	DY1	DX2	DY2
-0.00934	-0.00212	0.018883	0.012722
-0.00934	-0.00212	0.018883	0.012722
-0.00934	-0.00212	0.018883	0.012722
-0.00934	-0.00112	0.018883	0.012722
-0.00934	-0.00112	0.018883	0.012722
-0.00934	-0.00112	0.018883	0.012722
-0.00934	-0.00112	0.017883	0.012722
-0.00834	-0.00112	0.017883	0.012722
-0.00834	-0.00112	0.017883	0.012722
-0.00834	-0.00112	0.017883	0.012722
-0.00834	-0.00112	0.017883	0.012722
-0.00834	-0.00112	0.017883	0.012722
-0.00834	-0.00112	0.017883	0.012722
-0.00834	-0.00112	0.017883	0.011722
-0.00834	-0.00112	0.017883	0.011722
-0.00834	-0.00112	0.017883	0.011722
-0.00834	-0.00112	0.017883	0.011722
-0.00834	-0.00012	0.017883	0.011722
-0.00834	-0.00012	0.017883	0.011722
-0.00734	-0.00012	0.017883	0.011722

List of Figure Captions

- Figure 1.1 GPS satellites arranged in six orbital planes
- Figure 1.2 GPS elements
- Figure 1.3 the RTK-GPS sachem
- Figure 1.4 satellite-receiver double difference cases
- Figure 1.5 Common errors in GPS measurements
- Figure 1.6 Schematic of a linear time-invariant (LTI) system. The input signal is transformed into an output signal.
- Figure 1.7 Adaptive filter configurations.
- Figure 1.8 The geometry plane deformation monitoring (a) plan, (b) elevation
- Figure 1.9. The geometry polar coordinates system
- Figure 1.10. The geometry traffic loads affects on the deck and towers movement
- Figure 2.1. Elevation and system of health monitoring of the Bridge
- Figure 2.2. The structural health monitoring system of the Bridge
- Figure 2.3. The number of satellite and elevation angle of receivers
- Figure 2.4. GPS Dynamic Monitoring Scheme
- Figure 2.5. GPS network architecture
- Figure 2.6. The (a) global and local coordinate system and (b) layout of GPS positions of the bridge
- Figure 2.7. The sample of environment data observed (a) wind speed, (b) wind direction
- Figure 2.8. The time series of X (up) and Y (down)-direction for S. Tower (before and after KF) (1-8-2007)
- Figure 2.9. The time series of X (up) and Y (down)-direction for S. Tower (before and after KF) (1-6-2008)
- Figure 2.10. Corrected X coordinates deformation of S. Tower from PLS.
- Figure 2.11. Corrected Y coordinate deformation of S. Tower from PLS.
- Figure 2.12. Corrected X coordinate deformation of S. Tower from KF and PLS.

- Figure 2.13. Corrected Y coordinate deformation of S. Tower from KF and PLS.
- Figure 2.14. Cracks shape at (a) abutment and (b) mid span, respectively.
- Figure 2.15. The GPS original signals and linear fitting for south (up) and north tower
- Figure 2.16. The (a) load and (b) velocity traffic effects
- Figure 2.17. The environmental observation data (a) speed, (b) direction of wind and (c) temperature
- Figure 2.18. The time series original GPS data at north and south tower bridge
- Figure 2.19. The residual of original GPS data at (a) south and (b) north tower bridge
- Figure 2.20. The GPS original and KF signals at south (up) and north towers
- Figure 2.21. The deformation of south tower in two directions
- Figure 2.22. The deformation of north tower in two directions
- Figure 2.23. The SD of mean original, KF signals and PLS
- Figure 3.24. The power spectrum signals for south (up) and north X-direction signals (a) June 2007 (b) June 2008
- Figure 2.25. The power spectrum signals for south (up) and north Y-direction signals (a) June 2007 (b) June 2008
- Figure 2.26. The first peak PSD at south (X1, Y1) and north (X2, Y2) bridge towers
- Figure 2.27. The photo of cracks on the (a) south abutment, (b) mid span and (c) south tower
- Figure 2.28. AF results of June 2007 signals,(a) X and (b) Y-directions
- Figure 2.29. The tower movement (X-direction left)(Y-direction right), Aug., Dec. 2007, Mar., Jun., Jul. 2008 (up to down)
- Figure 2.30. Time-Frequency for the tower movement(the continous red color revealed to the high power), (X-direction left)(Y-direction right), Aug., Dec. 2007, Mar., Jun., Jul. 2008 (up to down)
- Figure 2.31. Movements of southern tower in X (longitudinal) and Y (lateral) directions (a) unload case (June 2007), and (b) damage case (June 2008).

- Figure 2.32. Statistical analysis of (a) GPS observation, (b) Velocity converted and (c) Acceleration converted, from GPS signals.
- Figure 2.33. Sample environmental observation (a) wind speed, (b) temperature in August 2007.
- Figure 2.34. The de-noised and coefficient for Haar wavelet analysis in X and Y-directions at (a) unload case (June 2007), (b) load case (December 2007), and (c) damage case (June 2008).
- Figure 2.35. Statistical mean and SD of the (a) approximate and (b) detail for the Haar wavelet coefficients with the time monitoring
- Figure 2.36. one and two D. Frequency for the tower movement in X and Y-direction at (a) June 2007, (b) May 2008 and (c) June 2008 (the continuous red color revealed to the high power).
- Figure 2.37. (a) The first mode frequency and (b) the maximum PSD of the first mode for the GPS signals
- Figure 2.38 A subset of the GPS results for the south tower site with the model kalman filter, in blue, superimposed (6 June 2007)
- Figure 2.39 The SD of KF and GPS signals for the X and Y coordinates
- Figure 2.40 The mean values of filters values for the south tower coordinates with the time monitoring
- Figure 2.41 The mean values of filters values for the north tower coordinates with the time monitoring
- Figure 2.42 The distortion of plane in (a) X-direction and (b) Y-direction respectively for the south tower
- Figure 2.43 The main signal (red) and prediction signal (blue) (a) distance PC and (b) angle PC
- Figure 2.44 The Maximum, Minimum and mean for the distance PC distortion
- Figure 2.45 The Maximum, Minimum and mean for the angle PC distortion
- Figure 2.46 The statistical test of the (a) distance and (b) angle for PC
- Figure 2.47 A subset of the span length calculated with the model kalman predictions, in blue, a-June 2007, b- August 2007, c- February 2008 and d- June 2008
- Figure 2.48 Statistical test of the span length distortion

- Figure 3.1 ARMAX Model Structure
- Figure 3.2. MLP-network scheme
- Figure 3.3. Observation,de-noised signals of tower displacements in (a) X and (b) Y-directions
- Figure 3.4. mean 20-min. displacement of de-noised signals for southern tower in (a) X and (b) Y-directions
- Figure 3.5. Variation in (a) Temperature, (b) Humidity, (c) Number of vehicle, and (d) Wind speed during the observation
- Figure 3.6. Input-output quantities and models considered in the development of transfer functions for the bridge tower
- Figure 3.7. Observation displacement and output produced by Robust fit regression of southern tower in (a) X and (b) Y-directions
- Figure 3.8. Displacements output of the NNARMAX models for the tower displacements
- Figure 3.9. ACF and 95% confidence intervals of NNARMAX models describing the displacements of the tower
- Figure 3.10. ACF and 95% confidence intervals of the residuals for the static multiple regression NNARMAX0100 model used to describe the displacements of the tower in the X (a) and Y (b) directions.
- Figure 4.1. Time history of movement of a southern tower bridge in (a) X and (b) Y-directions
- Figure 4.2. Time history of wind and temperature for the bridge (a) speed, (b) direction and (c) Temperature.
- Figure 4.3 Fundamental natural GPS signal frequency plot: (a) X-axis frequency; (b) Y-axis frequency
- Figure 4.4. Time history of accelerometer the southern tower bridge (a) X and (b) Y-directions
- Figure 4.5. Fundamental natural Accelerometer signal frequency plot: (a) X-axis frequency; (b) Y-axis frequency
- Figure 4.6 (a) Torsion displacement; (b) the distance error between the first and series positions
- Figure 4.7. continuous deformation analysis Scheme

Figure 4.8. continuous deformation (blue) statistical tests (a) X-direction; (b)
Y-direction

List of Table Captions

- Table 1.1. Non-GPS instruments for measuring deformation [89].
- Table 1.2. Summary of the Kalman filter.
- Table 2.1. The local Cartesian coordinates of bridge towers.
- Table 2.2. Temperature-induced deflection of tower and deck.
- Table 2.3. The results of statistical test.
- Table 2.4 The correlation coefficient between the GPS signals.
- Table 2.5 the total available vehicle loads and velocity (lane 1 from one side to another side)
- Table 2.6. The results of statistical test.
- Table 2.7. The movement observations relative to June 2007.
- Table 2.8. Summary of environmental observations with time selections.
- Table 2.9 The parameters of two assumed planes at south tower.
- Table 3.1. Robust fit model of the displacement of tower in X and Y directions with respect to the number of vehicle (V), wind speed (W), temperature (T), and humidity (H)
- Table 3.2. Parameters of NNARMAX models of the towers displacements in the X and Y-directions

Published Papers in the Ph.D.Period

Journal Papers

- 1- **Mosbeh R.Kalooop**, Hui Li , "Monitoring of Bridges Deformation Using GPS Technique ", KSCE journal of civil engineering, KSCE, 13 (2009), 423-431, DOI: 10.1007/s12205-009-0423-y. (**SCI, EI**)
- 2- **Mosbeh R.Kalooop**, Hui Li "Tower bridge movement analysis with GPS and accelerometer techniques: Case study Yonghe tower bridge", J. Information Technology 8 (2009) , 1213-1220. DOI: 10.3923/ijtj.2009.1213.1220 (**EI**)
- 3- **Mosbeh R.Kalooop**, Hui Li, 2010 "Simple Geometrical Model to Analyze the Motion Detection of Bridges Based-GPS Technique: Case study Yonghe bridge", Structural Engineering and Mechanics, An International Journal, (**Accepted**) (**SCI, EI**)(**IF=0.50**).
- 4- **Mosbeh R.Kalooop**, Hui Li, "Physical and Geometrical Design Methods for Bridge Movement and Damage Analysis", KSCE journal of civil engineering, KSCE,(under review) (**SCI, EI**)
- 5- **Mosbeh R.Kalooop**, Hui Li "Multi input Single Output Models Identification Tower Bridge Movements Using GPS monitoring System", Applied Mathematical Modelling Journal, (under review) (**SCI**).
- 6- **Mosbeh R.Kalooop**, Hui Li "Sensitivity and Analysis GPS Signals Based Bridge Damage using Wavelet Transform", Measurement Journal (Submit) (**SCI**)

Conference Papers

- 7- **Mosbeh R.Kalooop**, Hui Li, (2010) "Analysis of bridge movements and damage based on GPS monitoring technique" The 6th international exhibition and scientific congress "GEO-SIBERIA-2010" 27-29 April 2010, Novosibirsk, Russia, Vol.1, No.1,P.33-37.

Statement of Copyright

I am, the undersigned, declare this work has not previously been submitted in candidature for any degree. The dissertation is the result of my own work and investigation, explicit references. A complete list of references is appended.

Signed: *M.S. Wang*..... (candidate)

Date: *28.6.2010*

Letter of Authorization

Powers of discretion are granted to the University Library to allow the dissertation to be copied in part without further reference to the author. This permission covers only single copies made for study purposes, subject to normal conditions of acknowledgement.

Signed: *mes.h.n.*..... (candidate)

Date: 28.6.2010

Signed: (supervisor).....*李*..... (candidate)

Date: 28.6.2010

Acknowledgements

I wish to express my gratitude to Allah, the main source of knowledge and wisdom. Really, I have no words to express our gratitude to everyone shares in this work; There are many people whom I would like to thank and acknowledge for support and assistance during my doctoral program at HIT. I would especially like to express my cordial thanks, sincere gratitude and appreciation to my advisor Prof. Hui Li, for her generous time, commitment and enthusiasm for my education and research. Throughout my doctoral tenure, she encouraged me to refine the research skills and analytical abilities necessary to complete my course of studies.

Dr. Wensong Zhou, Dr. Abd-El Rahim Jassim, Dr. Wenli Chen, Dr. Shunlong Li, Dr. Ashraf A.Beshr, Dr. Mohammed EL-Diasty, Mr. Dongwang Tao and Eng. Amr Magdi deserve my special thanks for their technical support which were of a great value to this research.

Special thanks go to Dr. Chanxi Mao for helping me with my researches as well as my family during my study period in Harbin.

My warmest gratitude goes to my Wife, Mona, a woman of great patience and kindness deserves my deepest thanks. I greatly appreciate for her devotion, love and support all the time. The daily encouragement she provided makes this dissertation as much her as it is mine. I would also like to give special gratitude to my daughter, Razan, and my son, Khaled, for there smiles which light up my life. I shall remain indebted to my parents, my grandma 'Nasra', sisters, brothers and my wife's family for their love, constant care and encouragement during the course of my research.

Last but not least, I would like to thank Egyptian Ministry of Higher Education and Harbin Institute of Technology for allowing me to be a part of its first class research community. Finally, I would like to thank all of the professors, colleagues and friends who assisted me along the way until this dissertation has been completed and whose contributions are too numerous and diverse to mention in a few short paragraphs.

Resume

Mosbeh Rashed Mosbeh Kaloop
Assistant Lecturer

Work Address:
Faculty of Engineering – Dept. of
Public Works Engineering
University of Mansoura
EL-Mansoura
E-mail: mosbeh.kaloop@gmail.com

Personal
Birth place: North Sinai -
Egypt
Birth date: July 12, 1979
Marital status: Married
Citizenship: Egyptian



EDUCATION:

- **Doctoral:** Harbin Institute of Technology, PhD of Science in civil Engineering, under the title of: “**Structural Health Monitoring through Dynamic and Geometric Characteristics of Bridges Extracted from GPS Measurements**”.
- **Master:** Mansoura University, Egypt - Master of Science in Public works Engineering, 02/2006 under the title of: “**Leveling by using Global Positioning System**”.
- **Bachelor:** Faculty of Engineering, Mansoura University, Egypt - B.S., Civil Engineering, 06/2002, with a general grade of appreciation **Excellent with the Honor's** degree (Fourth). The grade of project (**survey project**) is Excellent.

WORK EXPERIENCE:

- Harbin Institute of Technology, China, 09/2007 to now – PhD student, School of Civil Engineering.
- Mansoura University, Egypt, 02 / 2006 to now - Assistant lecturer, Dept. of Public Works Engineering – Civil Engineering.
- Mansoura University, Egypt, 09/2002 to 12/ 2005: Assistant Teaching, Dept. of Public Works Engineering – Civil Engineering.

TEACHING:

University Courses (some selected topics are given for each course):

Mansoura University

- GPS Applied Survey Engineering.
- Plane Survey Engineering
- Aerial and Terrestrial Photogrammetry Engineering.
- Least Square Theory.
- Geodesy and Geographical Engineering.
- Undergraduate Students Seminar
- Statistical Analysis

Publications

Journal Publications

- 1- **Mosbeh R.Kaloop**, Hui Li , "Monitoring of Bridges Deformation Using GPS Technique ", KSCE journal of civil engineering, KSCE, 13 (2009), 423-431, DOI: 10.1007/s12205-009-0423-y. (SCI, EI)
- 2- **Mosbeh R.Kaloop**, Hui Li "Tower bridge movement analysis with GPS and accelerometer techniques: Case study Yonghe tower bridge", J. Information Technology 8 (2009) , 1213-1220. DOI: 10.3923/itj.2009.1213.1220 (EI)
- 3- **Mosbeh R.Kaloop**, Hui Li, 2010 "Simple Geometrical Model to Analyze the Motion Detection of Bridges Based-GPS Technique: Case study Yonghe bridge", Structural Engineering and Mechanics, An International Journal, (Accepted) (SCI,EI)(IF=0.50).
- 4- **Mosbeh R.Kaloop**, Hui Li, "Physical and Geometrical Design Methods for Bridge Movement and Damage Analysis", KSCE journal of civil engineering, KSCE,(under review) (SCI, EI)
- 5- **Mosbeh R.Kaloop**, Hui Li "Multi input Single Output Models Identification Tower Bridge Movements Using GPS monitoring System", Applied Mathematical Modelling Journal, (under review) (SCI).
- 6- **Mosbeh R.Kaloop**, Hui Li "Sensitivity and Analysis GPS Signals Based Bridge Damage using Wavelet Transform", Measurement Journal, (Submit) (SCI).

Conference Papers Publications

- 7- **M.Kaloop**, M. EL-Mowafi, M.Rabah “The simple polynomial technique to compute the orthometric height in Egypt”. The 6th International Engineering Conference (IEC 2008), Mansoura – Sharm El-Sheikh, Egypt. 18-23 March 2008, p.319-328.
- 8- Zaki Mohamed Zeidan , Ashraf A. A. Beshr, **Mosbeh R. Kaloop** “Studing the application accuracy of linear polynomial adjustment technique in monitoring the structural deformation”. The 6th International Engineering Conference (IEC 2008), Mansoura – Sharm El-Sheikh, Egypt. 18-23 March 2008, p.329-340.
- 9- **M.Kaloop**, H.El-shambaky and Ashraf A. Beshr “How can you estimate the geoid undulation by least square collocation technique and GPS data?” The fourth international exhibition and scientific congress “GEO-SIBERIA-2008” 22-24 April 2008, Novosibirsk, Russia Vol.1 p.197-202.
- 10- **Mosbeh R.Kaloop**, Ashraf A.Beshr, Mohammed Y.Elshiekh " Using Total Station for monitoring the deformation of high strength concrete beams" the 6 th international conference on vibration engineering (ICVE), June 4-5, 2008, Dalian, China, p.411-419.
- 11- **Mosbeh R.Kaloop** “Mathematical techniques to compute geoid undulation with GPS data” The fifth international exhibition and scientific congress “GEO-SIBERIA-2009” 21-23 April 2009, Novosibirsk, Russia Vol.1 p.307-313
- 12- **Mosbeh R.Kaloop**, Hui Li, (2010) "Analysis of bridge movements and damage based on GPS monitoring technique" The 6th international exhibition and scientific congress “GEO-SIBERIA-2010” 27-29 April 2010, Novosibirsk, Russia, Vol.1, No.,1 P.33-37.

Sessions:

- Six sessions in faculty and leadership development project (FLDP) from 01/2006 to 03/2006, Mansoura University, Egypt:-
 - Two sessions in research methodology.
 - Two sessions in development of the active communication.
 - Two sessions in development of the thought skills.

AWARDS

- CSC and Egyptian Ministry of Higher Education Scholarship, 2007.
- Awards for outstanding performance from Faculty of Engineering, Mansoura University, Egypt, 1998 to 2002.
- Awards for outstanding performance from the primary and secondary Rabaa School, North Sinai, Egypt, 1994 and 1997.

PROFESSIONAL:

The Engineering Syndicate of Egypt, Member

REFERENCES:

Available upon request